Research & Technology Transfer

Alaska Department of Transportation & Public Facilities

Pre-Stress Losses in Decked Bulb-Tee Girders (Phase 1-A: Sensor Study for Pre-Stress Loss Monitoring System)

FINAL REPORT

Prepared by:
Il-Sang Ahn, Ph.D., P.E.
Department of Civil and Environmental Engineering
University of Alaska Fairbanks

Report # FHWA-AK-RD-4000(178)
August 2020

Prepared for:
Alaska Department of Transportation & Public Facilities
Statewide Research Office
3132 Channel Drive
Juneau, AK 99801-7898

REPORT DOCUMENTATION PAGE

Form approved OMB No.

Public reporting for this collection of information is estimated to average 1 hour per response, including the time for reviewing instructions, searching existing data sources, gathering and maintaining the data needed, and completing and reviewing the collection of information. Send comments regarding this burden estimate or any other aspect of this collection of information, including suggestion for reducing this burden to Washington Headquarters Services, Directorate for Information Operations and Reports, 1215 Jefferson Davis Highway, Suite 1204, Arlington, VA 22202-4302, and to the Office of Management and Budget, Paperwork Reduction Project (0704-1833), Washington, DC 20503

1. AGENCY USE ONLY (LEAVE BLANK)	2. REPORT DATE	3. REPORT TYPE AND DATES COVERED
FHWA-AK-RD-4000(178)	8/31/2020	Final Report (January 2018 – March 2020)

4. TITLE AND SUBTITLE

Pre-Stress Losses in Decked Bulb-Tee Girders
(Phase 1-A: Sensor Study for Pre-Stress Loss Monitoring System)

5. FUNDING NUMBERS

Federal # 4000178
IRIS# HFHWY00081

6. AUTHOR(S)

Il-Sang Ahn

7. PERFORMING ORGANIZATION NAME(S) AND ADDRESS(ES)

Department of Civil and Environmental Engineering, PO Box 755900, 245 Duckering Building, 1760 Tanana Loop, University of Alaska Fairbanks, Fairbanks, AK 99775-5900

8. PERFORMING ORGANIZATION REPORT NUMBER

FHWA-AK-RD-4000-178

9. SPONSORING/MONITORING AGENCY NAME(S) AND ADDRESS(ES)

State of Alaska, Alaska Dept. of Transportation and Public Facilities
Research and Technology Transfer
3132 Channel Drive, Juneau, AK 99801-7898

10. SPONSORING/MONITORING AGENCY REPORT NUMBER

FHWA-AK-RD-4000-178

11. SUPPLENMENTARY NOTES

12a. DISTRIBUTION / AVAILABILITY STATEMENT

No restrictions

12b. DISTRIBUTION CODE

13. ABSTRACT (Maximum 200 words)

The research tested the performance of concrete-embedded strain sensors. The strain sensors are to use in a long-term pre-stress loss monitoring system of decked bulb-tee girders. Based on the measured total strain for 120 days, it was evaluated that the total strain can reach 3,000με over 5 years. Three types of vibrating wire strain gauges (VWSGs) and one type of fiber optic strain gauge (FOSG) were tested, and the measurement range of the VWSG-R sensor (5,000με) is wide enough for the expected strain change.

Both VWSG-B and VWSG-R were responsive through a wide range of temperatures. After applying five thermal cycles (-40°F ~73°F), VWSG-B and VWSG-R accurately measured the strain without any apparent deterioration from cold temperatures. Since each sensor was factory-calibrated, temperature correction can be performed more precisely with the VWSG-R sensor. The overall performance of the VWSG-R sensor is better than other tested sensors considering the significant temperature change that sensors will experience. The research concluded that the VWSG-R sensor is appropriate for use in long-term pre-stress loss monitoring.

14- KEYWORDS : pre-stress loss, long-term, concrete creep, concrete shrinkage, cold temperatures, long-term monitoring, vibrating wire strain gauge.

15. NUMBER OF PAGES

115

16. PRICE CODE

N/A

17. SECURITY CLASSIFICATION OF REPORT	18. SECURITY CLASSIFICATION OF THIS PAGE	19. SECURITY CLASSIFICATION OF ABSTRACT	20. LIMITATION OF ABSTRACT
Unclassified	Unclassified	Unclassified	N/A

Notice

This document is disseminated under the sponsorship of the U.S. Department of Transportation in the interest of information exchange. The U.S. Government assumes no liability for the use of the information contained in this document. The U.S. Government does not endorse products or manufacturers. Trademarks or manufacturers' names appear in this report only because they are considered essential to the objective of the document.

Quality Assurance Statement

The Federal Highway Administration (FHWA) provides high-quality information to serve Government, industry, and the public in a manner that promotes public understanding. Standards and policies are used to ensure and maximize the quality, objectivity, utility, and integrity of its information. FHWA periodically reviews quality issues and adjusts its programs and processes to ensure continuous quality improvement.

Author's Disclaimer

Opinions and conclusions expressed or implied in the report are those of the author. They are not necessarily those of the Alaska DOT&PF or funding agencies.

METRIC (SI*) CONVERSION FACTORS

APPROXIMATE CONVERSIONS TO SI UNITS

Symbol	When You Know	Multiply By	To Find	Symbol
		LENGTH		
in	inches	25.4		mm
ft	feet	0.3048		m
yd	yards	0.914		m
mi	Miles (statute)	1.61		km
		AREA		
in^2	square inches	645.2	millimeters squared	cm^2
ft^2	square feet	0.0929	meters squared	m^2
yd^2	square yards	0.836	meters squared	m^2
mi^2	square miles	2.59	kilometers squared	km^2
ac	acres	0.4046	hectares	ha
		MASS (weight)		
oz	Ounces (avdp)	28.35	grams	g
lb	Pounds (avdp)	0.454	kilograms	kg
T	Short tons (2000 lb)	0.907	megagrams	mg
		VOLUME		
fl oz	fluid ounces (US)	29.57	milliliters	mL
gal	Gallons (liq)	3.785	liters	liters
ft^3	cubic feet	0.0283	meters cubed	m^3
yd^3	cubic yards	0.765	meters cubed	m^3

Note: Volumes greater than 1000 L shall be shown in m^3

		TEMPERATURE (exact)		
°F	Fahrenheit temperature	5/9 (°F-32)	Celsius temperature	°C
		ILLUMINATION		
fc	Foot-candles	10.76	lux	lx
fl	foot-lamberts	3.426	candela/m^2	cd/cm^2
		FORCE and PRESSURE or STRESS		
lbf	pound-force	4.45	newtons	N
psi	pound-force per square inch	6.89	kilopascals	kPa

These factors conform to the requirement of FHWA Order 5190.1A *SI is the symbol for the International System of Measurements

APPROXIMATE CONVERSIONS FROM SI UNITS

Symbol	When You Know	Multiply By	To Find	Symbol
		LENGTH		
mm	millimeters	0.039	inches	in
m	meters	3.28	feet	ft
m	meters	1.09	yards	yd
km	kilometers	0.621	Miles (statute)	mi
		AREA		
mm^2	millimeters squared	0.0016	square inches	in^2
m^2	meters squared	10.764	square feet	ft^2
km^2	kilometers squared	0.39	square miles	mi^2
ha	hectares (10,000 m^2)	2.471	acres	ac
		MASS (weight)		
g	grams	0.0353	Ounces (avdp)	oz
kg	kilograms	2.205	Pounds (avdp)	lb
mg	megagrams (1000 kg)	1.103	short tons	T
		VOLUME		
mL	milliliters	0.034	fluid ounces (US)	fl oz
liters	liters	0.264	Gallons (liq)	gal
m^3	meters cubed	35.315	cubic feet	ft^3
m^3	meters cubed	1.308	cubic yards	yd^3

		TEMPERATURE (exact)		
°C	Celsius temperature	9/5 °C+32	Fahrenheit temperature	°F
		ILLUMINATION		
lx	lux	0.0929	foot-candles	fc
cd/cm^2	candela/m^2	0.2919	foot-lamberts	fl
		FORCE and PRESSURE or STRESS		
N	newtons	0.225	pound-force	lbf
kPa	kilopascals	0.145	pound-force per square inch	psi

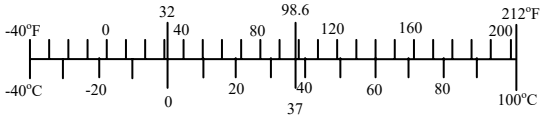

PRE-STRESS LOSSES IN DECKED BULB-TEE GIRDERS (PHASE 1-A: SENSOR STUDY FOR PRE-STRESS LOSS MONITORING SYSTEM)

FINAL REPORT

Prepared for
Alaska Department of Transportation & Public Facilities

Il-Sang Ahn, Ph.D, P.E.

Department of Civil and Environmental Engineering
University of Alaska Fairbanks
Fairbanks, AK

Report # FHWA-AK-RD-4000(178)

August 2020

Table of Contents

List of Figures

List of Tables

Acknowledgments

The research reported herein was performed by the Department of Civil and Environmental Engineering, University of Alaska Fairbanks. Dr. Il-Sang Ahn, Assistant Professor, was the principal investigator. The following individuals contributed to the research or advised material used in this report; their contributions are sincerely acknowledged:

- Mr. Elmer Marx, Mr. Jared Levings, and Mr. Nicholas Murray of DOT&PF for serving in the Technical Advisory Committee of the project
- Mr. Billy Connor at AUTC in UAF for advising and reviewing the final report
- Mr. David Schweigert for assisting in tests and data collection
- Mr. Xavier Schlee at Alaska Basic Industries for the donation of aggregates to make concrete cylinders

Abstract

The research tested the performance of concrete-embedded strain sensors. The strain sensors are to use in a long-term pre-stress loss monitoring system of decked bulb-tee girders. Based on the measured total strain for 120 days, it was evaluated that the total strain can reach 3,000με over 5 years. Three types of vibrating wire strain gauges (VWSGs) and one type of fiber optic strain gauge (FOSG) were tested, and the measurement range of the VWSG-R sensor (5,000με) is wide enough for the expected strain change.

Both VWSG-B and VWSG-R were responsive through a wide range of temperatures. After applying five thermal cycles (-40°F ~73°F), VWSG-B and VWSG-R accurately measured the strain without any apparent deterioration from cold temperatures. Since each sensor was factory-calibrated, temperature correction can be performed more precisely with the VWSG-R sensor. The overall performance of the VWSG-R sensor is better than other tested sensors considering the significant temperature change that sensors will experience. The research concluded that the VWSG-R sensor is appropriate for use in long-term pre-stress loss monitoring.

Summary of Findings

The following are findings of this research:

- Literature survey found no studies directly related to in-situ measurement of long-term pre-stress loss for decked-bulb tee girders in cold-climate regions.
- The pre-stress loss provisions in the current *AASHTO LRFD Bridge Design Specifications* (AASHTO 2017) are known to be less conservative than other pre-stress loss provisions.
- At cold temperatures (-40°F), concrete creep and shrinkage strains became infinitesimal.
- Based on the sensor test results, the total strain in the concrete is expected to reach 3,000με over five years.
- Among the three types of vibrating wire strain gauges and one type of fiber optic strain gauge tested, the VWSG-R was selected because of its measurement range of 5,000με.
- VWSG-R was responsive to the wide change of temperature (-40°F ~73°F) without any apparent deterioration through the entire temperature range.

CHAPTER 1. INTRODUCTION AND RESEARCH APPROACH

1.1 Problem Statement and Research Objective

In order to adapt to Alaska's short construction season, the Alaska Department of Transportation and Public Facilities (DOT&PF) has adopted the use of precast, pre-stressed, decked bulb-tee (DBT) girders to accelerate bridge construction across the state. Figure 1-1 shows a standard cross section of an Alaska-style DBT girder. The deck width can reach 8.5 feet (DOT&PF 2017). Using DBT girders eliminates the need to cast and cure a conventional cast-in-place concrete deck, consequently reducing the construction time of the superstructure (Daugherty and Marx 2014, DOT&PF 2017). In Alaska, about 80% of recently constructed bridges have DBT girders (with spans up to 145 feet). Once DBT girders are placed at the construction site, the bridge deck is constructed by connecting the wide top flanges of the girders with welded shear tabs spaced at 4-foot intervals and filling longitudinal keyways with high-strength, non-shrining grout.

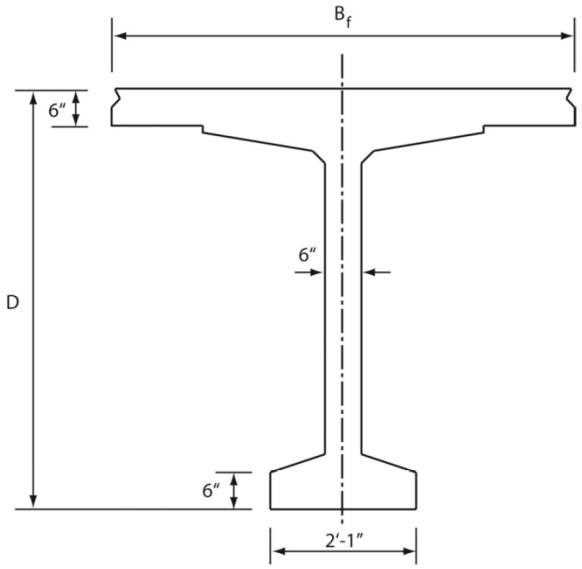

Figure 1-1. Standard Alaska-style precast DBT girder section (DOT&PF 2017)

In the design of DBT girders, the amount of pre-stress is one of the factors considered in determining the stress in the girder throughout its life. The pre-stress applied to the girder counteracts the dead and live loads, keeping the tensile stress in the bottom flange less than the tensile strength require by the design (e.g., zero tension under Service Load Combination III following DOT&PF practice). Over the life of the girder, the magnitude of pre-stress force decreases. This pre-stress loss must be accurately accounted for in girder design to assure the serviceability and safety of the bridge over its life.

If pre-stress loss is underestimated, the concrete of a girder at midspan may experience tensile cracks, which can compromise the durability and long-term performance of the girder. If pre-stress loss is overestimated, however, more pre-stressing strands will be required than are necessary, which may increase the cost of girder fabrication, reduce the maximum span length, or increase the number of girders used.

Total pre-stress loss is separated into two groups: (1) instantaneous losses and (2) long-term, time-dependent losses (AASHTO 2017). Losses due to anchorage set, friction, and elastic shortening are considered an instantaneous loss. Losses due to concrete creep, concrete shrinkage, and relaxation of pre-stressing strands are classified as time-dependent losses. Figure 1-2 demonstrates the change in pre-stress force that occurs during bridge construction activities:

- A – C: Pre-stress loss due to pre-stressing bed anchorage seating, relaxation between initial tensioning and transfer, and temperature change in strands embedded in concrete. Losses from the bed anchorage seating (A – B) are not present in either pre-stressing strands or concrete.
- C – D: Instantaneous pre-stress loss at transfer due to elastic deformation and self-weight.
- D – E and F – G: Time-dependent pre-stress loss due to shrinkage and creep of girder concrete and relaxation of pre-stressing strands.
- E – F: Increasing tensile stress due to superimposed dead loads (SIDL).

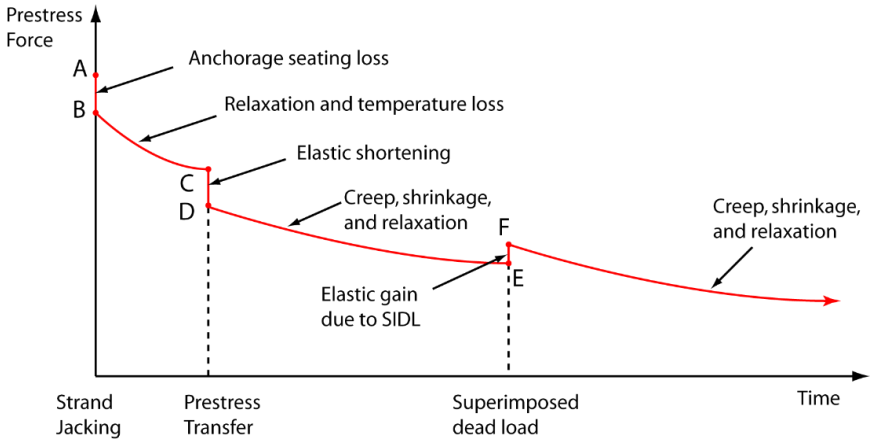

Figure 1-2. Pre-stressing strand force changes with time [modified from Tadros, Al-Omashi et al. (2003) to represent DBT girders]

At pre-stress transfer in Figure 1-2, compressive stresses are imposed on the concrete. In the current *AASHTO LRFD Bridge Design Specifications* or AASHTO-LRFD (AASHTO 2017), the maximum allowable compressive stress at pre-stress transfer is $0.65 f'_{ci}$, where f'_{ci} is concrete compressive strength at transfer.[1] Figure 1-3 shows corresponding compressive stress changes at the bottom fiber concrete (tension side when subject to gravity loads) of a girder. When superimposed dead loads are placed, the tensile stress increases in both the pre-stressing strands and the concrete, inducing stress "gain" in the pre-stressing strands (see Figure 1-2) and additional tensile stress at the bottom of the girder (see Figure 1-3). The tension side of the girder experiences only an increase in tensile stress, and the pre-stress "gains" do not equate to a reduction in pre-stress losses over time.

[1] This revision was made in the 2016 Interim.

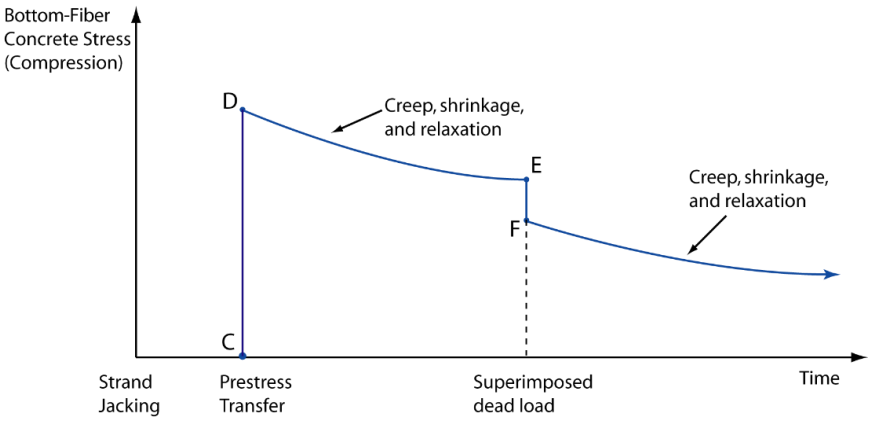

Figure 1-3. Bottom-fiber compressive stress changes [modified from Garber, Gallardo et al. (2013) to represent DBT girders]

Concrete shrinkage, concrete creep, and relaxation of pre-stressing strands are the major mechanisms that contribute to time-dependent pre-stress loss. Of these, creep is the most significant. The percentage of pre-stress loss to total time-dependent loss due to creep, shrinkage, and relaxation was 68%, 24%, and 8%, respectively, for two bridge examples in Tadros et al. (2003) and Roller et al. (2011).

While accurate estimation of pre-stress losses has been studied by many researchers, it is difficult to find research on DBT girders in cold-climate regions. The literature search summarized in Appendix A did not identify any studies on long-term, in-situ measurement of pre-stress loss in DBT girders.

The pre-stress loss provisions in the AASHTO-LRFD were substantially changed in the 2007 AASHTO-LRFD (AASHTO 2007). When the pre-stress loss was estimated from the two provisions, before and after the change, pre-stress losses from the 2017 AASHTO-LRFD (AASHTO 2017) provisions can be substantially less than those from the 2004 AASHTO-LRFD (AASHTO 2004) for DBT girders used by DOT&PF. As a result, the pre-stress loss provisions adopted by DOT&PF and included in the *Alaska Bridges and Structures Manual* (DOT&PF 2017) are from the 2004 AASHTO-LRFD, although the manual was mainly based on the 6th edition of the AASHTO-LRFD (2012).

The DOT&PF is concerned that the pre-stress loss provisions in the 2017 AASHTO-LRFD produce an unconservative estimation for DBT girders in Alaska. Further investigation requires field-measured, pre-stress loss data. In addition, field-measured data make it possible to better understand pre-stress losses that are related to Alaska-specific issues. In Alaska, long-term pre-stress losses can be quite different from those in other states for the following reasons:

- Different aggregate: The influence of different aggregate on the elastic modulus and creep coefficient of concrete was noted in Tadros, Al-Omashi et al. (2003).
- Few DBT girder fabricators in Alaska: There have been only three fabricators, with most of the work performed by one fabricator in Anchorage; thus, the material quality and workmanship can be relatively uniform among girders.

- Shorter time between fabrication and installation of girders: Typically, time spent in a storage yard is 60 days in Alaska[2]. Storage time is much longer in other states.
- Cold-climate: Ambient temperature in winter is significantly low, and annual temperature variation is substantial in Alaska.

Concerning concrete behavior at cold temperatures, Rostásy et al. (1979) showed that the compressive strength and elastic modulus of concrete increased at cold temperatures. Montejo et al. (2008) collected and compared early research. Lee et al. (1988a, 1988b) measured the mechanical properties of normal-strength and high-strength concrete and reported that compressive strength, splitting tensile strength, elastic modulus, and local bond strength increased at cold temperatures. Montejo et al. (2008, 2009) studied reinforced concrete columns under reversed cyclic loading at cold temperatures.

Compared with studies of other mechanical properties, studies of concrete creep and shrinkage at cold temperatures are rare. In general, creep becomes small at cold temperatures. Johansen and Best (1962) used specimens cured for 42 days at 68°F and sealed them to prevent moisture loss during the creep test. They observed that freezing made the initial creep rate high, but the rate dropped to zero quickly. Turner (1980) noticed that creep at cold temperatures was about half the creep at room temperature. Browne and Bamforth (1981) reported a reduction in creep at cold temperatures based on Japanese research.

1.2 Scope of Study

The scope of this research was to select a concrete-embedded strain sensor with the intent of using the sensor in several in-service DBT girders for long-term monitoring of pre-stress losses.

1.3 Research Approach

The research consisted of two tasks: a literature review and a sensor test. In the literature review, information on types of sensors and their durability was compiled and summarized. In addition, information on past and present long-term pre-stress loss monitoring systems was collected and compared. Appendix A is the result of the literature survey.

Vibrating wire strain gauges (VWSG), fiber-optic strain gauges (FOSG), and mechanical sensors for measuring concrete strain are commonly used in pre-stress loss monitoring systems. In the sensor study, sensors were installed in concrete cylinders, and the concrete cylinders were loaded in concrete creep frames and an MTS testing machine at temperatures ranging from 70°F down to -40°F. The performance data and analysis of the sensors are provided in Appendix B.

In Appendix C, pre-stress loss estimations from two provisions, the 2004 AASHTO-LRFD and the 2017 AASHTO-LRFD, are compared. The estimation used details of an actual bridge built by DOT&PF.

[2] Personal communication with an engineer in AggPro in Anchorage, AK.

CHAPTER 2. FINDINGS

2.1 State-of-the-Art Overview

Methods of pre-stress loss estimation can be grouped into three categories: lump-sum estimates, rational approximate methods, and detailed time-dependent analyses. The approximate estimation method (section 5.9.3.3) in the 2017 AASHTO-LRFD and the total-loss method in the *Precast/Prestressed Concrete Institute* (*PCI) Design Handbook* (PCI 2010) are lump-sum estimate methods. The refined estimation method (section 5.9.3.4) in the 2017 AASHTO-LRFD can be classified as a rational approximate method. Detailed time-dependent analyses may be required for special types of bridge construction. Some of these methods are presented in the *PCI Bridge Design Manual* (PCI 2000). In the present research, the following methods are of primary concern:

- 2004 AASHTO Lump-sum method
- 2004 AASHTO Refined method
- 2017 AASHTO Approximate estimation
- 2017 AASHTO Refined estimation

In the 2004 AASHTO-LRFD, pre-stress losses due to concrete creep and shrinkage are determined from the following equations.

$$\Delta f_{pCR} = 12.0 f_{cgp} - 7.0 \Delta f_{cdp} \tag{1}$$

$$\Delta f_{pSR} = 17.0 - 0.15H \tag{2}$$

where f_{cgp} is the concrete stress at the center of gravity of the pre-stressing, Δf_{cdp} is the concrete stress change due to permanent loads, and H is average relative humidity (%).

The *Alaska Bridges and Structures Manual* (DOT&PF 2017) adopted the pre-stress loss provision from the lump-sum method in the 2004 AASHTO-LRFD in Eq. (3). In this equation, the sum of time-dependent pre-stress losses is expressed as a function of concrete strength, $f_c^{'}$.

$$\Delta f_{pLT} = 33\left[1 - 0.15\left(\frac{f_c^{'} - 6}{6}\right)\right] - 2 \quad (ksi) \tag{3}$$

The pre-stress loss provisions in the 2017 AASHTO-LRFD were based on findings in NCHRP Project 18-07 (Tadros et al. 2003). The total pre-stress loss is

$$\Delta f_{pT} = \Delta f_{pES} + \Delta f_{pLT} \tag{4}$$

where Δf_{pES} is the instantaneous loss due to elastic shortening of members, and Δf_{pLT} is the sum of time-dependent losses. For the estimation of time-dependent losses, two methods were provided: approximate estimation and refined estimation methods. The approximate estimation

method was developed for pre-stressed I-beams and inverted tee beams with which a concrete deck was compositely built. Furthermore, it was assumed that the moment from live load was about 1/3 of the total load moments.

In the refined estimation method, the time-dependent loss is calculated from Eq. (5),

$$\Delta f_{pLT} = \left(\Delta f_{pSR} + \Delta f_{pCR} + \Delta f_{pR1}\right)_{id} + \left(\Delta f_{pSD} + \Delta f_{pCD} + \Delta f_{pR2} - \Delta f_{pSS}\right)_{df} \quad (5)$$

where $(\ )_{id}$ indicates the losses occurred between pre-stress transfer and deck placement, $(\ )_{df}$ indicates the losses occurred after deck placement, Δf_{pSR} and Δf_{pSD} are losses due to shrinkage of girder concrete, Δf_{pCR} and Δf_{pCD} are losses due to creep of girder concrete, Δf_{pR1} and Δf_{pR2} are losses due to relaxation of pre-stressing strands, and Δf_{pSS} is the gain due to shrinkage of the deck.

In Appendix C, time-dependent pre-stress losses were calculated from the four methods. The calculations were for the Tulsona Creek Bridge in Alaska. The following are time-dependent pre-stress losses from each method:

- 2004 AASHTO Lump-sum method: 29.8 ksi
- 2004 AASHTO Refined method: 38.9 ksi
- 2017 AASHTO Approximate estimation: 23.2 ksi
- 2017 AASHTO Refined estimation: 23.1 ksi

For the bridge used in the calculation, the approximate method and the refined method in the 2017 AASHTO-LRFD resulted in a similar value. The lump-sum method in the 2004 AASHTO-LRFD estimated about 28% more loss compared with the 2017 AASHTO-LRFD. The estimation from the refined method in the 2004 AASHTO-LRFD was 67% more than that from the 2017 AASHTO-LRFD.

The estimation of pre-stress loss from different methods was also compared in other studies. Garber, Gallardo et al. (2016) compared measured pre-stress losses with estimated losses from different methods as shown in Figure 2-1. The PCI simplified method and the 2004 AASHTO-LRFD were conservative; however, the other methods generated many cases where measured pre-stress losses were significantly larger than estimated losses.

When the 2004 AASHTO-LRFD and the 2007 AASHTO-LRFD were compared, Al-Omaishi, Tadros et al. (2009) used the pre-stress loss measurement of 31 girders in several states (Connecticut, Illinois, Nebraska, Ohio, Pennsylvania, Texas, and Washington). However, the bridges were not distributed well across the states and did not include a significant number of bridges in cold-climate regions. It is interesting to note that measured losses from 5 girders in Washington State (Stanton, Barr et al. 2000) were consistently greater than estimated losses from the 2007 AASHTO-LRFD.

Consequently, it is important to obtain pre-stress loss data that represent the bridge population in Alaska. Monitoring in-situ pre-stresses in bridge girders is a direct way to understand pre-stress losses and develop or verify design provisions.

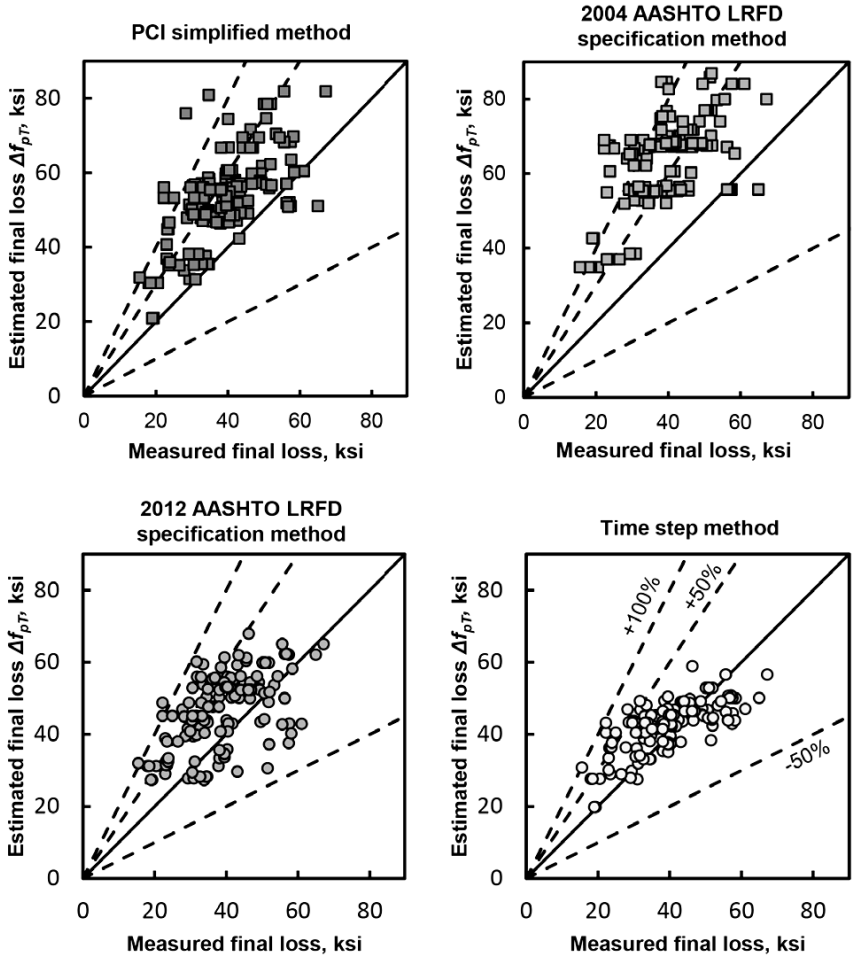

Figure 2-1. Estimated and measured pre-stress losses (Garber, Gallardo et al. 2016) [PCI simplified (PCI 2010), 2004 AASHTO-LRFD specifications (AASHTO 2004), 2012 AASHTO-LRFD specifications (AASHTO 2012), and time step approach (ACI 2014)]

Table 2-1 compares the sensors and data collection systems of a number of in-situ pre-stress loss monitoring systems implemented in other research projects. In most pre-stress loss monitoring systems, VWSG, FOSG, and electrical resistance strain gauges (ERSG) have been used. VWSG is the most widely used sensor type accounting for about 85% (Waldron 2004). Garber, Gallardo et al. (2013) collected 29 studies where pre-stress losses were measured. Among the 140 specimens, monitoring with VWSG (49%) and flexural cracking tests (41%) were most common.

Table 2-1. Comparison of in-situ pre-stress loss monitoring systems

Sensors	Number of sensors	Number of girders monitored	Data acquisition system	Data collection frequency	Reference
VWSG	12 (midspan and near support) 2 (deck over the instrumented girder)	5 girders	5 multiplexers + 1 datalogger	6 hours (monitoring period)	(Barr, Eberhard et al. 2000)
VWSG ERSG	6 VWSG + 1 ERSG (midspan) 4 VWSG + 1 ERSG (near support)	4 girders	1 system with remote access	NA	(Myers and Yang 2004)
VWSG	3 (per each girder)	3 girders (Chickahominy River Bridge); 6 girders (Pinner's Point Bridge);	1 system / site	2 hours	(Waldron 2004)
VWSG + ERSG	3 VWG + 1 ERSG (per girder)	3 girders	1 system	2 hours	
FOSG	2 or 4 (per girder)	6 girders	6 connection boxes + 1 reading unit	6 hours (monitoring period)	(Idriss and Liang 2009)
VWSG	5 (per girder) 7 (in the deck)	4 (at midspan)	1 system with remote access	1 hour (monitoring for 1 year)	(Roller, Russell et al. 2011)
VWSG	3-4 (per girder)	18 (at midspan)	1 system at each site	1 hour	(Garber, Gallardo et al. 2013)
VWSG	3 (per girder)	7 girders	1 system	12 hours (monitoring period)	(Peterman and Holste 2016)
VWSG	86 (total)	6 (2 girders in 3 spans)	2 systems with wireless connection	5 min. (monitoring stage)	(Alghazali and Myers 2017)

NOTE: VWSG: vibrating wire strain gauge; FOSG: fiber optic strain gauge using fiber Bragg grating; ERSG: electrical resistance strain gauge.

Kowalsky, Zia et al. (2002) used plane strain bars, ERSG, and VWSG to measure concrete strain in a high-performance concrete girder in Raleigh, North Carolina. The durability of VWSG proved better than other sensor types. Myers and Yang (2004) noted that strain values from ERSGs became inaccurate after the polymer encasing the ERSG was damaged by heat during

concrete hydration. In some applications, ERSGs were not sufficiently durable or reliable for long-term monitoring.

2.2 Sensor Test Summary

The objective of the sensor study was to observe accuracy and reliability in measured strain from different strain sensors at cold temperatures. The aggregate used in this study is the same as that used by Pre-Cast Concrete (PCC) in Anchorage, a DBT girder fabricator in Alaska. The PCC's concrete mix design for DBT girders was adopted for this study using aggregates from PCC's supplier, thus minimizing differences in strain caused by variances in concrete aggregates.

From the literature review, we chose three vibrating wire strain gauges (VWSG) and a fiber optic strain gauge (FOSG) in the sensor study. They were:

- VWSG-NA: Geokon Concrete Embedded Strain Gauge model 4200 (non-adjustable)
- VWSG-B: Geokon Concrete Embedded Strain Gauge model 4200 (adjustable)
- VWSG-R: Geokon Concrete Embedded Strain Gauge model 4200-6 (adjustable)
- FOSG: Micron Optics Embeddable Strain Sensor os3500

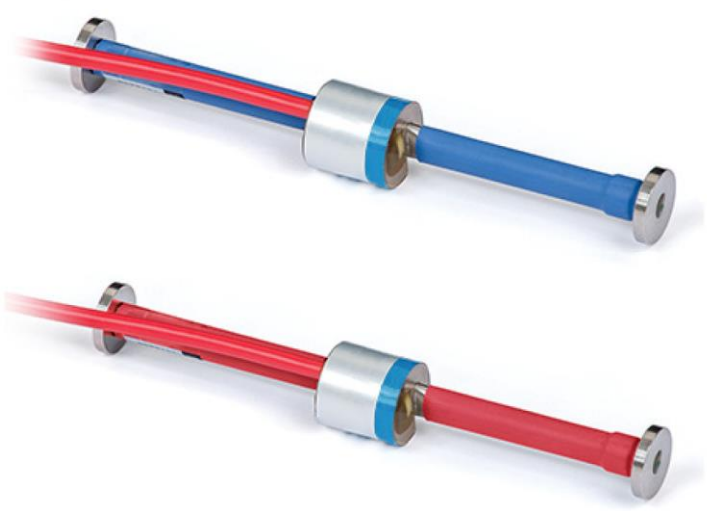

Figure 2-2. Geokon vibrating wire strain gauge (VWSG-B and VWSG-R)

Each strain gauge was embedded in a ϕ6″×12″ concrete cylinder. The strain was monitored as each specimen was loaded with a constant stress. For longer-term tests, specimens were loaded with a hydraulic jack in concrete creep frames. The MTS testing machine was used to load a specimen for shorter-term tests. The details of the test are described in Appendix B. The total strain is the sum of the initial strain (or elastic strain), creep strain, and shrinkage strain. If the temperature changed during the test, the measured strain was the sum of the total strain and thermal strain. The thermal strain can be removed by correcting temperature effects in the measured strain.

Seven concrete batches in Table 2-2 were made to mold ϕ4″×8″ and ϕ6″×12″ cylinders. The ϕ4″×8″ cylinders were used for compressive strength test, and ϕ6″×12″ cylinders were used to measure strain.

Table 2-2. Concrete compressive strength using ϕ4″×8″ cylinders

Batch	Strength when Loaded		28-day strength (psi)	Remark
	Test Age (day)	Strength (psi)		
0125-F	7	7,512	10,992	Measured at -40F
0125-S	5	7,859	9,286 11,149	Loaded at the 9th day Measured at -40F
0405	6	9,255	9,897	Loaded at the 12th day
0514	5	8,771	10,090	
0516	6	8,199	8,708	
0624	4	7,900	9,976	29-day strength
0819	3	7,804	10,958	Loaded at the 5th day

For each batch, the elastic modulus of concrete was measured. Figure 2-3 shows the measured elastic modulus with compressive strength. In addition, the elastic modulus estimated from the AASHTO-LRFD equation, Eq. (6), was compared in the figure.

$$E_c = 120,000 K_1 w_c^{2.0} f_c'^{0.33} \quad (6)$$

where $K_1 = 1.0$ is a correction factor for source of aggregate and $w_c = 0.15 kcf$ is the unit weight of concrete.

The measured modulus was considerably smaller than the calculated values. If $K_1 = 0.8$, measured and calculated moduli became closer. Given that concrete strength has reached the design strength for each batch, the factors that induced small elastic modulus were not clear. The properties of aggregates in concrete, consolidation method, and curing method could be factors. More material tests are required to clarify the causes.

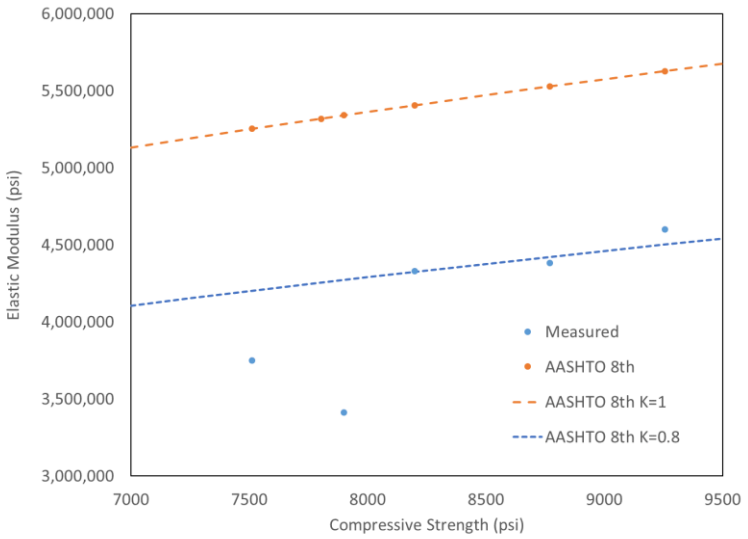

Figure 2-3. Measured elastic modulus vs. estimated modulus

Table 2-3 shows the seven sensor tests conducted in the sensor study. Specimens for the two long-term test types loaded in creep frames to maintain a constant applied stress for the time specified in the table. The long-term tests were conducted at room temperature and at -40°F to compare total strains at these temperatures. The results of the long-term tests were used to eliminate the types of sensors that did not perform satisfactorily.

The temperature dependence test compared strains in two specimens. When they were loaded, one specimen was at 68°F and the other was at -40°F. This test showed the effect of cold temperatures on elastic, creep, and shrinkage strains. The stress dependence test investigated the dependence of strain on the applied stress. The applied stresses on the two specimens were $0.23f_{ci}^{'}$ and $0.72f_{ci}^{'}$. The thermal cycling test investigated the reliability and resilience of VWSG sensors under frequently changing temperature. After the long-term 2 (low temperature) test, several temperature cycles were applied to the same specimens.

The temperature dependence and stress dependence tests were conducted in the MTS testing machine. The ϕ6″×12″ specimens were loaded by the MTS testing machine as the temperature of the specimen was controlled by the environmental chamber that contained the specimen.

Table 2-3. Summary of sensor test types

Test type	Number of specimens	Sensors	Period of Measurement	Test condition	Concrete Batch
Long-term 1 (Room temperature)	2 + 1 (shrinkage)	VWSG-NA, DEMEC	41 days	Room Temperature, Creep Frame	0125-F
Long-term 1 (Low temperature)	2 + 1 (shrinkage)	VWSG-NA, DEMEC	83 days	Cold Room (-40°F), Creep Frame	0125-S
Long-term 2 (Room temperature)	3	VWSG-B, VWSG-R, FOSG, DEMEC	120 days	Room Temperature, Creep Frame	0514
Long-term 2 (Low temperature)	2	VWSG-B, VWSG-R, DEMEC	120 days	Cold Room (-40°F), Creep Frame	0514
Temperature dependence	1	VWSG-NA	7 days	MTS, Environ. Chamber	0405
	1	VWSG-B	26 days	MTS, Environ. Chamber	0819
Stress dependence	1 (53kips)	VWSG-B	15 days	MTS, Environ. Chamber	0516
	1 (160 kips)	VWSG-B	10 days	MTS, Environ. Chamber	0624
Thermal cycling	2	VWSG-B, VWSG-R	30 days	Cold Room, Creep Frame	0514

Figure 2-4 shows the total strain measured from the long-term test 1 (room temperature) where two specimens (0125-F batch), VW3 and VW6, were loaded at 66°F – 72°F. The two specimens were loaded to 3,749 psi on the day when the compressive strength reached 7,512 psi. The ratio of applied stress to strength was 3,749 psi/7,512 psi = 0.50. Another unloaded specimen, VW5 (0125-F batch), was used for shrinkage measurement. The shrinkage strain gradually increased and reached around 450με at the end of the test.

In Figure 2-4, total strain reached the maximum measurement range of the VWSG-NA sensors. The VWSG-NA in VW6 stopped working at 42 days, and the sensor in VW3 stopped at 25 days. For VW6, the total strain at 37 days was 2,312με. The anticipated total strain over 5 years was around 3,000με. Consequently, the VWSG-NA sensor is not appropriate to measure the expected total strain.

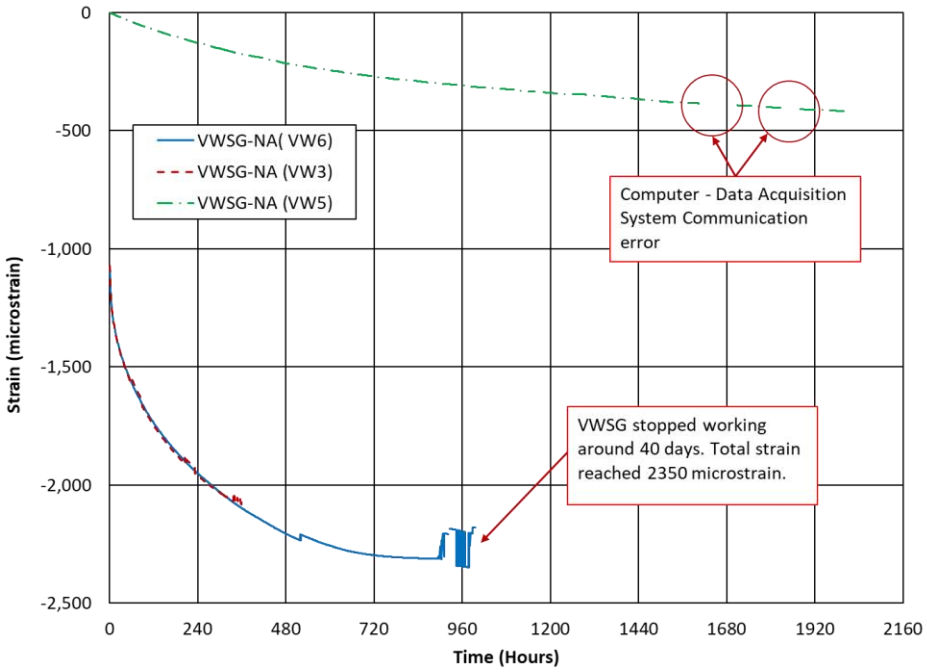

Figure 2-4. Strain measurement from the long-term 1 (room temperature) test

Figure 2-5 shows measured total strain from the long-term test 2 (room temperature). Three ϕ6″×12″ specimens (0514 batch), VWSG-B, VWSG-R, and FOSG, were loaded to 3,537 psi when the concrete strength reached 8,771 psi. The ratio of applied stress to strength was 3,537 psi/8,771 psi = 0.40. The specimens were unloaded and reloaded to check whether the sensors were working properly and to remove the FOSG specimen at 57 days (1,371 hours).

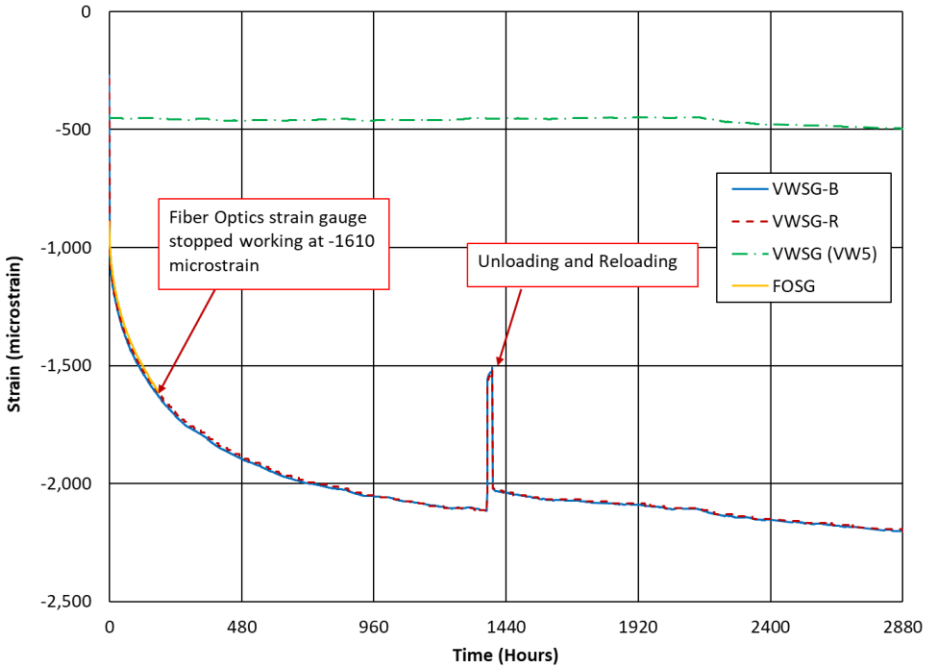

Figure 2-5. Strain measurement from the long-term 2 (room temperature) test

The measured strains from the three specimens were very close. However, the FOSG sensor stopped working at 7.5 days (180 hours) when the total strain reached 1,610με. The initial reading of the FOSG sensor before loading was 788με in compression. The sensor reached its specified measurement range (788+1,610 = 2,398με) when it stopped working. At 120 days, total strain reached 2,223με in the VWSG-B specimen and 2,221με in the VWSG-R specimen. Both VWSG-B and VWSG-R sensors measured total strain for more than 120 days.

Figure 2-6 shows the result from the long-term 2 (low temperature) test where VWSG-B and VWSG-R (0514 batch) were used at cold temperatures. The two specimens were loaded to 3,537 psi when the concrete strength was 8,771 psi. The ratio of applied stress to strength was 3,537 psi/8,771 psi = 0.40. The VW1 specimen from the long-term 1 (low temperature) test was continuously used to measure shrinkage strain. The measured strains decreased and increased as the temperature changed since the measured strain contained thermal strain. Overall, the total strain from VWSG-B and VWSG-R as well as the shrinkage strain from VW1 became infinitesimal at cold temperature.

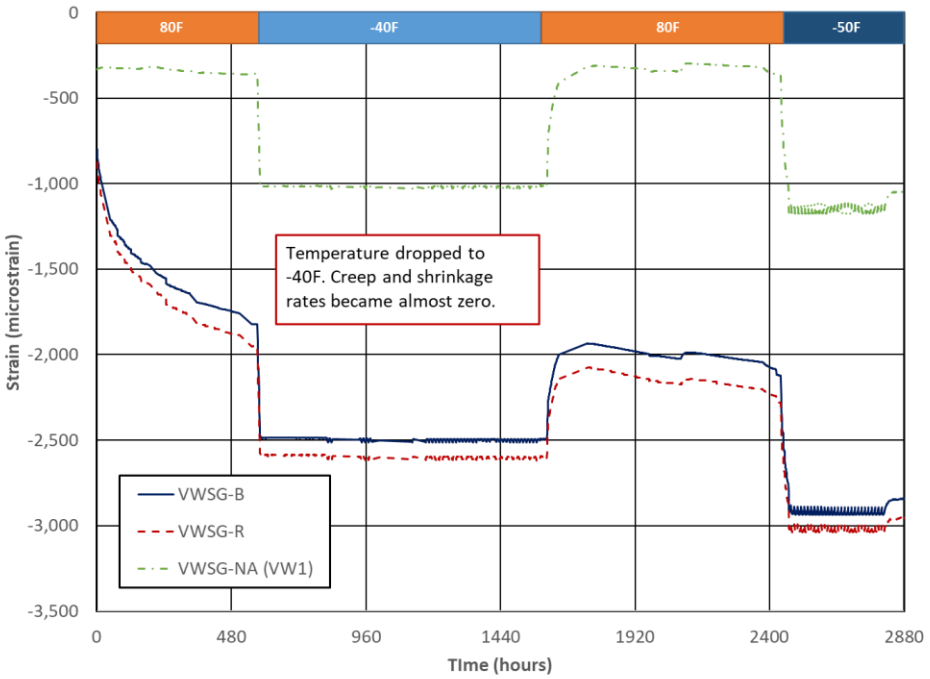

Figure 2-6. Strain measurement from the low-temperature 2 (low temperature) test

Table 2-4 shows the measured strains from two types of sensors, VWSG-B and VWSG-R, at 20 days after loading. Four specimens from both room temperature and low temperature tests in the long-term 2 were used to collect data. All four specimens were prepared with the same aggregate and loaded with the same amount at the same age. The temperature decreased for two specimens in the low-temperature test after 20 days. Therefore, the differences in measured strain were primarily due to the sensors.

Table 2-4. Strains between long-term 2 test (at 20 days)

Sensor	Test	Total (με)	Initial (με)	Shrinkage (με)	Creep (με)	Creep Coefficient
VWSG-R	Room temperature	1,885	841	214	830	0.99
	Low temperature	1,877	792	214	871	1.10
VWSG-B	Room temperature	1,895	874	214	807	0.92
	Low temperature	1,747	735	214	798	1.09

The total strain was separated into initial strain, shrinkage strain, and creep strain in Table 2-4. The initial strain was calculated from the measured elastic modulus and applied stress when specimens were loaded. The shrinkage strain was measured shrinkage strain from VW5 at the same age. Then, creep strain and a creep coefficient were evaluated for each case. The creep coefficient is the ratio of creep strain to initial (elastic) strain. The creep coefficients between the two VWSG-R sensors were closer than those between the VWSG-B sensors. The VWSG-R sensor had a smaller variation between sensors than VWSG-B sensor did.

The creep and shrinkage strains became infinitesimal and the strain did not change in the long-term 2 (low temperature) test at -40ºF. To confirm that this is a characteristic of concrete at cold temperatures, sensors were checked to ensure they were working properly at cold temperatures. Figure 2-7 shows results from the 2nd specimen of the temperature dependence test.

Five stress cycles (354 psi – 3,537 psi) were applied at 264 hours after loading when the temperature was -40°F. The temperature increased to 68°F at 284 hours after loading. Then, five stress cycles (354 psi – 3,537 psi) were applied at 385 hours and 405 hours. During the last two sets of stress cycles, the temperature was 75°F. The change in strain was 568με at -40°F. The change in strain at 75°F were 610με and 604με. The smaller change at -40°F is likely the result of increased stiffness of concrete at cold temperatures. These results indicated the VWSG-B sensor was responsive to the change of stress, and the measured strains were reasonable at cold temperatures.

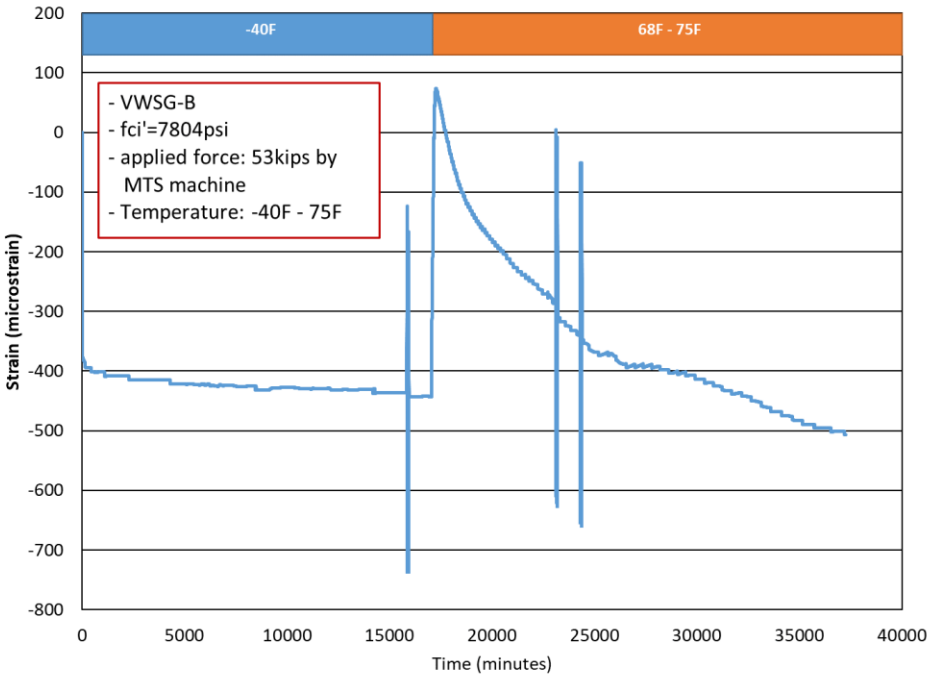

Figure 2-7. Strain measurement from the temperature dependence test (0819 batch)

The performance of VWSG-B and VWSG-R through large temperature changes was tested in the thermal cycling test. Figure 2-8 shows the change of measured strain from the thermal cycling test where the temperature changed between -40°F and 73°F in each cycle. The strain changes during temperature cycles correspond to the thermal strain of concrete. Both VWSG-B and VWSG-R were responsive to the wide temperature change.

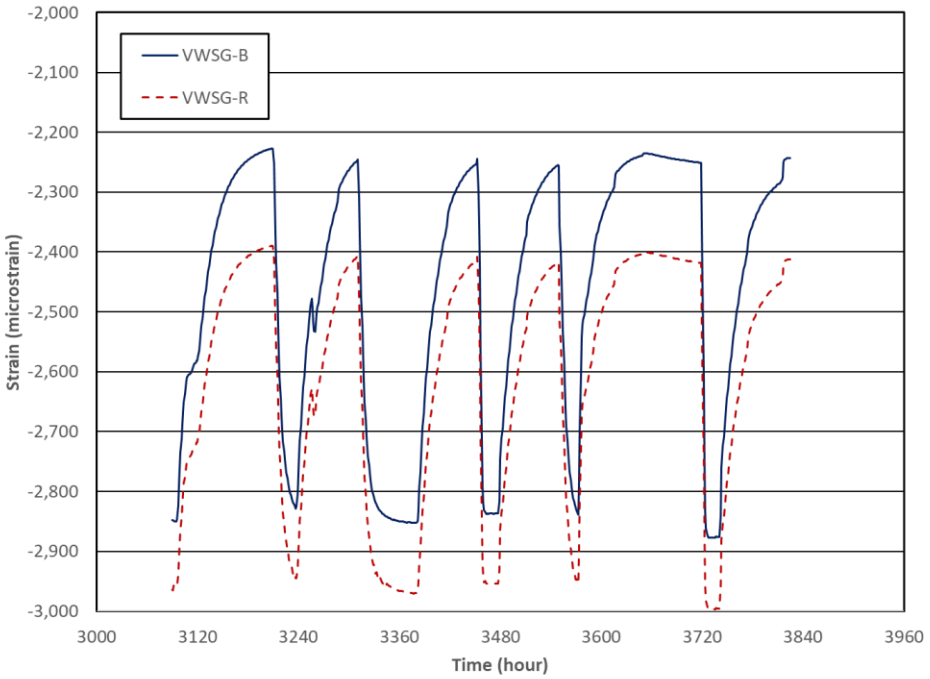

Figure 2-8. Strain measurement from the thermal cycling test

2.3 Concrete Creep and Shrinkage

Among many factors that influence concrete creep and shrinkage, the temperature and applied stress were investigated from test results in Table 2-3. In the temperature dependence test in Table 2-3, temperature was set before applying stress to a specimen. Figure 2-9 shows results from two specimens of which temperature was set to 68°F and -40°F, respectively, before stress was applied. Both specimens were loaded to 1,874 psi in the MTS testing machine. The applied stress ratio to strength was 1,874 psi/8,199 psi = 0.23 and 1,874 psi/7,804 psi = 0.24 for the specimen from the 0516 batch and the 0819 batch, respectively.

Since the applied stress ratios were almost the same between the two specimens, the temperature was the main factor for any difference in the total strain. When a force was applied to the specimen at -40°F, and the force and the temperature were kept unchanged, creep and shrinkage occurred in the specimen as shown in Figure 2-9. Whereas, the total strain did not change at -40°F in the long-term 2 (low temperature) test (Figure 2-6) where the force was first applied at room temperature and the temperature changed to -40°F. This implies that the amount of total strain at cold temperature depends on the history of loading and temperature change.

The initial strain and measured strain of the two specimens in Figure 2-9 at 200 hours (12,000 minutes) are summarized in Table 2-5. The initial strain of the specimen from the 0819 batch was smaller because the elastic modulus increased at cold temperatures. The strain change was also small at cold temperatures. The total strain changed by 52με at -40°F, and the total strain change was 462με at 68°F. The ratio of total strain to the initial strain is much smaller for the specimen at -40°F.

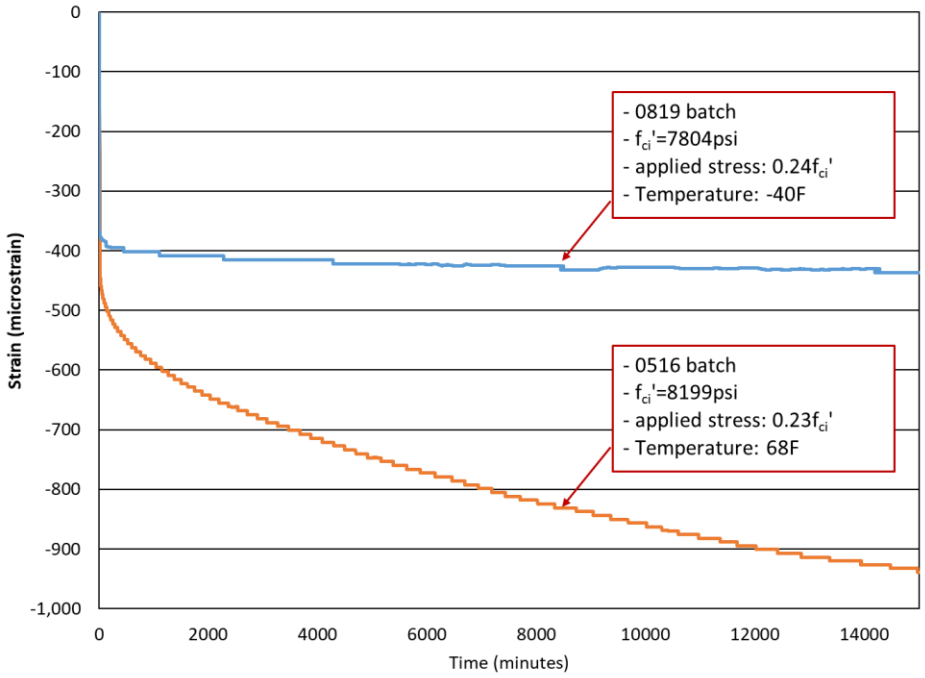

Figure 2-9. Comparison of measured strain (68°F vs. -40°F)

Table 2-5. Strain comparison (68°F vs. -40°F)

Temperature	Initial Strain (με)	200 hours Strain (με)	Ratio
68°F	433	895	2.07
-40°F	377	429	1.14

In the stress dependent test in Table 2-3, applied stress to the two specimens were $0.23f_{ci}^{'}$ and $0.72f_{ci}^{'}$, respectively. Figure 2-10 shows the measured strain of the two specimens at room temperature. In addition, the measured strain of the VWSG-R specimen from the long-term 2 (room temperature) was added. The applied stress to this specimen was $0.40f_{ci}^{'}$.

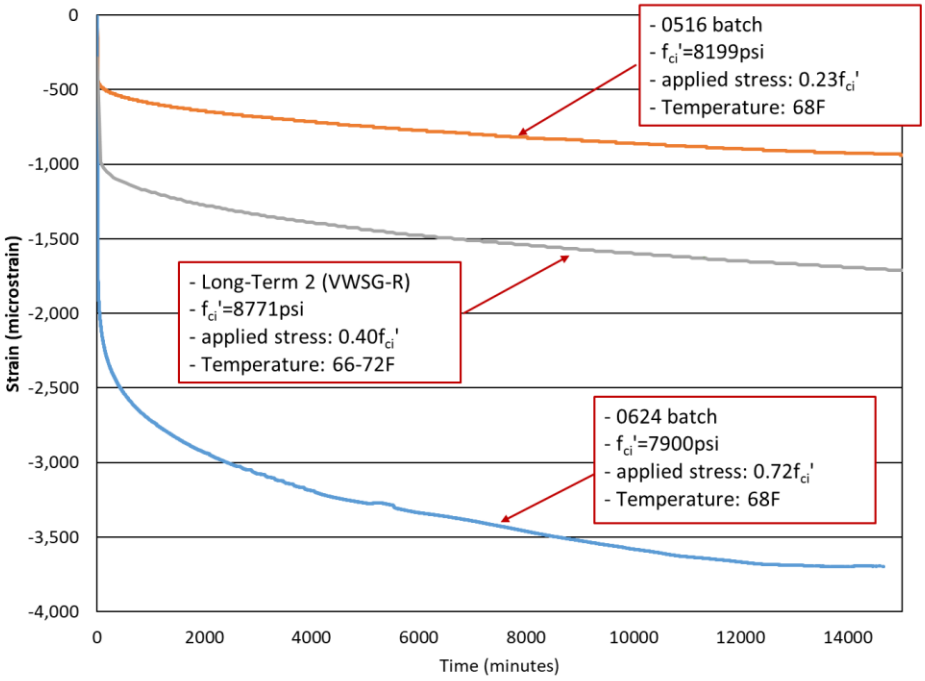

Figure 2-10. Comparison of measured strain ($0.23f_{ci}^{'}$ vs. $0.40f_{ci}^{'}$ vs. $0.72f_{ci}^{'}$)

In Table 2-6, the measured strains from the three specimens at 200 hours (12,000 minutes) are separated into their components. The shrinkage strain was from the VW5 specimen which was used for shrinkage strain measurement in the long-term 1 (room temperature) test. The initial strain of each specimen was calculated from the measured stiffness and applied stress. The creep coefficient at the last column is the ratio of the creep strain to the initial strain. The creep coefficient was in the range of 0.80–0.85 for specimens with an applied stressed below $0.40f_{ci}^{'}$. However, the creep coefficient significantly increased for the specimen stressed to $0.72f_{ci}^{'}$. The increase of creep strain may be related to the small elastic modulus of the concrete used for the

specimen stressed to $0.72f_{ci}^{'}$.[3] However, the trend of having larger creep strain under greater applied stress can be observed. Further, the increase of creep strain was not proportional to the applied stress. The stress at mid-span of a DBT girder is in the range of $0.40f_{ci}^{'}$ - $0.60f_{ci}^{'}$. For example, the stress was $0.54f_{ci}^{'}$ from the example in Appendix C.

Table 2-6. Strain components at 200 hours

Applied stress	Initial strain (με)	Total strain (με)	Shrinkage strain (με)	Creep strain (με)	Creep coefficient
$0.23f_{ci}^{'}$	433	895	111	351	0.81
$0.40f_{ci}^{'}$	841	1,647	111	695	0.83
$0.72f_{ci}^{'}$	1,658	3,668	111	1,899	1.15

Figure 2-11 shows the shrinkage strain measured for 4,500 hours (188 days). An unloaded ϕ6″×12″ specimen (VW5) at room temperature was used from the beginning of the long-term test 1 to the end of the long-term test 2. The shrinkage strain reached its maximum of about 450με at around 120 days.

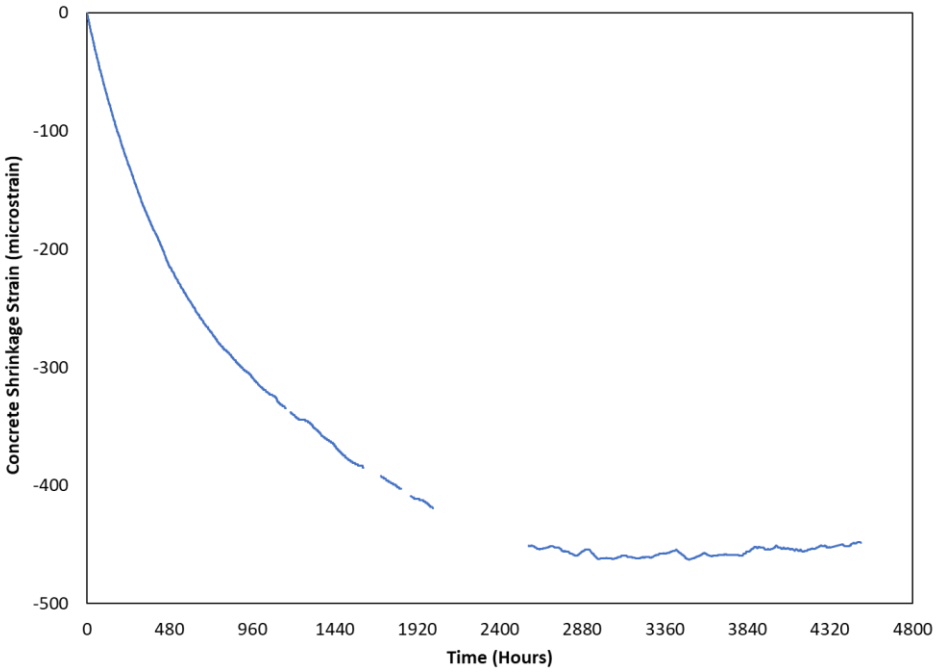

Figure 2-11. Measured shrinkage strain from long-term test

[3] The material properties of concrete used in the test are described in Appendix B.

CHAPTER 3. INTERPRETATION, APPRAISAL, AND APPLICATIONS

3.1 Sensor Selection

Four types of concrete-embedded strain gauge were tested for this project. Table 3-1 summarizes the test results. The major shortcoming of VWSG-NA and FOSG was the measurement range. The initial setting is adjustable for VWSG-B and VWSG-R sensors. In the test, the initial setting of VWSG-B sensors was adjusted to measure compressive strain up to approximately 3,000με. Also, VWSG-R sensors were adjusted to measure a compressive strain of about 4,000με in the test. Both VWSG-B and VWSG-R performed well at room temperature and cold temperature (-40°F) in the long-term tests. In addition, both sensors accurately measured the total strain without apparent deterioration trough five thermal cycles (-40°F ~73°F).

Table 3-1. Strain sensor performance

Sensor	Measurement Range (με)	Initial strain setting	Long-term performance	Low-temperature performance	Thermal cycling performance
VWSG-NA	1,000 – 4,000	Not adjustable	NG	OK	NA
VWSG-B	1,000 – 4,000	Adjustable	OK	OK	OK
VWSG-R	1,000 – 5,000	Adjustable	OK	OK	OK
FOSG	±2500	Not adjustable	NG	NA	NA

In order to predict the total strain over 5 years, the measured strain from the long-term 2 (room temperature) test was used. The red line in Figure 3-1 shows measured strain with an applied stress of $0.40 f_{ci}^{'}$, and a trendline is drawn based on the measured strain. The predicted total strain from the trendline over five years is about 3,000με. Since the strain was measured at room temperature, the actual measured strain can be different. The total strain change will be reduced in the cold weather, while the total strain will increase with greater applied stress (more than $0.40 f_{ci}^{'}$). Further, if the elastic modulus is different from the used specimen (4,206,000 psi), the resulting total strain will also change. Nevertheless, 3,000με is a reasonable amount of strain for sensor selection.

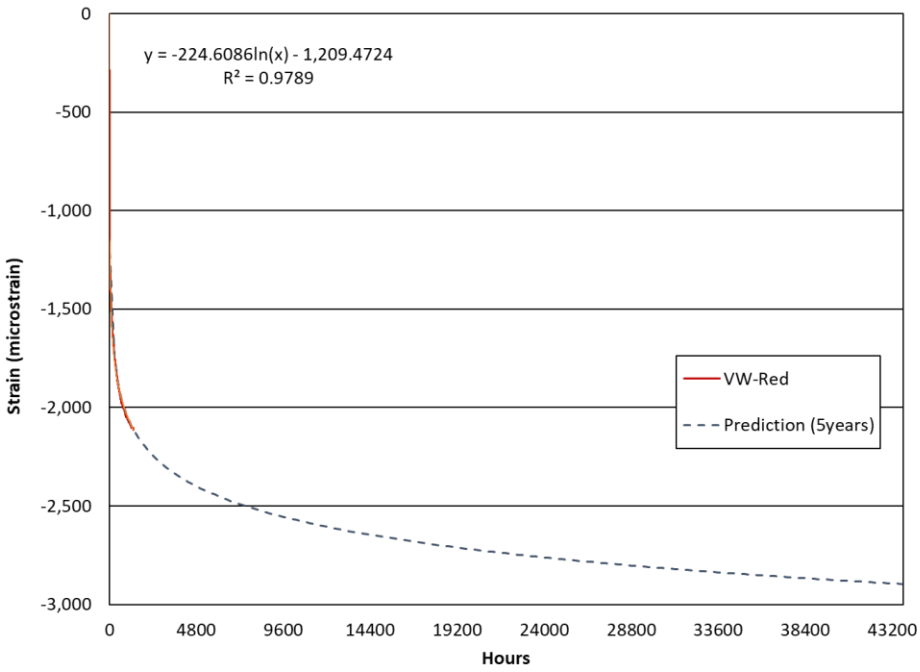

Figure 3-1. Prediction of total strain over 5 years

This anticipated total strain exceeds the manufacturers stated measurement range of VWSG-NA and FOSG sensors. The measurement range of VWSG-B is marginal. The VWSG-R is the only sensor that can reasonably measure the anticipated strain measurement over 5 years. In addition, the VWSG-R sensor is individually calibrated for temperature at the factory. The strain correction of temperature effects is more accurate for the VWSG-R than for the VWSG-B sensor.

3.2 Sensor Installation

When sensors are embedded in a concrete girder, installing sensors in accurate positions and protecting sensors and wires during concrete placement, vibration, and curing are important. Myers and Yang (2004) used a rebar welded cage where a VWSG gauge was tied, as shown in Figure 3-2. The rebar cage was tied to rebar in a girder. The size of rebar in the cage was small and the length was short. Such details minimize the influence of rebar cage in strain measurement.

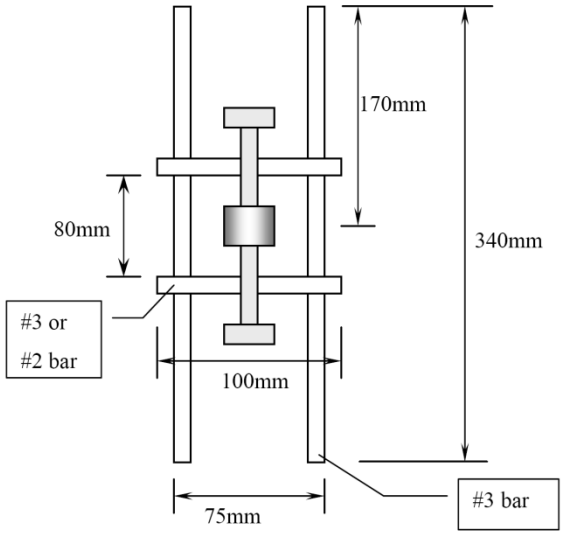

Figure 3-2. Welded grid rebar cage for VWSG (Myers and Yang 2004)

Figure 3-3 shows the anticipated strain sensor location on the cross section of a DBT girder. From sensors, a strain profile over the section is known. Since it is not always possible to place a sensor at the center of gravity of pre-stressing strands (c.g.s.) where the pre-stress losses are evaluated, the strain at the c.g.s. can be calculated from the strain profile. Multiple sensors are required at the bottom and the top flange of a girder to consider shear-lag phenomenon.

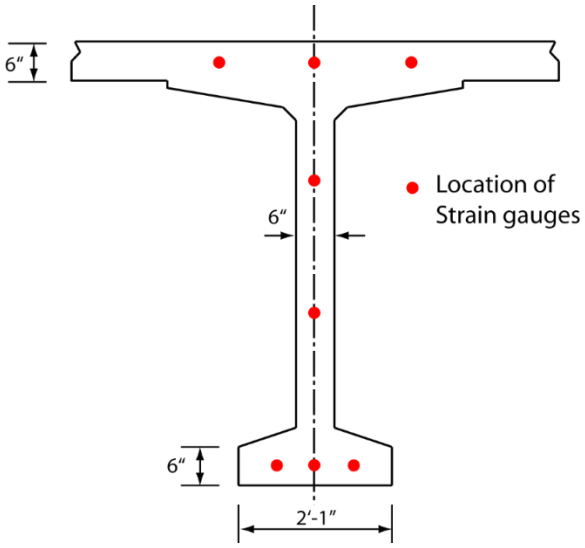

Figure 3-3. Anticipated sensor location on DBT girder cross section

CHAPTER 4. CONCLUSIONS AND SUGGESTED RESEARCH

In the present research, the performance of four concrete-embedded strain sensors was tested. The sensor will be used for measuring the concrete total strain of a DBT girder, to monitor pre-stress losses for at least 5 years. From the literature review, VWSG and FOSG sensors were selected. They have been successfully used in pre-stress loss monitoring systems located in warm- or moderate-climate regions. However, the performance of sensors in cold-climate regions needed to be tested. In addition, concrete creep and shrinkage at cold temperatures were investigated during the sensor study. Specifically, it was observed that concrete creep and shrinkage became infinitesimal at cold temperatures. Therefore, the maximum expected strain change can be measured from specimens at room temperature. The following are conclusions of the research.

- The total strain can reach 3,000 με over 5 years.
- Among the sensors studied in the research, the anticipated total strain exceeds the measurement range of VWSG-NA and FOSG sensors.
- The measurement range of VWSG-B is marginal.
- The measurement range of VWSG-R (5,000 με) is wide enough for the anticipated strain change.
- VWSG-B and VWSG-R were responsive to the wide change of temperature. After applying five thermal cycles (-40°F ~73°F), VWSG-B and VWSG-R accurately measured the strain without indicating deterioration from the cold temperatures.
- The VWSG-R sensor is individually calibrated for temperature at the factory. The strain correction of temperature effects is more accurate for the VWSG-R than for the VWSG-B sensor.

The research concluded that the VWSG-R sensor is sufficient for use in long-term, pre-stress loss monitoring.

As suggested research, concrete material tests to measure elastic modulus are needed. The research showed that the elastic modulus of concrete was smaller than estimates based on the AASHTO-LRFD equation. Since the same cement and aggregates were used in the research, the factors that induce small elastic modulus could be aggregates themselves, consolidation method, and curing method. We recommend a comparison of the elastic modulus of steam-cured specimens, moisture-cured specimens, and ambient cured specimens consolidated with different methods.

REFERENCES

AASHTO (2004). *AASHTO LRFD Bridge Design Specifications (3rd ed.)*, American Association of State Highway and Transportation Officials.

AASHTO (2007). *AASHTO LRFD Bridge Design Specifications (4th ed.)*, American Association of State Highway and Transportation Officials.

AASHTO (2012). *AASHTO LRFD Bridge Design Specifications (6th ed.)*, American Association of State Highway and Transportation Officials.

AASHTO (2017). *AASHTO LRFD Bridge Design Specifications (8th ed.)*, American Association of State Highway and Transportation Officials.

ACI (2005). *Report on Factors Affecting Shrinkage and Creep of Hardened Concrete (ACI 209.1R-05)*, American Concrete Institute.

ACI (2008). *Guide for Modeling and Calculating Shrinkage and Creep in Hardened Concrete (ACI 209.2R-08)*, American Concrete Institute.

ACI (2014). *Guide to Estimating Prestress Loss (ACI Committee 423)*. Farmington Hills, MI, American Concrete Institute.

Al-Omaishi, N., M. K. Tadros and S. J. Seguirant (2009). Estimating prestress loss in pretensioned, high-strength concrete members. *PCI Journal* **54**(4): 132-159.

Alaywan, W. (2011). *Long-Term Monitoring of the HPC Charenton Canal Bridge*. L. T. R. Center.

Alghazali, H. H. and J. J. Myers (2017). Time-dependent prestress loss behavior of girders in Missouri bridge A7957 compared with a U.S. data set of high performance concrete bridge girders. *PCI Journal* **62**(6): 76-87.

Angomas, F. B. (2009). *Behavior of Prestressed Concrete Bridge Girders*. MS Thesis, UTAH State University.

ASTM (2014). *C469/C469M-14: Standard Test Method for Static Modulus of Elasticity and Poisson's Ratio of Concrete in Compression*. West Conshohocken, PA, ASTM International.

ASTM (2016). *C192/C192M-16a: Standard Practice for Making and Curing Concrete Test Specimens in the Laboratory*. West Conshohocken, PA, ASTM International.

Barr, P. J., M. O. Eberhard, J. F. Stanton, B. Khaleghi and J. C. Hsieh. (2000). *High Performance Concrete in Washington State SR 18/SR 516 Overcrossing: Final Report on Girder Minitoring*.

Berner, D., J. B.C. Gerwick and M. Polivka (1985). Static and Cyclic Behavior of Structural Lightweight Concrete at Cryogenic Temperature. *Temperature Effects on Concrete*. ASTM STP 85. T. R. Naik. Philadelphia, American Society for Testing and Materials**:** 21-37.

Brewe, J. E. and J. J. Myers (2010). High-strength self consolidating concrete girders subjected to elevated compressive fiber stresses, part 1: Prestress loss and camber behavior. *PCI Journal*(Fall): 59-77.

Brewe, J. E., J. J. Myers and J. Myers (2008). Prestress Loas Behavior of High-Strength Self-Consolidating Concrete Girders Subjected to Elevated Compressive Fiber Stresses. *National Bridge Conference*.

Browne, R. D. and P. B. Bamforth (1981). The use of concrete for cryogenic storage: a summary of research, past and present. *Cryogenic concrete: proceedings of the 1st international conference*, The Concrete Society**:** 135–166.

Collins, M.P. and D. Mitchell (1997). *Prestressed Concrete Structures*. Response Publications.

Daugherty, L. and E. Marx (2014). Alaska: Concrete bridges in extreme and remote environments. *ASPIRE***:** 34-35.

DeRosa, D., N. A. Hoult and M. F. Green (2015). Effects of varying temperature on the performance of reinforced concrete. *Materials and Structures* **48**: 1109–1123.

DOT&PF (2017). *Alaska Bridges and Structures Manual*, Alaska Department of Transportation and Public Facilities.

Elices, M. (1987). Cryogenic prestressed concrete: Fracture aspects. *Theoretical and Applied Fracture Mechanics* **7**: 51-63.

Garber, D., J. Gallardo, D. Deschenes, D. Dunkman and O. Bayrak (2013). *Effect of New Prestress Loss Estimates on Pretensioned Concrete Bridge Girder Design (FHWA/TX-12/0-6374-2)*, Center for Transportation Research, The University of Texas at Austin; Texas Department of Transportation.

Garber, D. B., J. M. Gallardo, D. J. Deschenes and O. Bayrak (2016). Prestress loss calculations: Another perspective. *PCI Journal*(May-June): 68-85.

Hale, W. M. and B. W. Russell (2006). Effect of allowable compressive stress at release on prestress losses and on the performance of precast, prestressed concrete bridge girders. *PCI Journal*(March-April).

Holland, R. B., J. Dunbeck, J.-H. Lee, L. F. Kahn and K. E. Kurtis (2011). *Evaluation of a Highway Bridge Constructed Using High Strength Lightweight Concrete Bridge Girders*. Georgia Department of Transportation.

Holste, J., R. J. Peterman and A. Esmaeily (2014). Evaluation and Long-Term Monitoring of the Time-Dependent Characteristics of Self-Consolidating Concrete in an Instrumented Kansas Prestressed Concrete Bridge. Kansas Department of Transportation.

Huynh, T.-C. and J.-T. Kim (2017). FOS-Based Prestress Force Monitoring and Temperature Effect Estimation in Unbonded Tendons of PSC Girders. *Journal of Aerospace Engineering* **30**(2).

Idriss, R. and Z. Liang (2009). *Monitoring Of An Interstate-25 High Performance Concrete Bridge With An Embedded Optical Fiber Sensor System*. New Mexico Department of Transportation.

Johansen, R. and C. H. Best (1962). Creep of concrete with and without ice in the system. *RILEM Bulletin*. **16:** 47-57.

Kogbara, R. B., S. R. Iyengar, Z. C. Grasley, E. A. Masad and D. G. Zollinger (2013). A review of concrete properties at cryogenic temperatures: Towards direct LNG containment. *Construction and Building Materials* **47**: 760-770.

Kowalsky, M. J., P. Zia, M. C. Wagner and B. A. Warren (2002). *The Behavior of Prestressed High Performance Concrete Bridge Girders for US Highway 401 over the Neuse River in Raleigh, NC*, North Carolina Department of Transportation; North Carolina State University, Raleigh.

Kukay, B., P. J. Barr and M. W. Halling (2007). A Comparison of Time Dependent Prestress Losses in a Two-Span, Prestressed Concrete Bridge. *2007 Structures Congress: New Horizons and Better Practices*. Long Beach, California.

Lee, G. C., T. S. Shih and K. C. Chang (1988a). Mechanical properties of concrete at low temperature. *Journal of Cold Regions Engineering-ASCE* **2**(1): 13-24.

Lee, G. C., T. S. Shih and K. C. Chang (1988b). Mechanical properties of high-strength concrete at low temperature. *Journal of Cold Regions Engineering-ASCE* **2**(4): 169-178.

Lewis, M. and V. M. Karbhari (2006). *Experimental Verification of the Influence of Time-Dependent Material Properties on Long-Term Bridge Characteristics*. California Department of Transportation.

Menn, C. (1986). *Prestressed Concrete Bridges*. Birkhäuser.

Mertol, H. C., S. Rizkalla, P. Zia and A. Mirmiran (2010). Creep and shrinkage behavior of high-strength concrete and minimum reinforcement ratio for bridge columns. *PCI Journal*(summer): 138-154.

Miura, T. (1989). The properties of concrete at very low temperatures. *Materials and Structures* **22**: 243-254.

Montejo, L. A., M. J. Kowalsky and T. Hassan (2009). Seismic Behavior of Flexural Dominated Reinforced Concrete Bridge Columns at Low Temperatures. *Journal of Cold Regions Engineering-ASCE* **23**(1): 18-42.

Montejo, L. A., J. E. Sloan, M. J. Kowalsky and T. Hassan (2008). Cyclic Response of Reinforced Concrete Members at Low Temperatures. *Journal of Cold Regions Engineering-ASCE* **22**(3): 79-102.

Myers, J. J. and Y. Yang (2004). *HIGH PERFORMANCE CONCRETE FOR BRIDGE A6130-ROUTE 412, PEMISCOT COUNTY, MO*. Missouri Department of Transportation.

Neville, A. M. (2011). *Properties of concrete (5th ed)*, Pearson.

O'Neill, C. R. and C. E. W. French (2012). *Validation of Prestressed Concrete I-Beam Deflection and Camber Estimates*. Minnesota Department of Transportation.

Oesterle, R. G., A. F. Elremaily, Z. J. Ma, R. Eriksson and C. Prussack (2009). *Design and Construction Guidelines for Long-Span Decked Precast, Prestressed Concrete Girder Bridges (Final Report, NCHRP Project 12-69)*, National Cooperative Highway Research Program; Transportation Research Board.

Park, R. and T. Paulay (1975) *Reinforced Concrete Structures*. John Wiley and Sons.

PCI (2000). *Precast Prestressed Concrete Bridge Design Manual*. Chicago, IL, PCI.

PCI (2010). *PCI Design Handbook: Precast and Prestressed Concrete. MNL-120 (7th ed.)*. Chicago, IL, Precast/Prestressed Concrete Institute.

PCI (2014). *Chapter 6. Preliminary Design. Bridge Design Manual (3rd Ed. Second Release)*, Precast/Prestressed Concrete Institute.

Persson, B. S. M. (1999). Shrinkage of High-performance Concrete. *Autogenous Shrinkage of Concrete*. E.-i. Tazawa, Taylor & Francis.

Peterman, R. J. and J. R. Holste (2016). *Long-Term Monitoring of a Pretensioned Concrete Bridge Near Winfield, Kansas*. Kansas Department of Transportation.

Rizkalla, S., P. Zia and T. Storm (2011). *Predicting Camber, Deflection, and Prestress Losses in Prestressed Concrete Members*. North Carolina Department of Transportation.

Roller, J. J., H. G. Russell, R. N. Bruce and W. R. Alaywan (2011). Evaluation of prestress losses in high-strength concrete bulb-tee girders for the Rigolets Pass Bridge. *PCI Journal* **56**(1): 110-134.

Rosa, M. A., J. F. Stanton and M. O. Eberhard (2007). *Improving Predictions for Camber in Precast, Prestressed Concrete Bridge Girders*. Washington State Department of Transportation.

Rostásy, F. S., U. Schneider and G. Wiedemann (1979). Behaviour of mortar and concrete at extremely low temperatures. *CEMENT and CONCRETE RESEARCH* **9**(3): 365-376.

Rüsch, H. (1960). Researches Toward a General Flexural Theory for Structural Concrete. *ACI-Journal Proceedings* 57(7): p. 1-28.

Stanton, J. F., P. J. Barr and M. O. Eberhard (2000). *Behavior of High-Strength HPC Bridge Girders (Preliminary review paper)*. Seattle, WA, University of Washington.

Tadros, M. K., N. Al-Omashi, S. J. Seguirant and J. G. Gallt (2003). *Prestress Losses in Pretensioned High-Strength Concrete Bridge Girders (NCHRP Report 496)*. Washington, D.C., Transportation Research Board.

Tazawa, E.-i. (1999). *Autogenous Shrinkage of Concrete*, Taylor & Francis.

Turner, F. H. (1980). Concrete and Cryogenics – Part 1. *Concrete* **14**(5): 29–40.

Waldron, C. J. (2004). *Investigation of Long-term Prestress Lossed in Pretensioned High Performance Concrete Girders*. Ph.D., Virginia Polytechnic Institute and State University.

Webb, G. T., P. J. Vardanega and N. A. Hoult (2017). Analysis of Fiber-Optic Strain-Monitoring Data from a Prestressed Concrete Bridge. *Journal of Bridge Engineering* **22**(5).

Xie, J., X. Chen, J.-B. Yan, G. Lei and L. Zhu (2017). Ultimate strength behavior of prestressed concrete beams at cryogenic temperatures. *Materials and Structures* **50**: 81.

APPENDIX A.

LITERATURE REVIEW

A.1 Introduction

Among numerous types of precast, pre-stressed concrete girders, Decked Bulb-Tee (DBT) girders are widely used in Alaska to accelerate bridge construction since the climate conditions shorten the construction season. The DBT girder is a precast, pre-stressed concrete, bulb-tee girder with the deck that is cast monolithically and pre-stressed with the girder (Oesterle, Elremaily et al. 2009, PCI 2014). Figure A-1 shows the standard cross-section of Alaska-style DBT girders, where the deck width can reach 8.5 feet (DOT&PF 2017). After the erection of DBT girders at construction site, bridge deck is finished by connecting wide top flanges of the girders with welded shear tab connections spaced at a 4-ft interval and filling longitudinal keyways with high-strength grout. Employing DBT girders eliminates the need to form, cast, and cure a conventional cast-in-place concrete deck, which greatly accelerates the superstructure construction (Daugherty and Marx 2014). About 80% of recently constructed bridges with spans up to 145 feet are of the DBT girder type (DOT&PF 2017).

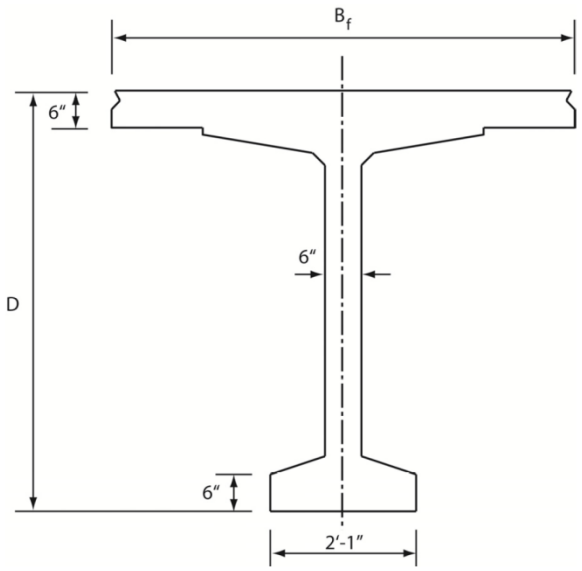

Figure A-1. Standard Alaska-Style Precast DBT girder section (DOT&PF 2017)

In the design of DBT girders, the amount of pre-stress is one of the deciding factors that determine the short-term and long-term concrete stress in the girder. The pre-stress applied to a bridge girder counteracts the dead and live loads, in order to keep the tensile stress of the girder (i.e., the bottom flange) less than a specified tensile stress limit in the design (e.g., zero tension under Service Load Combination III). Meanwhile, the magnitude of pre-stress force in a girder decreases over time; from the fabrication of a girder to the end of the bridge's service life. The amount of pre-stress change, or pre-stress loss, should be well-known for girder design to assure the serviceability and safety of the bridge over the structure's life.

If the pre-stress loss is underestimated, the concrete of a girder at midspan may experience the tensile stresses that exceed the bottom flange tension limit of concrete, which can compromise the durability and long-term performance of the girder. If the pre-stress loss is overestimated, however, more pre-stressing strands will be required than necessary, which may increase the cost of girder fabrication, reduce the maximum span length, or increase the number of girders. The accurate estimation of pre-stress losses, therefore, is essential in the design process. While this subject has been long studied by many researchers, it is hard to find research focused on DBT girders. Specifically, in-situ measurement of pre-stress loss data for DBT girders over a long period of time is extremely rare or does not exist.

The *AASHTO LRFD Bridge Design Specifications* or AASHTO-LRFD (AASHTO 2017) provides guidance for the calculation of pre-stress losses in precast concrete girders using either simplified or refined calculation method. The changes in pre-stress loss provisions adopted in AASHTO-LRFD (2007) result in inconsistent pre-stress loss predictions for DBT girders used by DOT&PF. Specifically, pre-stress losses from the simplified calculation procedure are much less than those from the previous versions of the AASHTO-LRFD (2004) and are less than those calculated from the refined method. As a result, the *Alaska Bridges and Structures Manual* (DOT&PF 2017) was mainly based on the 6th edition of the AASHTO-LRFD (2012), but provisions for the estimation of time-dependent pre-stress losses for DBT girders were adopted from an earlier edition of the AASHTO-LRFD (2004).

It is necessary to update the pre-stress loss provisions for DBT girders. In the process of revising the provisions, field-measured data are required to resolve the discrepancy between the simplified and refined methods and to develop design provisions that can be properly applied to DBT girders. In addition, the field-measured data make it possible to better understand pre-stress losses that may be related to Alaska specific issues. In Alaska, long-term pre-stress losses can be quite different from those in other states for the following reasons.

- Different aggregate: the influence of different aggregate on the elastic modulus and creep coefficient of concrete was noted in Tadros, Al-Omashi et al. (2003).
- Few DBT girder fabricators in Alaska: there have been only three fabricators, with most of the work performed by one fabricator in Anchorage; so the material quality and workmanship can be relatively uniform among girders.
- Shorter time between fabrication and placement of girders: typically the time period in a storage yard is 60 days[1] in Alaska. Storage time is much longer in other states.
- Cold climates and extreme annual temperature variation in Alaska.

[1] From a DBT girder fabricator in AggPro in Anchorage, AK. Girders have been known to be placed two weeks after being cast while others sit in storage through the winter.

A.2 Pre-stress Loss Provisions

The total pre-stress loss is conveniently separated into two groups: (1) instantaneous losses and (2) long-term time-dependent losses (AASHTO 2017). Losses due to anchorage set, friction, and elastic shortening are grouped as an instantaneous loss; losses due to concrete creep, concrete shrinkage, and relaxation of pre-stressing strands are classified as time-dependent losses. Figure A-2 demonstrates the change in pre-stress force that occurs during bridge construction activities.

- A – C: Pre-stress loss due to pre-stressing bed anchorage seating, relaxation between initial tensioning and transfer, and temperature change in strand embedded in concrete. The losses from the bed anchorage seating (A – B) are not present in either pre-stressing strands or concrete for pre-tensioned girders.
- C – D: Instantaneous pre-stress loss at transfer due to elastic deformation and self weight.
- D – E and F – G: Time-dependent pre-stress loss due to shrinkage and creep of girder concrete and relaxation of pre-stressing strands.
- E – F: Increasing tensile stress due to superimposed dead loads (SIDL).

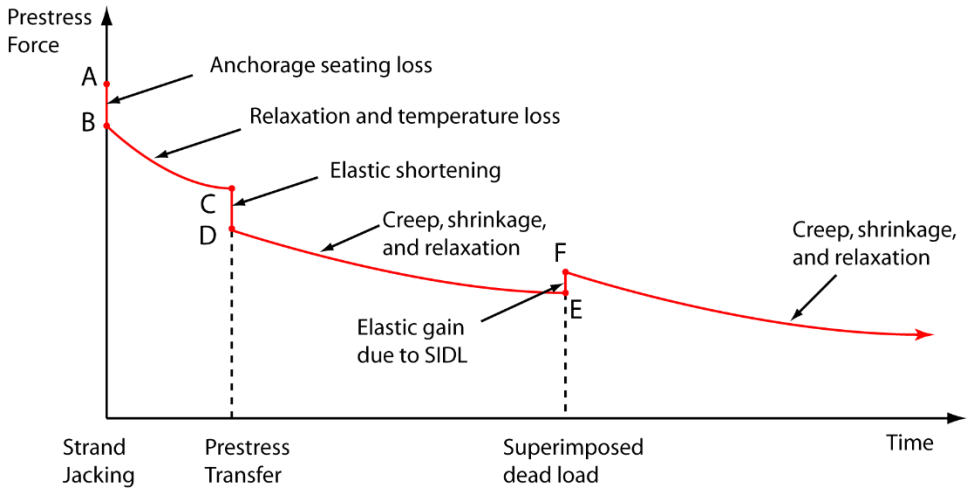

Figure A-2. Pre-stressing strand force changes with time [modified from Tadros, Al-Omashi et al. (2003) to represent DBT girders]

At transfer, compressive stresses are imposed to the concrete. In the current AASHTO-LRFD (AASHTO 2017), the maximum allowable compressive stress at pre-stress transfer is $0.65 f_{ci}^{'}$ where $f_{ci}^{'}$ is concrete strength at transfer[2]. Figure A-3 shows corresponding compressive stress changes at the bottom fiber concrete (tension side when subject to gravity loads) of a girder. When superimposed dead loads (SIDL) are placed, tensile stress increases both in the pre-

[2] This revision was made in 2016 Interim

stressing strands and the concrete. This induces stress "gain" in the pre-stressing strands (see Figure A-2) and additional tensile stress at the bottom of the girder (see Figure A-3). The tension side of the girder experiences only an increase in tensile stress and pre-stress "gains" do not equate to a reduction in pre-stress losses over time.

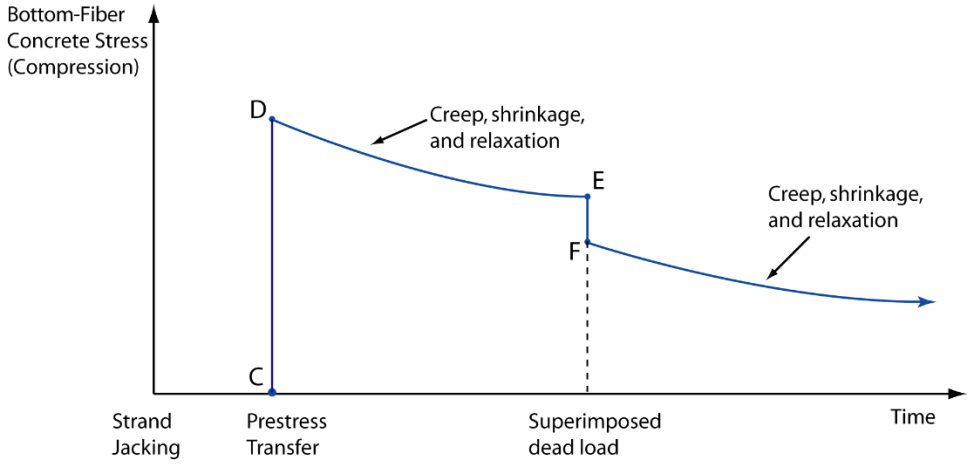

Figure A-3. Bottom-fiber compressive stress changes [modified from Garber, Gallardo et al. (2013) to represent DBT girders]

Concrete shrinkage, concrete creep, and relaxation of pre-stressing strands are three major mechanisms contributing to time-dependent pre-stress losses. Among them, pre-stress loss due to creep is the most significant. For instance, the percentages of pre-stress losses due to creep, shrinkage, and relaxation to the total time-dependent losses were 68%, 24%, and 8%, respectively, for two example bridges in Tadros et al. (2003) and Roller et al. (2011). Due to creep, concrete strain under a constant stress increases with time. This occurs because the elastic modulus of the concrete under a constant stress decreases with time.

Figure A-4 shows the concrete stress-strain relationships that depend on the rate of loading (Rüsch 1960). When hardened concrete cylinders were loaded with a slow rate of loading (longer than 1 hour), the strength of concrete decreased compared to the strength observed from a loading occurring in minutes, which is typical for a concrete cylinder test. Collins and Mitchell (1997) reported that the strength reduction was about 20% of the 28-day strength. Also, concrete typically gains 20 to 40% in strength due to continuing hydration. These two phenomena compensate for each other, resulting in a conservative assumption on the 28-day concrete strength, so the strength reduction caused by long-term loading was not considered in the design (Collins and Mitchell 1997).

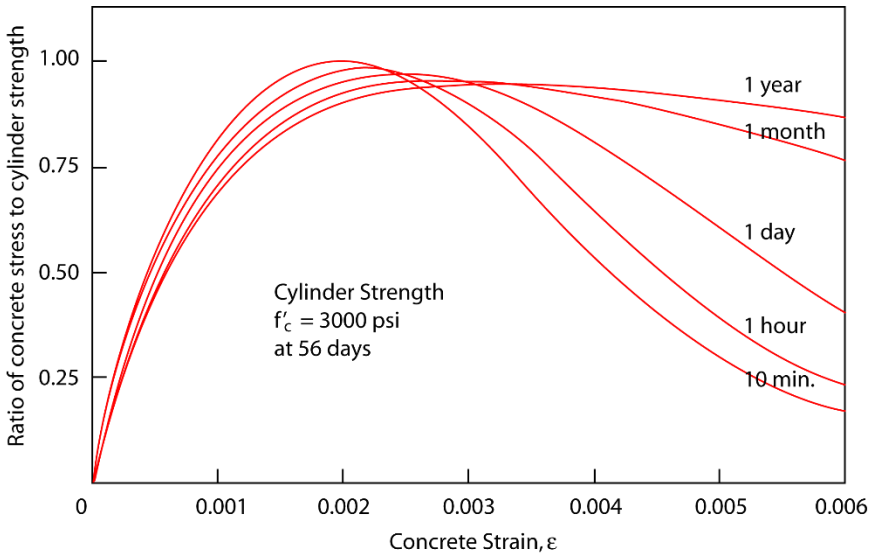

Figure A-4. Stress-strain relationships for eccentric compression after various durations of loading at constant strain rates (Rüsch 1960)

Figure A-5 demonstrates concrete creep in stress-strain relationships (Rüsch 1960). When a stress is applied to a concrete cylinder with a rate of $t = 20\,\text{min}.$ and held constant for a long time, the strain increases as the stress-strain relationship changes with time. Theoretically, the creep stops as the strain reaches the creep limit, a stress-strain relationship for a load with a rate of $t = \infty$. For estimating concrete creep, therefore, the stress-strain relationship of concrete at different ages and under different stress histories should be known.

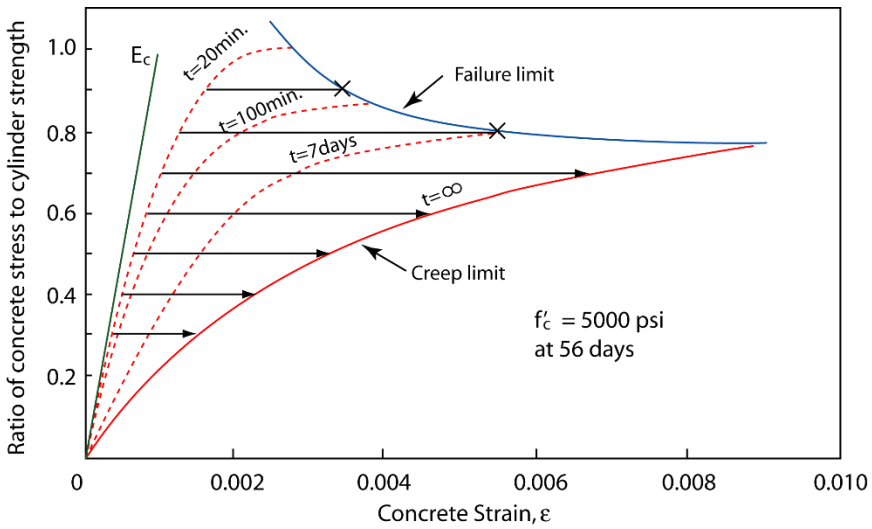

Figure A-5. Influence of load intensity and duration on concrete strain (Rüsch 1960)

The creep deformation of concrete with time under constant axial compressive stress is illustrated in Figure A-6 (Park and Paulay 1975). The creep would proceed at a decreasing rate with time. If the load is removed, the elastic strain is immediately recovered. However, the

elastic recovery is less than the initial elastic strain, because the elastic modulus of concrete increases with age[3]. The creep strain occurring over a given period of time is proportional to the applied stress if the stress level is not high. For the usual range of concrete stress used in structural design, the assumption of a linear relationship between creep strain and applied stress is acceptable.

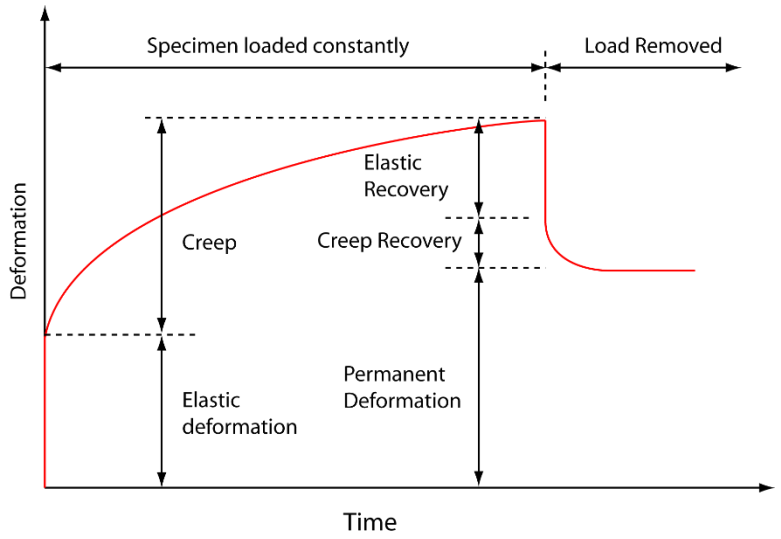

Figure A-6. Typical creep curve for concrete with constant axial compressive stress (Park and Paulay 1975)

The stress-strain relationship of concrete can be represented by various models, and a linear elastic relationship in Eq. (A-1) can be used if the stress is low, $f_c < 0.6 f_c^{'}$ (Collins and Mitchell 1997).

$$f_c = E_c \varepsilon_{cf} \tag{A-1}$$

where f_c is the concrete stress, $f_c^{'}$ is the maximum stress (strength), ε_{cf} is the concrete strain caused by f_c, and E_c is the tangent modulus when $\varepsilon_{cf} = 0$. In AASHTO-LRFD (AASHTO 2017), Eq. (A-2) is used for the estimation of E_c.

$$E_c = 120{,}000 K_1 w_c^{2.0} \left(f_c^{'} \right)^{0.33} \qquad (ksi) \tag{A-2}$$

where K_1 is a correction factor for source of aggregate. The difference between this secant modulus and the tangent modulus is negligible for the concrete used in typical pre-stressed concrete (Collins and Mitchell 1997).

[3] After the start of concrete hardening, the stress-strain relationship under short-term loading is different from the stress-strain relationship under long-term loading for the same concrete.

The total concrete strain due to a sustained stress $f_{c,long}$ can be expressed as the sum of an elastic strain $\varepsilon_{c,el}$ and a creep strain $\varepsilon_{c,c}$:

$$\varepsilon_{c,long} = \varepsilon_{c,el} + \varepsilon_{c,c} = \varepsilon_{c,el} + \phi(t,\tau)\varepsilon_{c,el} = \frac{f_{c,long}}{E_c}\left[1+\phi(t,\tau)\right] \tag{A-3}$$

where $\phi(t,\tau)$ is a creep function, t is the age of the concrete, and τ is the age when the stress $f_{c,long}$ is applied. The creep function can be expressed as (Menn 1986):

$$\phi(t,\tau) = \phi_n k(\bar{\tau}) f(t-\tau) \tag{A-4}$$

where ϕ_n is the creep coefficient that depends on material properties and environmental conditions, $k(\bar{\tau})$ is a correction factor for the age of concrete at time of loading, and $f(t-\tau)$ describes the time-varying behavior of creep and depends on an effective thickness parameter.

The pre-stress loss provisions in AASHTO-LRFD (AASHTO 2017) were based on findings in NCHRP Project 18-07 (Tadros et al. 2003). The total pre-stress loss is:

$$\Delta f_{pT} = \Delta f_{pES} + \Delta f_{pLT} \tag{A-5}$$

where Δf_{pES} is the instantaneous loss due to elastic shortening in members and Δf_{pLT} is the sum of time-dependent losses. For the estimation of the time-dependent losses, two methods were provided: approximate estimation and refined estimation methods. The approximate estimation method was developed for pre-stressed, I-beams and inverted tee beams with which a concrete deck was compositely built. Furthermore, it was assumed that moment from live load was about 1/3 of the total load moments. Therefore, the application of the approximate estimation method to DBT girders is questionable, and modification of the method may be necessary.

In the refined estimation method, the time-dependent loss is calculated from Eq. (A-6).

$$\Delta f_{pLT} = \left(\Delta f_{pSR} + \Delta f_{pCR} + \Delta f_{pR1}\right)_{id} + \left(\Delta f_{pSD} + \Delta f_{pCD} + \Delta f_{pR2} - \Delta f_{pSS}\right)_{df} \tag{A-6}$$

where $(\ )_{id}$ indicates the losses occurred between pre-stress transfer and deck placement, $(\ )_{df}$ indicates the losses occurred after deck placement, Δf_{pSR} and Δf_{pSD} are losses due to shrinkage of girder concrete, Δf_{pCR} and Δf_{pCD} are losses due to creep of girder concrete, Δf_{pR1} and Δf_{pR2}

are losses due to relaxation of pre-stressing strands, and Δf_{pSS} is the gain due to shrinkage of deck.

For the estimation of each component in time-dependent pre-stress losses, the concrete strain is estimated based on the stress-strain relationship of slow-loading which can be represented by elastic modulus, $E_c^{"}$ (Tadros et al. 2003):

$$E_c^{"} = \frac{E_{ci}}{1 + \chi \psi_b \left(t_f, t_i\right)} \tag{A-7}$$

where E_{ci} is the concrete elastic modulus at pre-stress transfer, $\chi = 0.7$ is the relaxation coefficient, and $\psi_b \left(t_f, t_i\right)$ is the creep coefficient. The creep coefficient in Eq. (A-8) is the ratio of creep strain at time $t = t_f$ to elastic strain when a load is applied at time $t = t_i$ and held constant (Tadros et al. 2003).

$$\psi_b(t_f, t_i) = \frac{\varepsilon_{cc}}{\varepsilon_e} = \psi_u \cdot \gamma_{cr} = 1.9 \cdot \left(k_{td} k_s k_{hc} k_f t_i^{-0.118}\right) \tag{A-8}$$

where ψ_u is an ultimate creep coefficient, k_{td} is the time-development factor, k_s is the factor for the effect of the volume-to-surface ratio, k_{hc} is the humidity factor, and k_f is the factor for effect of concrete strength.

For pre-stress loss estimation, three methods have been used: lump-sum estimates, rational approximate methods, and detailed time-dependent analyses. The approximate estimation method (section 5.9.3.3) in the AASHTO-LRFD (AASHTO 2017) and the total-loss method in the PCI Design Handbook (PCI 2010) are lump-sum estimate methods. The refined estimation method (section 5.9.3.4) in the AASHTO-LRFD and a method in the PCI Design Handbook can be classified as rational approximate methods. Detailed time-dependent analyses may provide accurate prediction of pre-stress losses. Some of these methods are presented in the PCI Bridge Design Manual (PCI 2000). In the present study, the following methods are of primary concern.

- 2004 AASHTO Lump-sum method
- 2004 AASHTO Refined method
- 2017 AASHTO Approximate estimation
- 2017 AASHTO Refined estimation

In the third edition of the AASHTO-LRFD specifications (AASHTO 2004), pre-stress losses due to concrete creep and shrinkage were determined from the following equations.

$$\Delta f_{pCR} = 12.0 f_{cgp} - 7.0 \Delta f_{cdp} \tag{A-9}$$

$$\Delta f_{pSR} = 17.0 - 0.15H \tag{A-10}$$

where f_{cgp} is the concrete stress at the center of gravity of the pre-stressing, Δf_{cdp} is the concrete stress change due to permanent loads, and H is average relative humidity (%).

The *Alaska Bridges and Structures Manual* (DOT&PF 2017) was mainly based on the 6th edition of the AASHTO-LRFD (2012), but provisions for the estimation of time-dependent prestress losses for DBT girders in Eq. (A-11) were adopted from the lump-sum method in the 3rd edition (or before) of the AASHTO-LRFD. Specifically, the equation of average loss for single T or double T girders was adopted with a pre-stress loss reduction of -8 ksi for low-relaxation strands. In this equation, the sum of time-dependent pre-stress losses is expressed as a function of concrete strength, $f_c^{'}$.

$$\Delta f_{pLT} = 33\left[1 - 0.15\left(\frac{f_c^{'} - 6}{6}\right)\right] - 2 \quad (ksi) \tag{A-11}$$

Mertol, Rizkalla et al. (2010) investigated creep and shrinkage of high-strength concrete of which compressive strengths were 10 ksi, 14 ksi, and 18 ksi. It was shown that the creep coefficient in AASHTO-LRFD (AASHTO 2017) was closer to the measured value for moist-cured HSC specimens but overestimated the measured value for heat-cured HSC specimens. For shrinkage strain, AASHTO-LRFD provided reasonably good predictions compared to the measured strains except that the predicted shrinkage strains are higher than the measured values at an early age. In addition, there was less shrinkage for heat-cured specimens than for the moist-cured cylinders. The difference in the shrinkage having different strength (10 ksi to 18 ksi) was small.

There are various factors that affect concrete creep and shrinkage, and Table A-1 shows the ones in ACI 209.2R-08 *Guide for Modeling and Calculating Shrinkage and Creep in Hardened Concrete* (ACI 2008).

Table A-1. Factors affecting concrete creep and shrinkage (ACI 2008)

Factors			Variables considered
Concrete (creep and shrinkage)	Concrete composition	Cement paste content	Type of cement
		Water-cement ratio	Slump
		Mixture proportions	Air content
		Aggregate characteristics	Fine aggregate percentage
		Degrees of compaction	Cement content
	Initial curing	Length of initial curing	Moist cured
			Steam cured
		Curing temperature	Moist cured
			Steam cured
		Curing humidity	Relative humidity
Member geometry and environment (creep and shrinkage)	Environment	Concrete temperature	Concrete temperature
		Concrete water content	Ambient relative humidity
	Geometry	Size and shape	Volume-surface ratio or minimum thickness
Loading (creep only)	Loading history	Concrete age at load application	Moist cured
			Steam cured
		During of loading period	Sustained load
		Duration of unloading period	—
		Number of load cycles	—
	Stress conditions	Type of stress and distribution across the section	Compressive stress
		Stress/strength ratio	Stress/strength ratio

Concrete creep and shrinkage can significantly vary depending on its thermal environment. While this subject has been long studied by many researchers, it is hard to find research focused on in-situ measurement of creep and shrinkage in ambient cold temperatures.

Early studies found that the mechanical properties of concrete increased at low temperatures. Rostásy et al. (Rostásy, Schneider et al. 1979) collected studies about compressive strength, elastic modulus, and thermal strains of concrete at low temperature. Also, changes of strain and strength of concrete under thermal cycles were measured. Montejo et al. (Montejo, Sloan et al. 2008) collected and compared early research. Miura (Miura 1989) summarized early Japanese researches on concrete properties at low temperatures. Berner et al. (Berner, B.C. Gerwick et al. 1985) observed that compressive strength, elastic modulus, and splitting tensile strength of high-strength, lightweight concrete also increased due to cold temperature. It was argued that formation of ice within the pores and capillaries of the hardened cement paste contributes to the increases in strength and elastic modulus observed at low temperatures. Consequently, saturated concrete exhibited larger strength gains than dry concrete at low temperatures. Neville (Neville 2011) also discussed different strength increase between wet and dry concrete at low temperature, which is related to the formation of ice in the hydrated cement paste.

Elices (Elices 1987) provided a review about the fracture characteristics of reinforced concrete and pre-stressed concrete at low temperatures. The bond strength and thermal expansion of concrete were main interest in the review. Lee et al. (Lee, Shih et al. 1988, Lee, Shih et al. 1988) measured mechanical properties of normal-strength and high-strength concrete and presented that compressive strength, splitting tensile strength, elastic modulus, and local bond strength increased at low temperature. Montejo et al. (Montejo, Sloan et al. 2008, Montejo, Kowalsky et al. 2009) studied reinforced concrete columns under reversed cyclic loading at low temperature. The results were applied to the seismic design of a bridge in cold climate regions. Kogbara et al. (Kogbara, Iyengar et al. 2013) reviewed then-current development on concrete properties at cryogenic temperatures for applications to Liquefied Natural Gas containment. Concrete permeability, coefficient of thermal expansion, tensile strength, and bond strength at cryogenic temperatures were main interests to investigate and compare. It was mentioned that variation in concrete properties at cryogenic temperatures depends on the moisture content of concrete. Xie et al. (Xie, Chen et al. 2017) tested unbonded pre-stressed concrete beams at low temperatures. The beams loaded with a four-point bending scheme showed that the bending capacity of a beam increased as temperature decreased.

Compared to other mechanical properties, studies on concrete creep and shrinkage at low temperatures were rare. In general, creep became small at cold temperature. Johansen and Best (Johansen and Best 1962) used specimens cured for 42 days at 20°C and sealed them to prevent moisture loss during creep test. It was observed that freezing made the initial creep rate high, but the rate dropped to zero quickly. Also, creep from the specimens that experienced temperature change from -20°C to 20°C was greater than creep from specimens at 20°C. Turner (Turner 1980) noticed that the creep at low temperature was about a half of the creep at room temperature. Browne and Bamforth (Browne and Bamforth 1981) reported a reduction in creep at low temperatures based on Japanese researches. DeRosa et al. (DeRosa, Hoult et al. 2015) measured the deflection of a simply supported beam under sustained point loads, and it was gradually increasing. At low temperature, the deflection stopped increasing since the creep was very small or zero. However, the measurement lasted for 50 hours after loading, and it was too short to observe actual creep behavior.

A.3 In-Site Pre-stress Loss Measurement

Measuring in-situ pre-stress in bridge girders is a direct way to understand pre-stress losses. Measured pre-stress losses have been collected in many researches, and they have been used to formulate and verify design provisions. In this section, several examples of in-situ pre-stress measurement are summarized.

Barr, Eberhard et al. (2000) studied the long-term behavior of a High-Performance concrete (HPC) pre-stressed concrete girder bridge. Several types of sensors were installed in girders to measure concrete strains and temperatures, strand slip-back, girder camber, and strand stress. Figure A-6 shows the location of Vibrating Wire Strain Gages (VWSG) on the cross section of a girder.

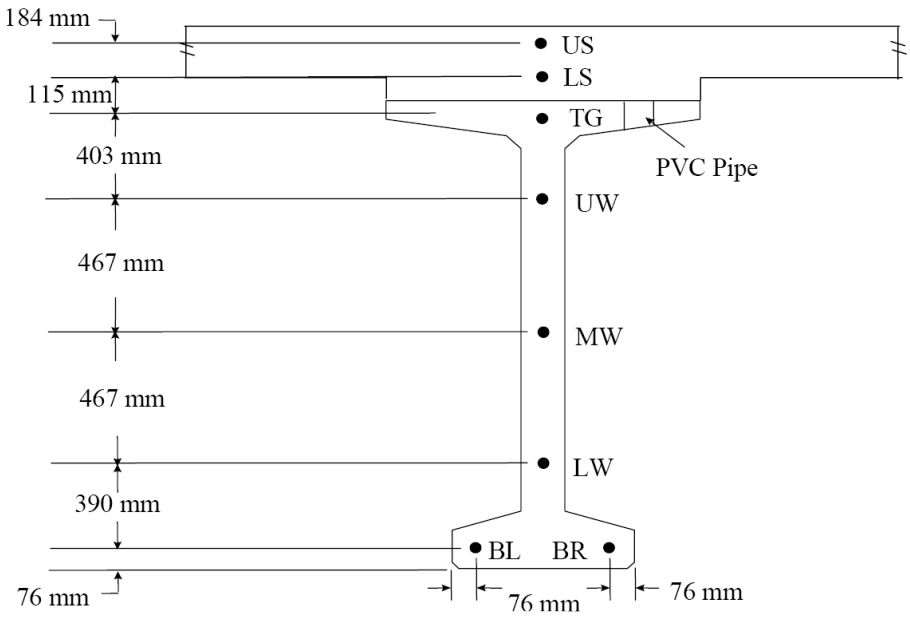

Figure A-6. Location of VWSGs installed on a Washington W74MG girder cross-section (Barr, Eberhard et al. 2000)

Among 15 girders of a three-span bridge, VWSGs were installed at 2 locations (midspan and near support) of 5 girders. VWSG cables were connected to the multiplexer attached to the web of each girder, and 5 multiplexers were connected to a datalogger at a pier. During a long-term monitoring period, data were collected at an interval of 6 hours.

Myers and Yang (2004) investigated the performance of HPC bridge girders of a 5-span bridge in Missouri. They installed various types of sensors including VWSGs and Electrical Resistance Strain Gages (ERSG) and monitored temperature, strain, and deflection of the bridge. Figure A-7 shows the location of concrete strain sensors installed in a girder.

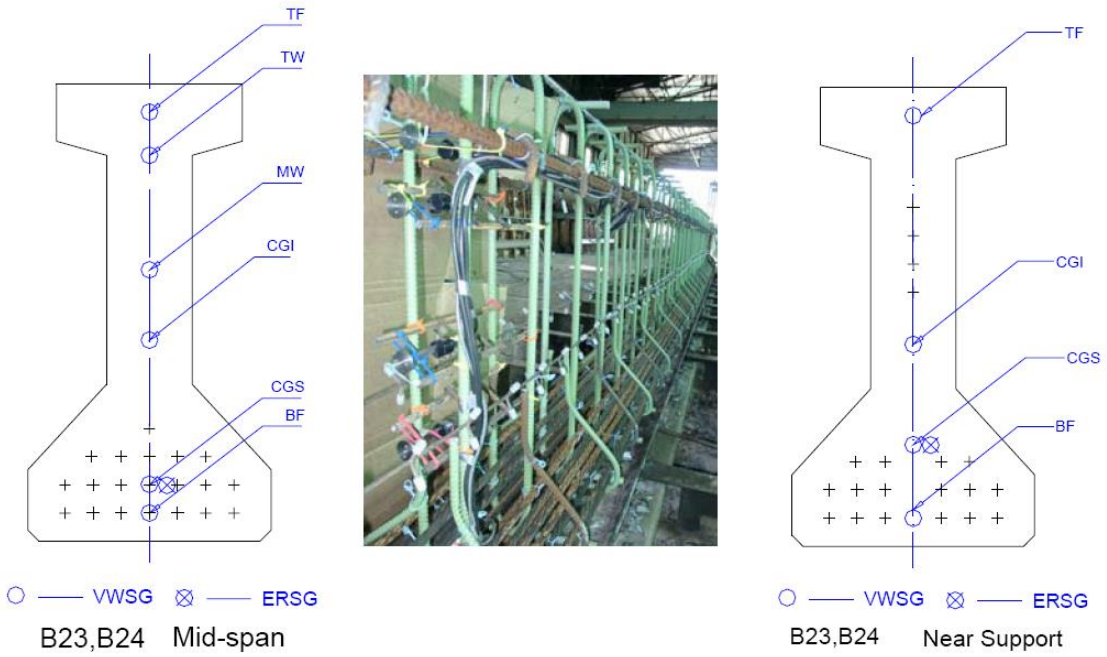

Figure A-7. Location of VWSG and ERSG in a girder (Myers and Yang 2004)

Waldron (2004) studied pre-stress losses of three bridges in Virginia. Also, VWSGs were installed at midspan of girders as shown in Figure A-8. During the fabrication and storing of girders, data were recorded every two hours. Recording was suspended while the girders were transported to bridge site and resumed once the girders were placed at the site at a two hour frequency through the placing of a deck. Then, the monitoring continued for over two years.

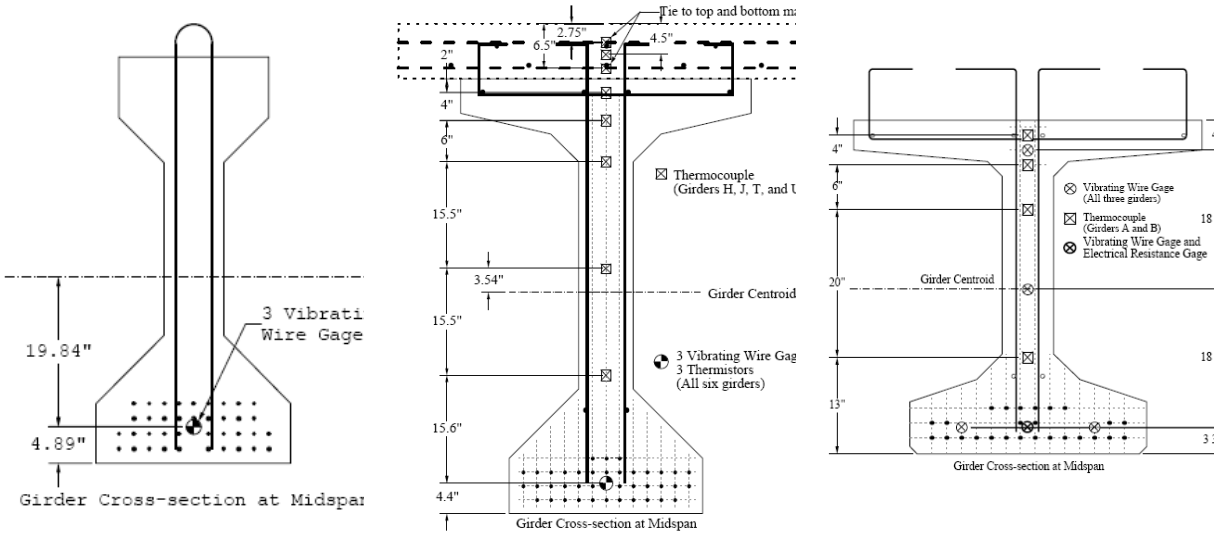

Chickahominy River Bridge Pinner's Point Bridge Dismal Swamp Bridge

Figure A-8. VWSGs in Virginia girders (Waldron 2004)

Among recently reported research on pre-stress loss monitoring, Roller, Russell et al.(2011) installed a long-term monitoring system in the Rigolets Pass Bridge in Orleans and St. Tammany Parishes, Louisiana. One span of the bridge was instrumented to measure concrete strains and temperatures of four girders. Five VWSGs were installed at midspan during girder fabrication, and girders were cured at ambient temperature. Figure A-9 shows the location of VWSGs installed at midspan.

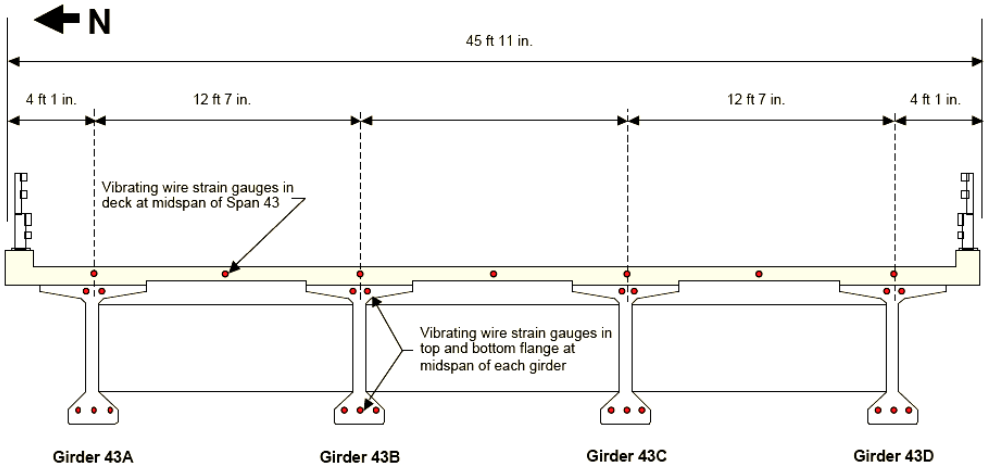

Figure A-9. Location of VWSGs in Bulb-Tee girders in the Rigolets Pass Bridge (Roller, Russell et al. 2011)

For the research of pre-stress loss in Texas girders, Garber, Gallardo et al. (2013) monitored 18 girders with VWSGs. Figure A-10 shows the location of strain gages at midspan. To protect sensor cables during concrete placement and concrete compaction, cables were carefully routed under the pre-stressing strands to exit locations in the girder.

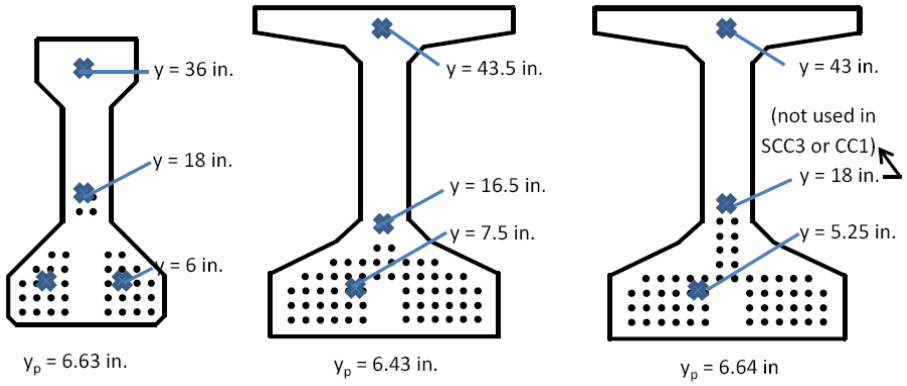

Figure A-10. Vibrating wire strain gage location in UT-Austin study (Garber, Gallardo et al. 2013)

Figure A-11 shows an example of Data Acquisition (DAQ) systems configured with vibrating wire type strain gages (Garber, Gallardo et al. 2013). It should be noted that the girders were monitored at girder conditioning sites (storage yards) not at bridge sites.

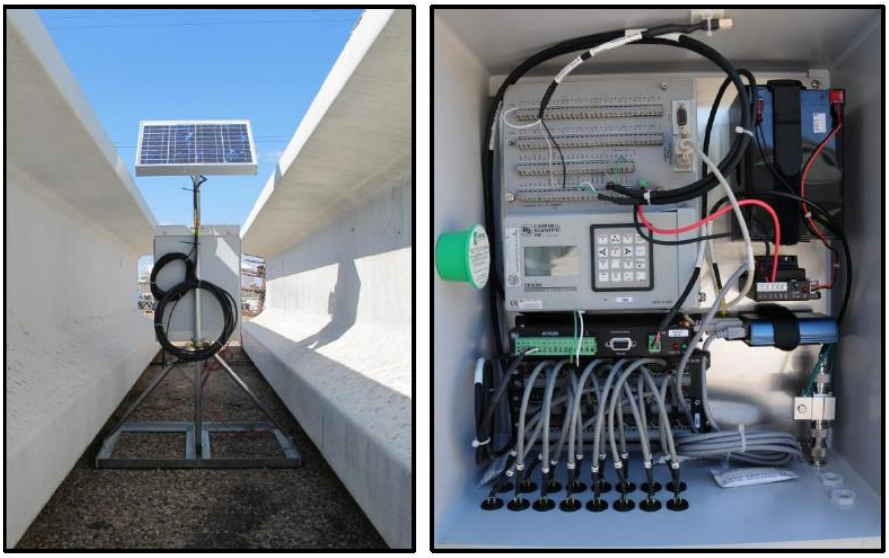

Figure A-11. Remote DAQ system for pre-stress loss monitoring system (Garber, Gallardo et al. 2013)

Alghazali and Myers (2017) investigated pre-stress loss in the girders made of high-strength concrete (HSC), self-consolidating concrete (SCC), and high-strength SCC. Nebraska University (NU) 53 girders were fabricated from the three different concrete types. Girders of the same concrete type were used to build each span of a three span bridge. Concrete strains were monitored by 86 VWSGs from girder fabrication to in-service stage of the bridge. Figure A-12 shows the location of strain gauges in girders.

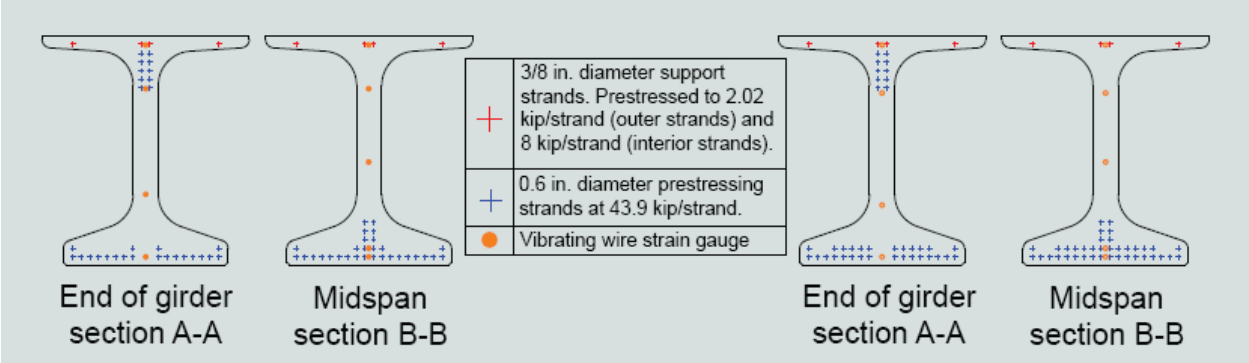

Figure A-12. VWSG locations in girders (Alghazali and Myers 2017)

The researchers reported that the losses in the HSC and high-strength SCC bridges were approximately 6.21% and 4.86%, respectively, of the nominal jacking stress. It was concluded that the AASHTO-LRFD specifications overestimated the pre-stress losses of HSC by 23% and high-strength SCC by 57% when the measured modulus of elasticity was used in the estimation. The PCI Design Handbook model was not as accurate and overestimated the total pre-stress loss by 24% for HSC and 85% for high-strength SCC when the measured modulus of elasticity was used in the estimation.

Alaywan (2011) reported the long-term pre-stress monitoring result of HPC girders in the Charenton Canal Bridge in Louisiana. Three VWSGs were installed at midspan of five girders. Figure A-13 shows the monitoring results of four girders. The measurement began in 1998 and ended in 2010. The time interval of the last measurement is more than 4 years. This result indicates that VWSG reliably measures pre-stress loss for more than 7 years (around 2500 days). In addition, it should be noted that the amount of the total loss is close to the estimation based on the 2004 AASHTO-LRFD.

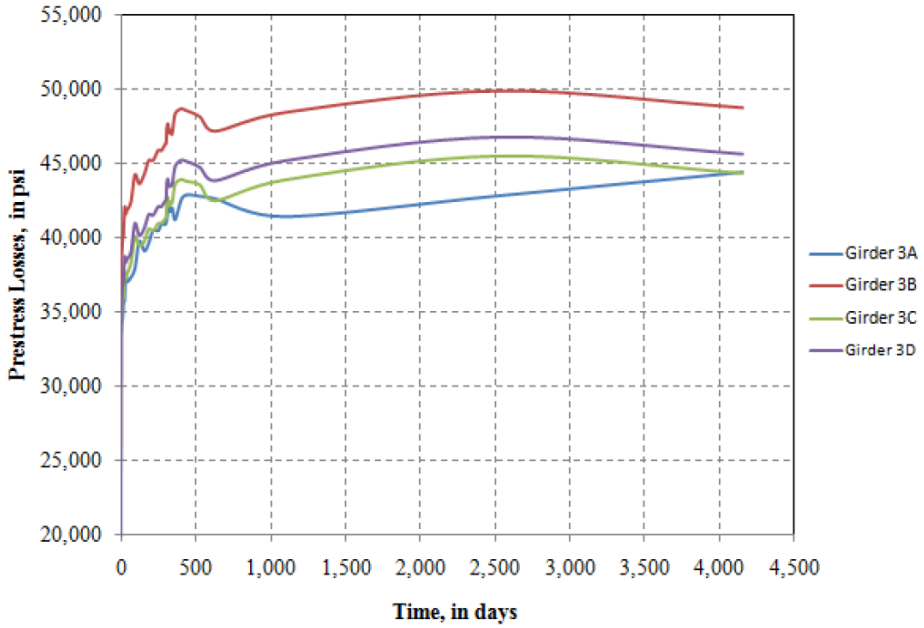

Figure A-13. Prestress loss of girders in Charenton Canal Bridge (Alaywan 2011)

Peterman and Holste (2016) reported long-term pre-stress loss monitoring results of girders made of conventional concrete and SCC. The monitoring system has collected data for more than 8 years although the system was not technically maintained for most of the time. Some data were lost since the system buffer was only able to store 3-year long data. Figure A-14 shows the change of pre-stress for almost 3000 days. If the jacking stress was 203 ksi, the total pre-stress loss is about 18 ksi and 43 ksi for Girders B1 and C3, respectively. The total loss for Girder B1

seems too small. Malfunctioning of sensor or significant long-term drifting of signal can be speculated as possible causes.

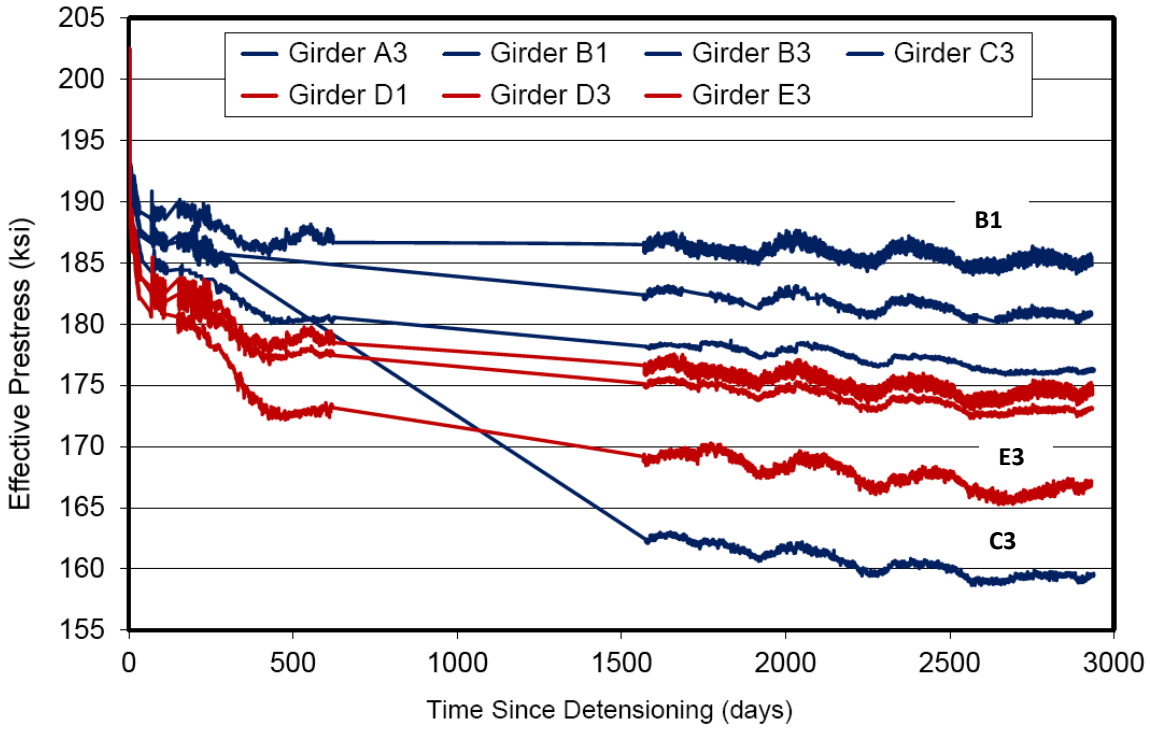

Figure A-14. Long-term pre-stress loss monitoring results (Blue: Conventional Concrete; Red: Self-Consolidating Concrete) (Peterman and Holste 2016)

Holste, Peterman et al. (2014) monitored pre-stress changes of SCC bridge girders of the new Amelia Earhart Bridge in Kansas for 3 ½ years. Three girders were used for monitoring and each girder was selected from different span. In one girder, 10 VWSGs were installed to measure concrete strains at midspan and both ends of a girder. Figure A-15 shows measured pre-stress changes during monitoring period.

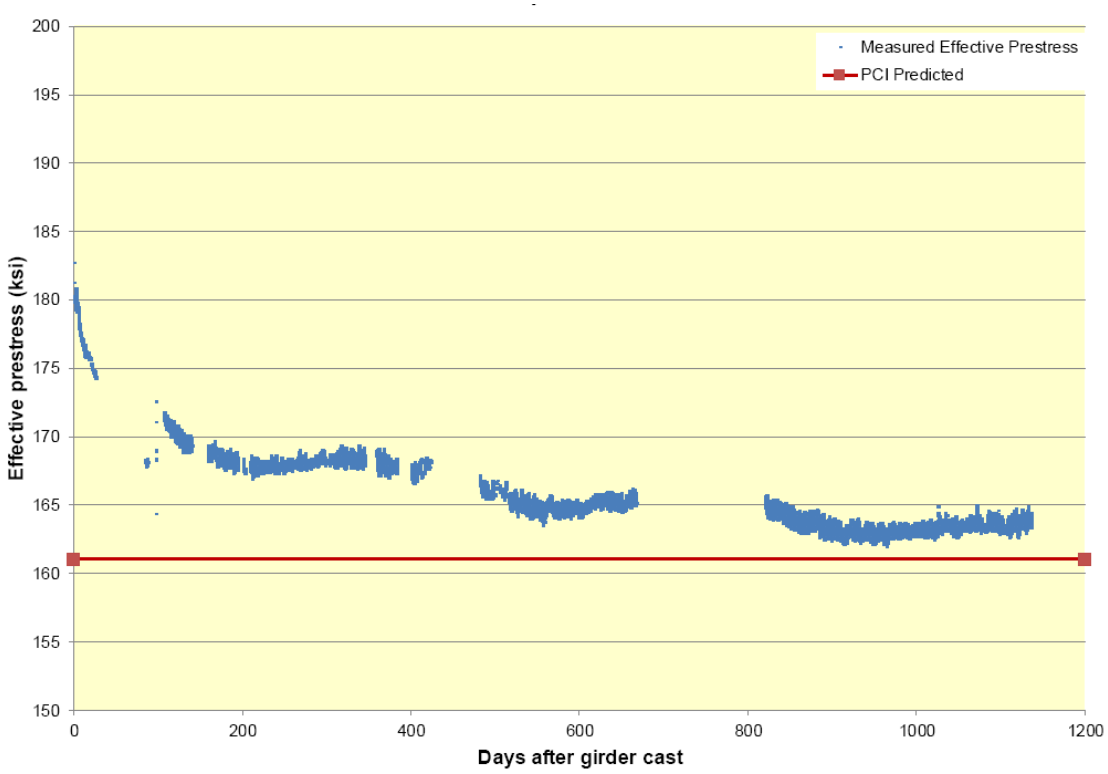

Figure A-15. Measured pre-stress changes in the New Amelia Earhard Bridge (Holste, Peterman et al. 2014)

Kukay, Barr et al. (2007) monitored four SCC girders of a two-span bridge in Logan, Utah. Four VWSGs were installed at midspan of each girder and long-term pre-stress losses were monitored for 1 year. Angomas (2009) monitored pre-stress losses in 6 girders of a three-span bridge near Farmington, Utah. In total, 24 VWSGs were installed at midspan of girders. One-year long monitoring result showed that the losses were close to values predicted by the 2004 AASHTO-LRFD refined method and the 2017 AASHTO-LRFD refined method.

Holland, Dunbeck et al. (2011) monitored pre-stress losses of High Strength Light Weight concrete girders in Georgia. All five girders in the second span of a 4-span bridge were used for monitoring. Five VWSGs were installed at midspan of each girder, and strains were collected for more than 800 days. The measured total loss was 58.5 ksi which was close to an estimated value of 61.4 ksi based on the 2017 AASHTO-LRFD refined method.

Recently, the application of Fiber Optic Sensors (FOS) has been increased to measure pre-stress force in bridge girders. Huynh and Kim (2017) used a FOS-based smart tendon to measure pre-stress force of unbounded tendons. Webb, Vardanega et al. (2017) applied the Brillouin Optical Time Domain Reflectometry (BOTDR) technique to measure concrete strain with fiber-optic cables. Idriss and Liang (2009) used fiber Bragg grating optical fiber deformation sensors to monitor the behavior including pre-stress losses of a HPC girder bridge in Las Cruces, NM.

Figure A-15 shows the change of pre-stress measured at midspan of girders for two years. If the jacking stress is 203 ksi, the largest total pre-stress loss is about 43 ksi in CMB shown with the purple color.

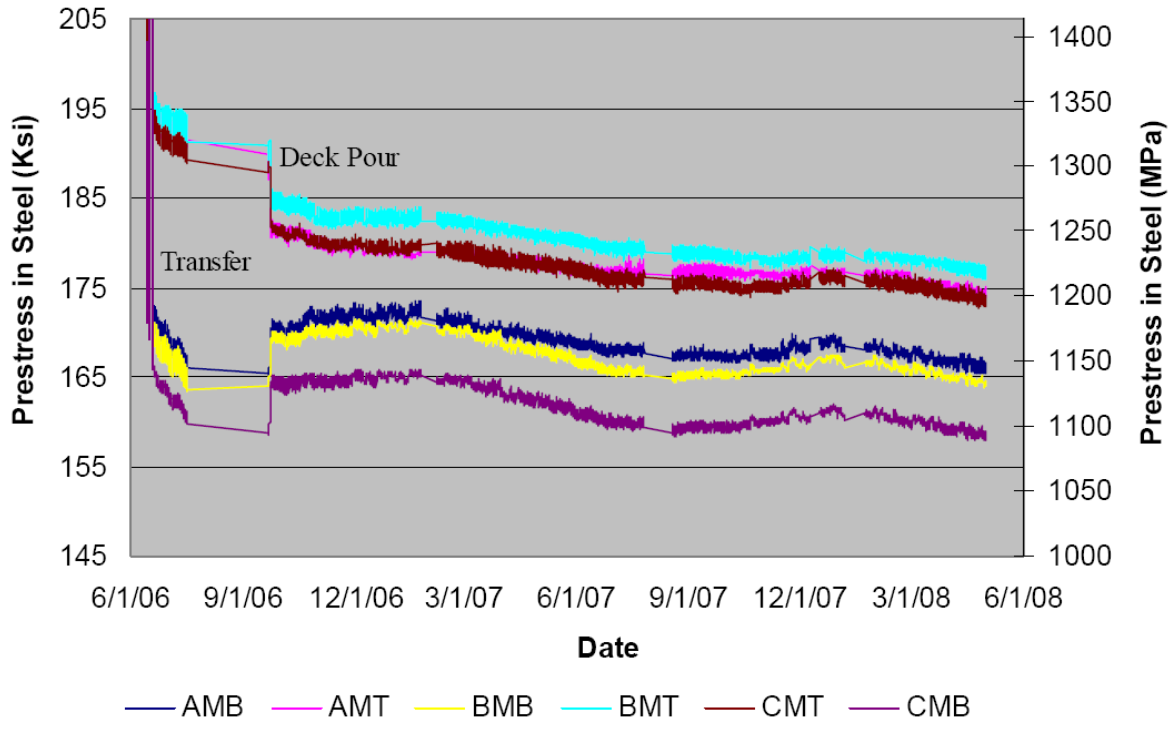

Figure A-15. Long-Term pre-stress monitoring results using FBG optical fiber sensors (Idriss and Liang 2009)

Several characteristics of pre-stress measurement schemes are compared in Table A-2.

Table A-2. Comparison of in-situ pre-stress measurement schemes

Sensors	***Number of sensors***	***Number of girders monitored***	***Data acquisition system***	***Data collection frequency***	***Reference***
VWSG	12 (midspan and near support) 2 (deck over the instrumented girder)	5 girders	5 multiplexers + 1 datalogger	6 hours (monitoring period)	(Barr, Eberhard et al. 2000)
VWSG ERSG	6 VWSG + 1 ERSG (midspan) 4 VWSG + 1 ERSG (near support)	4 girders	1 system with remote access		(Myers and Yang 2004)
VWSG	3 (per each girder)	3 girders (Chickahominy River Bridge); 6 girders (Pinner's Point Bridge);	1 system / site	2 hours	(Waldron 2004)
VWSG + ERSG	3 VWG + 1 ERSG (per girder)	3 girders	1 system	2 hours	
FOSG	2 or 4 (per girder)	6 girders	6 connection boxes + 1 reading unit	6 hours (monitoring period)	(Idriss and Liang 2009)
VWSG	5 (per girder) 7 (in the deck)	4 (at midspan)	1 system with remote access	1 hour (monitoring for 1 year)	(Roller, Russell et al. 2011)
VWSG	3-4 (per girder)	18 (at midspan)	1 system at each site	1 hour	(Garber, Gallardo et al. 2013)
VWSG	3 (per girder)	7 girders	1 system	12 hours (monitoring period)	(Peterman and Holste 2016)
VWSG	86 (total)	6 (2 girders in 3 spans)	2 systems with wireless connection	5 min. (monitoring stage)	(Alghazali and Myers 2017)

NOTE: VWSG: vibrating wire strain gage with built-in thermistor; FOSG: fiber optic strain gauge using fiber Bragg grating; ERSG: Electrical Resistance Strain Gauge.

In most pre-stress monitoring system, VWSG, FOSG, and ERSG have been used. Among them, VWSG is the most widely used sensor type (about 85% as reported in Waldron (2004)). Also, Garber, Gallardo et al. (2013) collected 29 studies where pre-stress losses were measured for 237

specimens. For selected 140 specimens, VWSG (49%) and flexural cracking tests (41%) were used in most cases.

Kowalsky, Zia et al. (2002) used plane strain bars, embedded ERSGs and VWSGs to measure concrete strain in a HPC girder in Raleigh, NC. The durability of VWSGs was much better than other types. Many strain bars were damaged during girder fabrication and transportation. Strain values from the ERSGs became inaccurate after encasing polymer of ERSG was damaged by concrete hydration heat. In some applications, ERSGs were not durable or reliable for long-term monitoring (Myers and Yang 2004).

When gages are embedded in a concrete girder, installing gages in accurate positions and protecting gages and wires during concrete placement, vibration, and curing are important. In some cases, a gage was tied to a rebar welded cage and the cage was tied to rebar in a girder as shown in Figure A-16 (Myers and Yang 2004).

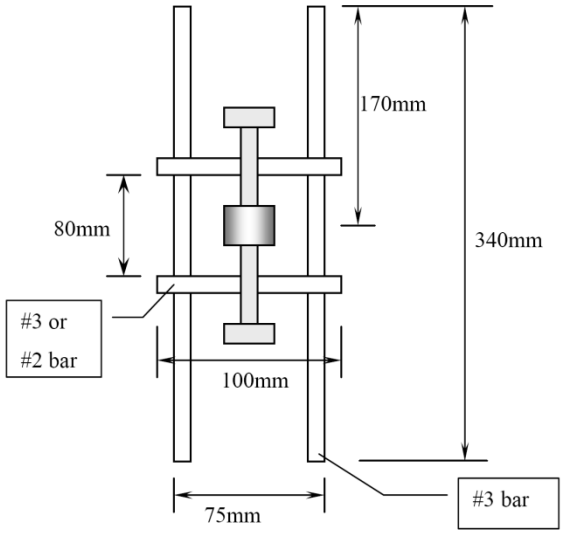

Figure A-16. Welded grid rebar cage for VWSG (Myers and Yang 2004)

It was recommended to use a hard material such as wood, concrete, or plastic as standoffs when VWSGs were installed (Lewis and Karbhari 2006). Styrofoam was easily dislodged and damaged during pouring of concrete. Also, it was noted that the amount of measured shrinkage cannot be accurate when a gage was placed near shrinkage reinforcement in a girder.

A.4 Some Issues

Since the adoption of the current pre-stress loss provisions in the AASHTO-LRFD, the accuracy and usability of the provisions have been called into question. For example, in a study comparing

measured and calculated pre-stress losses, a significant discrepancy was found in the time-dependent losses of high-strength concrete bulb-tee girders (Roller, Russell et al. 2011). Brewe, Myers et al. (2008) observed that the 2017 AASHTO-LRFD refined method underestimates the total pre-stress losses for all beams by an average of 22%. Garber, Gallardo et al. (2013) discussed that the current refined estimation method resulted in underestimation of the pre-stress loss by nearly half.

Based on measured pre-stress loss data, different methods for estimating pre-stress losses were compared as shown in Figure A-17 (Garber, Gallardo et al. 2016). The PCI simplified method and 2004 AASHTO-LRFD provisions are conservative in the estimation of the final pre-stress loss; whereas, the other methods generate many cases where measured pre-stress losses are significantly larger than estimated losses. It was mentioned that the current provisions were less conservative and significantly more complex without accurately predicting pre-stress losses.

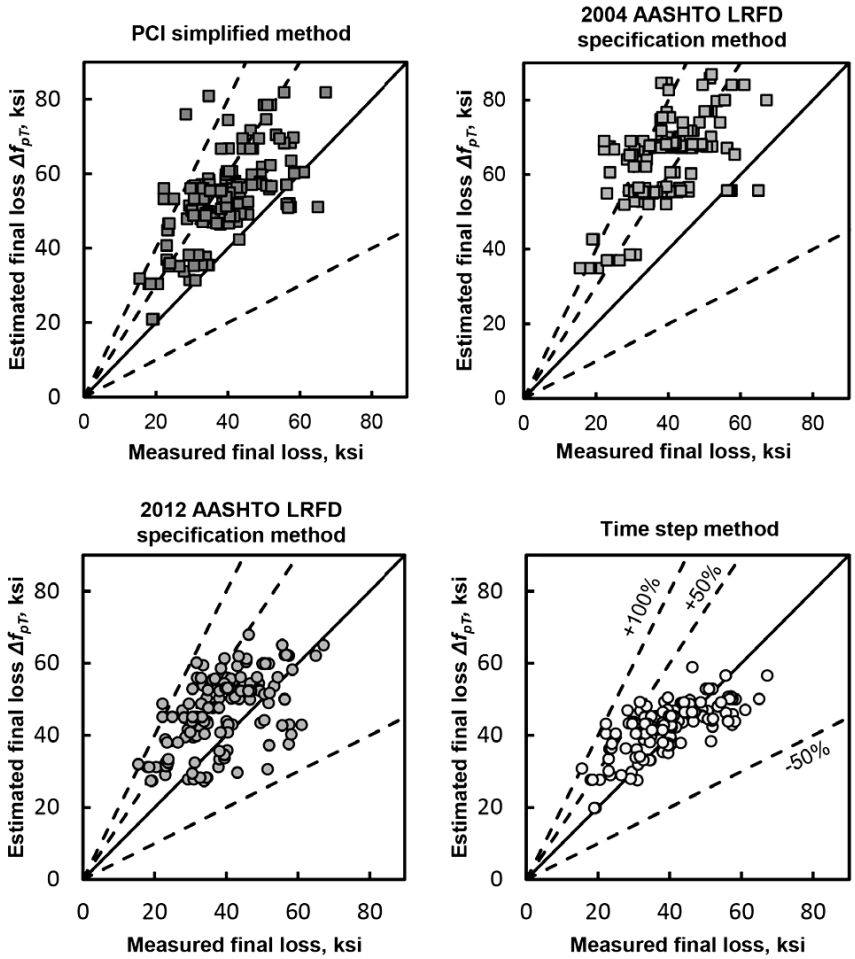

Figure A-17. Estimated and measured pre-stress losses (Garber, Gallardo et al. 2016) [PCI simplified (PCI 2010), 2004 AASHTO-LRFD specifications (AASHTO 2004), 2012 AASHTO-LRFD specifications (AASHTO 2012), and time step approach (ACI 2014)]

The long-term pre-stress losses become greater as applied pre-stress force increases. Higher allowable concrete stress at release, therefore, makes long-term pre-stress losses greater. Several studies that support higher concrete stress at release include Hale and Russell (2006). Hale and Russell recommended increasing the allowable compressive stress immediately after release to $0.70f_{ci}^{'}$. Brewe and Myers (2010) studied effects of elevated compressive fiber stresses on high-strength SCC girders. It was observed that increasing the allowable compressive stress at lease to $0.70f_{ci}^{'}$ was feasible. The maximum allowable compressive stress at pre-stress transfer was increased to $0.65f_{ci}^{'}$ in the AASHTO-LRFD (AASHTO 2017).

Since the amount of concrete creep is closely related to the elastic modulus of concrete, the provisions of elastic modulus in specifications are also important (O'Neill and French 2012). Rosa, Stanton et al. (2007) showed that the camber of a girder was sensitive to the elastic modulus of the concrete, creep coefficient, and pre-stress losses. It was discussed that the AASHTO-recommended values for the elastic modulus and the creep coefficient had to be multiplied by adjustment factors. Rizkalla, Zia et al. (2011) also recommended using a factor of $K_1 = 0.85$ (the aggregate adjustment factor) to estimate elastic modulus of concrete when the 2010 AASHTO-LRFD equation was used.

Once in-situ pre-stress loss data are available from long-term monitoring, the data will be used to formulate or verify design provisions. The monitoring results will become data points, and it will be required to add more data points from bridges in other states to acquire statistically meaningful results. Garber, Gallardo et al. (2013) built a database to generate Figure A-17, and the database contained many bridges in Texas. When the 2004 AASHTO-LRFD and the 2007 AASHTO-LRFD specifications were compared, Al-Omaishi, Tadros et al. (2009) used pre-stress loss measurement of 31 girders in many states. It is interesting to note that measured losses from 5 girders in Washington (Stanton, Barr et al. 2000) are consistently greater than those from the 2007 AASHTO-LRFD specifications. Therefore, selection of proper bridges is crucially important to verify or validate provisions.

APPENDIX B.

EXPERIMENT REPORT

B.1 Introduction

Concrete under stress experiences various types of strain. Figure B-1 shows various strains related to load, creep, and shrinkage of concrete. The total strain is the sum of initial or elastic strain, creep strain, and shrinkage strain if there is no temperature change. The creep strain consists of basic creep and drying creep strains, and the shrinkage strain is the sum of autogenous shrinkage strain and drying shrinkage strain.

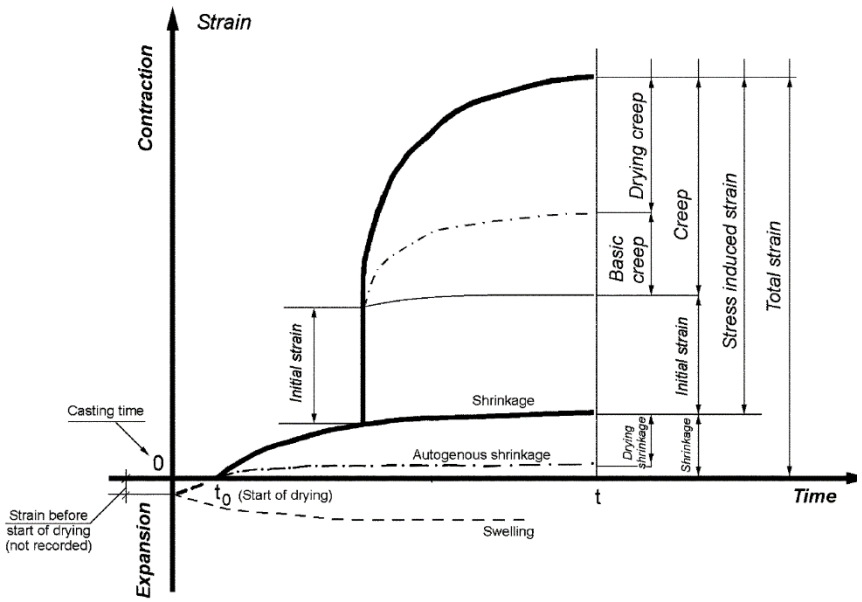

Figure B-1. Relationship between various measured and derived strains (ACI 2005)

Basic creep strain is time-dependent that increases under a sustained constant load in the absence of moisture exchange with surroundings (sealed specimen) (ACI 2005, ACI 2008). Also, autogenous shrinkage occurs in the absence of moisture exchange due to the hydration reactions in the cement matrix. It is also termed as basic shrinkage or chemical shrinkage. Drying creep is additional creep to the basic creep in a loaded specimen exposed to a drying environment and allowed to dry. Also, drying shrinkage occurs in the concrete allowed to dry. Autogenous shrinkage is usually small for normal strength concrete and can usually be neglected (ACI 2005). When the water-cement ratio (w/c) was 0.55, the autogenous shrinkage was about 18% of the shrinkage strain (Persson 1999). For concrete with the w/c ratio less than 0.40, such as that commonly used for precast, prestressed concrete girders, autogenous shrinkage can be significant. For example, the autogenous shrinkage was about 40% of the total shrinkage for concretes of which w/c ratio was 0.40 (Tazawa 1999). It was about 50% for concretes of which w/c ratio was 0.30.

The strain measured from a strain gauge in the present study corresponds to the total strain following the definition in Figure B-1. Also, the measured strain contains thermal strain as the temperature changes. From the total strain, creep strain, shrinkage strain, and elastic strain are identified and separated for further investigation.

B.2 Experiment Setup

B.2.1 Concrete Cylinder Specimens

The concrete mix design was adopted from the design by Pre-Cast Concrete Company (PCC) in Anchorage used for Decked Bulb-Tee (DBT) girder fabrication. Anchorage Sand and Gravel donated the same materials used in DBT girder construction. The air-entraining admixture was added in the PCC mix design, but it was not used in concrete batches for specimens. Table B-1 shows the concrete mix design for the specimens.

Table B-1. Concrete mix design

	Cement	Water	Coarse aggregate	Inter-mediate aggregate	Sand	PS-1466	air-entraining admixture	Total Volume
PPC mix design	lb	lb	lb	lb	lb	floz	floz	ft^3
	758	252	815	970	1,265	68.2	2.5	27.18
Specimens	g	g	g	g	g	ml	ml	ft^3
	12,650	4,206	13,601	16,188	21,111	74.2	0	1

Concrete used for specimens was mixed in a 3 ft^3 capacity drum mixer. From concrete batches, φ6″×12″ cylinders and φ4″×8″ cylinders were molded. A vibrating wire strain gauge was installed as shown in Figure B-2 in the φ6″×12″ cylinders. φ4″×8″ cylinders were used for strength test and were not instrumented with internal sensors.

Three layers were used to mold φ6″×12″ cylinders, and two layers were used for φ4″×8″ cylinders. Since rodding concrete can damage strain gauge in a mold, each layer was vibrated for one minute on a vibration table. The consolidation method using vibration was different from rodding in ASTM C192/C192M: *Standard Practice for Making and Curing Concrete Test Specimens in the Laboratory* (ASTM 2016). The strength of concrete cylinders consolidated for different vibration duration was compared with the strength of cylinders consolidated by rodding, and one-minute of vibration was selected to get a similar effect of consolidation by rodding. Also, the cylinder mold was regularly

tapped during the vibration. Overall, the concrete was well consolidated without segregation.

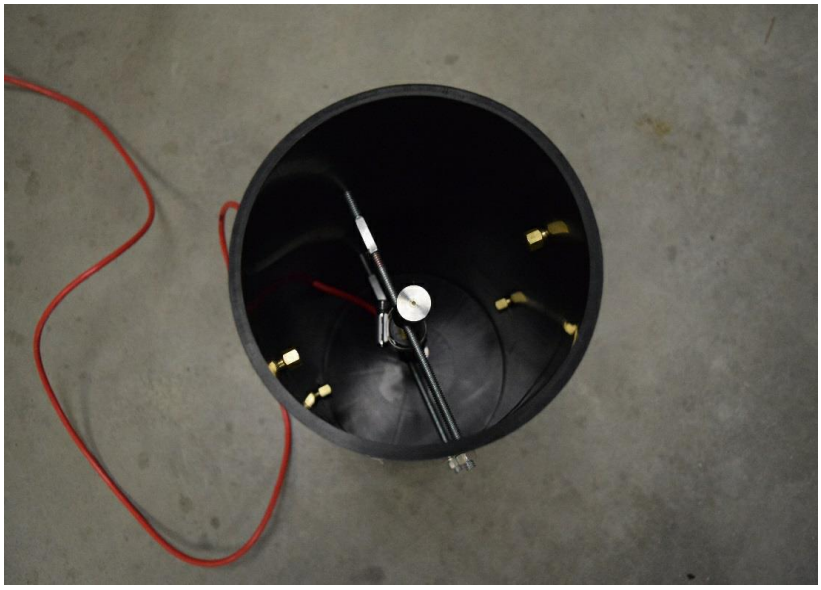

Figure B-2. Strain gauge installed in a cylinder mold

After 24 hours, the specimens were demolded and the top and bottom surfaces were cut with a concrete saw. Then, the specimens were coated with UNITEX Solvent Seal 1315 for ambient curing. The initial concrete hardening and strength gaining were different from real DBT girders since DBT girders were usually steam cured during fabrication. The specimens were cured in an ambient air in the coating until their strength reached design stress transfer strength.

Figure B-3 shows the specimens stored for ambient curing. Before loading φ6″×12″ cylinders for creep measurement, the coating was removed with paint thinner.

Figure B-3. Specimens in ambient curing

Compressive strength of concrete was tested with φ4″×8″cylinders. Table B-2 shows the compressive strength test results of all batches used in the research. The φ6″×12″ cylinders were loaded when the compressive strength measured from the φ4″×8″ specimens was found to be more than 7,500 psi. The second and the third columns in Table B-2 show the age and measured strength of concrete when corresponding φ6″×12″ cylinders were loaded. Due to preparation of specimens and loading scheme, some cylinders were not loaded on the day when the strength was measured. They are identified in the remark column.

Concrete batches were identified by their mixing date. For the batches identified as 0405 and 0514 (mixed on 4/5 and 5/14, respectively), the strength at the test day was much greater than 7,500 psi. The initial strength gaining of these batches was faster than anticipated. When the 28-day strength was measured for specimens stored in a cold room at -40°F, the strength was about 20% greater than the specimens stored at ambient temperature. This comparison was made from 0125-F and 0125-S batches.

Table B-2. Concrete compressive strength

Batch	Strength when Loaded		28-day strength (psi)	Remark
	Test Age (day)	Strength (psi)		
0125-F	7	7,512	10,992	Measured at -40F
0125-S	5	7,859	9,286 11,149	Loaded at the 9th day Measured at -40F
0405	6	9,255	9,897	Loaded at the 12th day

0514	5	8,771	10,090	
0516	6	8,199	8,708	
0624	4	7,900	9,976	29-day strength
0819	3	7,804	10,958	Loaded at the 5th day

Table B-3 shows the elastic modulus of concrete measured from φ6″×12″ cylinders on the day of loading. Procedures in ASTM C469/C469M: *Standard Test Method for Static Modulus of Elasticity and Poisson's Ratio of Concrete in Compression* (ASTM 2014) were adopted. Before loading specimens to designed amount, each specimen was loaded to 100 kips and unloaded two or three times in order to measure elastic modulus. The specimens in Table B-3 experienced 38% - 47% of their strength when a compressive force of 100 kips was applied. The force was slightly different from 40% of the strength as specified in ASTM C469, but the stress-strain relationship of specimens showed no deviation in the elastic modulus measured under 38% - 47% of strength. Figure B-4 shows measured stress-strain relationship of selected specimens where the elastic modulus was evaluated from the slope of trendlines. The moduli in Table B-3 are averages of multiple measurements. The elastic modulus is used to evaluate initial strain of each specimen.

Table B-3. Elastic modulus of concrete on the day of loading

Batch	Specimen	Elastic Modulus (psi)	Specimen	Elastic Modulus (psi)
0125-F	VW3	3,661,058	VW6	3,642,404
0125-S	VW2	3,919,855	VW7	3,771,039
0405		4,601,252		
0514	Blue (Long-term 2)	4,044,345	Red (Long-term 2)	4,206,251
	Blue (Low-temp 2)	4,810,119	Red (Low-temp 2)	4,462,953
0516		4,331,368		
0624		3,412,957		
0819		4,969,142*		

NOTE: * was measured at -40°F

Figure B-5 compares measured elastic modulus with estimated values in AASHTO-LRFD (AASHTO 2017). The estimated elastic modulus was calculated from Eq. (B-1).

$$E_c = 120,000 K_1 w_c^{2.0} f_c'^{0.33}$$

(B-1)

where $K_1 = 1.0$ is a correction factor for source of aggregate and $w_c = 0.15kcf$ is the unit weight of concrete. The measured modulus was quite smaller than the calculated values. If $K_1 = 0.8$, measured and calculated modulus became closer. The elastic modulus is important to estimate initial strain and creep strain, and measured modulus was used in strain calculation.

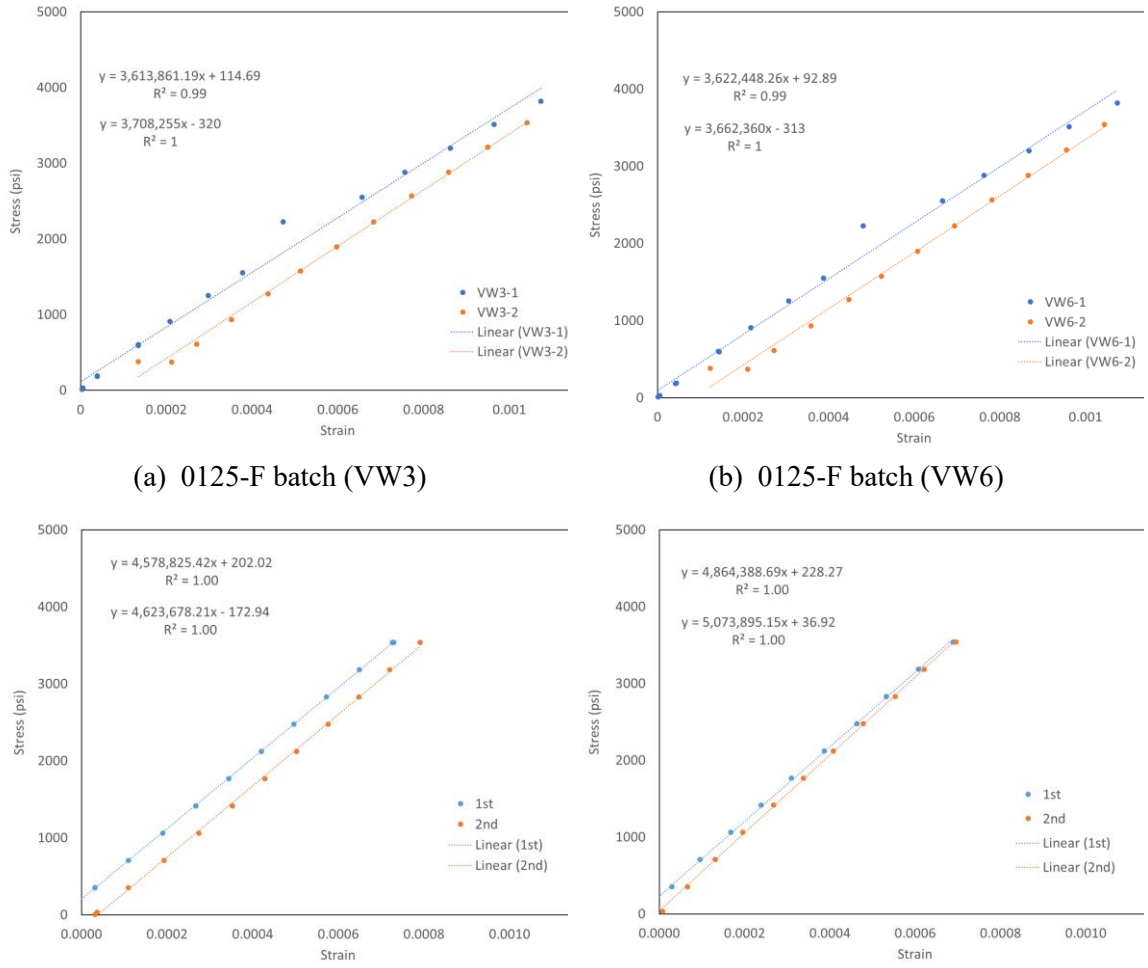

(a) 0125-F batch (VW3)

(b) 0125-F batch (VW6)

(c) 0405 batch

(d) 0819 batch (at -40°F)

Figure B-4. Stress-strain relationship of selected specimens

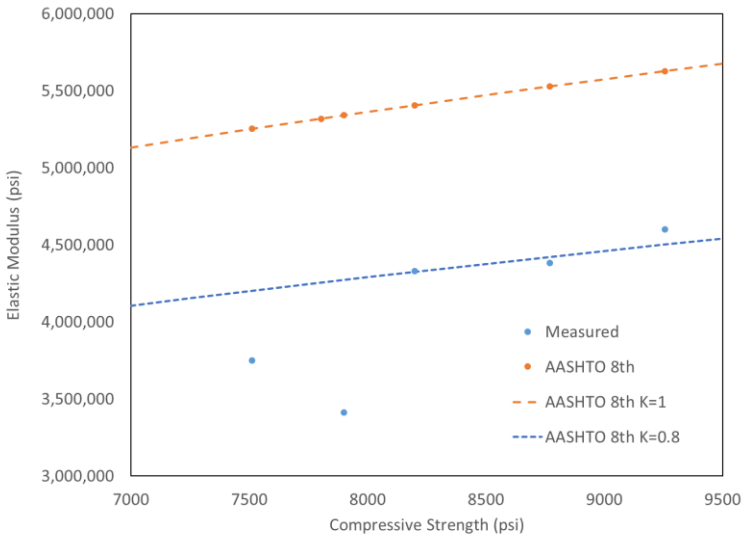

Figure B-5. Measured elastic modulus vs. estimated modulus

B.2.2 Sensor Types

The total strain from φ6″×12″ cylinders was measured with the following four types of strain gauges embedded in the cylinder. The gauges were selected based on the information collected during literature survey. They were durable and convenient to install. The first three gauges are vibrating wire strain gauge (VWSG), and the last one is fiber optic strain gauge (FOSG). Figures B-6 and B-7 show the shape of gauges. Technical detail about the strain gauges can be found in Appendix D.

- VWSG-NA: Geokon Concrete Embedded Strain Gauge model 4200 (non-adjustable)
- VWSG-B: Geokon Concrete Embedded Strain Gauge model 4200 (adjustable)
- VWSG-R: Geokon Concrete Embedded Strain Gauge model 4200-6 (adjustable)
- FOSG: Micron Optics Embeddable Strain Sensor os3500

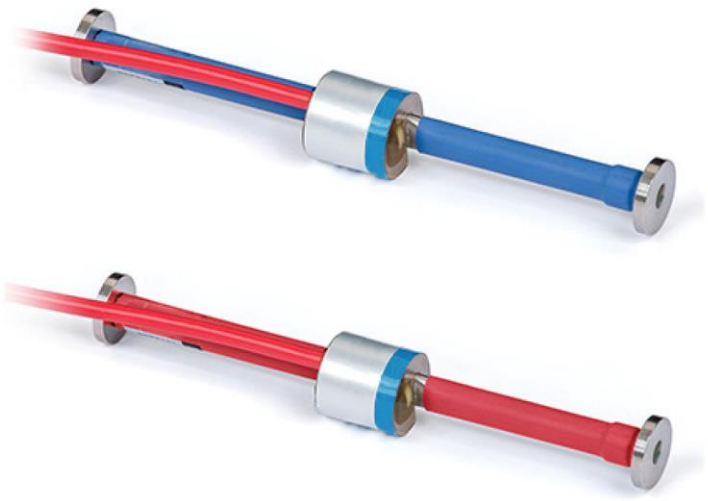

Figure B-6. Geokon vibrating wire strain gauge (VWSG-B and VWSG-R)

The VWSG-NA has a measurement range of 1,000 – 4,000με, but the initial strain value is not adjustable. Since the target strain is compressive strain, the half of the measurable range is useless if the initial strain value is fixed to the mid-point in the range. In fact, the initial strain before applying load was in compressive strain from installing, molding, and initial curing processes. Table B-4 shows measured strains from the specimens made from the 0125 batch. They are strains before sensor installation and after concrete hardening.

Table B-4. Initial strain measurement of VWSG-NA sensors (unit: με)

Sensor	VW1	VW2	VW3	VW4	VW5	VW6	VW7
before molding	2,300	2,866	2,808	2,440	1,730	2,923	2,959
after concrete hardening	2,053	2,678	2,607	2,100	1,532	2,736	2,756

The VWSG-B is almost the same as VWSG-NA except that the initial strain can be adjusted. The initial strain was adjusted to measure compressive strain up to approximately 3,000με. The measurement range of VWSG-R is increased to 5,000με with the capability of adjusting initial strain. The initial strain was adjusted to measure about 4,000με of compressive strain in the tests. Each VWSG-R sensor was calibrated at the factory, and a calibration sheet was provided for each. The measured strain is more

accurate than the one from VWSG-B. Factory calibration was not performed for every VWSG-B sensor. Factory calibration assures the reliability of each sensor and provides parameters for more accurate temperature correction.

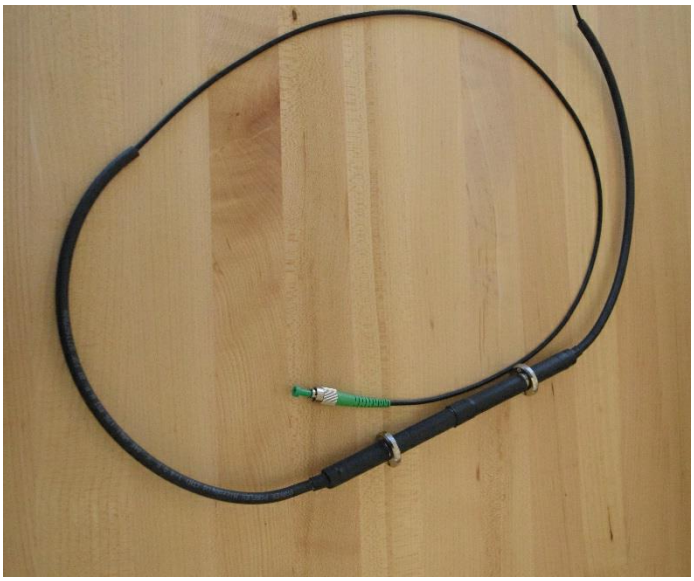

Figure B-7. Fiber optics strain gauge (FOSG)

The measurement range of FOSG is ±2500με, but the initial strain cannot be adjusted. The measured initial strain of the gauge used in the test was compressive strain, and the measurable range was substantially reduced.

For VWSG, strain can be calculated from the measured frequency of a wire inside a gauge based on a vibration theory. The wave velocity of a wire can be expressed as in Eq. (B-2).

$$v = \sqrt{\frac{T}{m}}$$

(B-2)

where T is the tension of a wire and m is the mass of the wire per unit length. The frequency of the wire can be expressed as:

$$f = \frac{v}{\lambda} = \frac{1}{\lambda}\sqrt{\frac{T}{m}}$$

(B-3)

where f is frequency in Hz, λ is a wave length which is equal to $2L_w$ for the 1st mode of vibration, and L_w is the length of the wire. For the 2nd mode of vibration, $\lambda = L_w$. The tension, T, and the mass per unit length, m, can be expressed as:

$$T = \varepsilon_w EA$$

(B-4)

where ε_w is the strain of the wire, E is the Young's modulus of the wire, and A is the cross-sectional area of the wire.

$$m = \frac{W}{L_w g} = \frac{\rho A L_w}{L_w g} = \frac{\rho A}{g}$$

(B-5)

where W is the weight of the wire, g is the gravitational constant, and ρ is the unit weight of the wire.

Therefore, the 1st mode frequency equation becomes:

$$f = \frac{1}{2L_w}\sqrt{\frac{T}{m}} = \frac{1}{2L_w}\sqrt{\frac{Eg\varepsilon_w}{\rho}}$$

(B-6)

Since the change of length between the wire and the sensor body is the same, Eq. (B-7) can be used to change Eq. (B-6) for the strain of the body such as:

$$\varepsilon_w L_w = \varepsilon L_g$$

(B-7)

where L_g is the gage length.

$$f = \frac{1}{2L_w}\sqrt{\frac{T}{m}} = \frac{1}{2L_w}\sqrt{\frac{Eg}{\rho}\frac{L_g}{L_w}\varepsilon}$$

(B-8)

For Geokon model 4200, the parameter values are $L_w = 5.875 inches$, $L_g = 6.000 inches$, $E = 30\times10^6\ psi$, $g = 386\ in/s^2$, and $\rho = 0.283\ lb/in^3$. Based on these values, the relationship between measured frequency and strain becomes:

$$f = 17397.8\sqrt{\varepsilon}$$
$$\varepsilon = 3.3038\times10^{-9} f^2 = 3.3038\times10^{-3} f^2 (\text{in } \mu\varepsilon)$$

(B-9)

For higher mode, the relationship is:

$$\varepsilon = \frac{3.3038\times10^{-3}}{n^2} f^2 (\text{in } \mu\varepsilon)$$

(B-10)

where $n = 1, 2, \ldots, n$ is the mode number.

For VWSG-NA and VWSG-B, Eq. (B-9) or Eq. (B-10) is directly used to evaluate strain. For VWSG-R, value from Eq. (B-9) is an intermediate value. This intermediate value is used either in a linear equation or a cubic equation with calibration factors provided in the calibration sheet attached to an individual gauge. The cubic equation was used to calculate strain in the present study.

$$\varepsilon = a\varepsilon_{tmp}^3 + b\varepsilon_{tmp}^2 + c\varepsilon_{tmp} + d$$
$$\varepsilon_{tmp} = 3.3038\times10^{-3} f^2 (\text{in } \mu\varepsilon)$$

(B-11)

where a, b, c, *and* d are calibration factors.

If the measured strain is ε_i at a temperature of T_i, the strain change from an initial ε_0 at T_0 can be calculated using a batch factor for VWSG-NA and VWSG-B sensors as in Eq. (B-12).

$$\Delta\varepsilon_{apparent} = \left(\varepsilon_i - \varepsilon_0\right) \cdot B$$

(B-12)

where B is a batch factor. $B = 0.97$ for VWSG-NA, and $B = 0.98$ for VWSG-B. Temperature correction can be done based on coefficients of thermal expansion. For VWSG-NA and VWSG-B, the load-related strain in concrete becomes:

$$\Delta\varepsilon_{load} = \left(\varepsilon_i - \varepsilon_0\right) \cdot B + \left(T_i - T_0\right) \cdot \left(C_g - C_c\right)$$

(B-13)

where $C_g = 12.2\mu\varepsilon / °C$ is the coefficient of thermal expansion for the gage, and $C_c = 10\mu\varepsilon / °C$ is the coefficient of thermal expansion for concrete. Without temperature correction for concrete, the actual strain (total strain) of concrete becomes:

$$\Delta\varepsilon_{actual} = \left(\varepsilon_i - \varepsilon_0\right) \cdot B + \left(T_i - T_0\right) \cdot C_g$$

(B-14)

The VWSG-R uses a different temperature correction method. The temperature correction is directly applied to ε_{tmp} in Eq. (B-11) to produce ε_i as in Eq. (B-15).

$$\begin{aligned}
\varepsilon_i &= a\varepsilon_{temp}^3 + b\varepsilon_{temp}^2 + c\varepsilon_{temp} + d \\
\varepsilon_{temp} &= \varepsilon_{tmp} + \left(0.000401 \cdot \varepsilon_{tmp} - 1.067\right) \cdot \left(T_i - T_0\right) \\
\varepsilon_{tmp} &= 3.3038 \times 10^{-3} f^2 (\text{in } \mu\varepsilon)
\end{aligned}$$

(B-15)

The actual strain (total strain) can be calculated as:

$$\Delta\varepsilon_{actual} = (\varepsilon_i - \varepsilon_0) + (T_i - T_0) \cdot C_g$$

(B-16)

Each strain gauge is equipped with a thermistor to measure temperature inside of a concrete cylinder. An additional thermistor was installed close to the cylinder to measure surrounding air temperature. The applied force to the specimen was measured from a load cell.

For data acquisition, CR1000 or CR5000 system by Campbell Scientific was used. Strain and internal temperature from FOSG were collected and stored in a Micron Optics' system.

B.2.3 Loading and Temperature Control Setup

Concrete cylinders were loaded under controlled temperature in two test setups. However, some tests (long-term tests explained in the next section) were not temperature controlled and specimens were left at room temperature (66°F – 72°F). Concrete creep frames were used for long-term and low-temperature strain measurement, and MTS testing system was used for shorter-term strain measurement.

The concrete creep frame installed in the laboratory can load three φ6″×12″ cylinders as shown in Figure B-8(a). Whereas, the concrete creep frame in the cold room can load two cylinders as in Figure B-8(b). The temperature can be dropped to -50°F in the cold room.

(a) setup in the laboratory

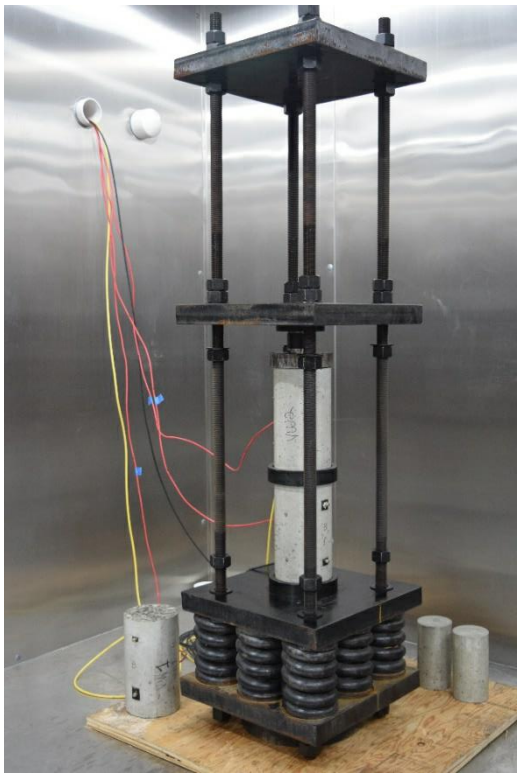

(b) setup in the cold room

Figure B-8. Concrete creep frame setups

The MTS testing machine with an environmental chamber can load a specimen to 250 kips as the temperature can be dropped to -45°F. Figure B-9 shows the overview of the system and Figure B-10 shows the specimen setup in the loading pad in the environmental chamber.

Figure B-9. MTS testing machine and environmental chamber

Figure B-10. Specimen setup in the MTS testing machine and environmental chamber

B.2.4 Test Types

The main objective of the test was to acquire data about the long-term performance of VWSG in the cold temperature. The characteristics of concrete creep in the cold temperature and the mechanical properties of concrete from the used concrete mix design were additional objectives in the tests. Table B-5 shows the types of tests performed. The concrete shrinkage strain was continuously measured for 228 days from the two specimens used in the long-term 1 test and the low-temperature 1 test.

Table B-5. Summary of sensor test types

Test type	Number of specimens	Sensors	Period of Measurement	Test condition	Concrete Batch
Long-term 1	2 + 1 (shrinkage)	VWSG-NA, DEMEC	41 days	Room Temperature, Creep Frame	0125-F
Low-temperature 1	2 + 1 (shrinkage)	VWSG-NA, DEMEC	83 days	Cold Room, Creep Frame	0125-S
Long-term 2	3	VWSG-B, VWSG-R, FOSG, DEMEC	120 days	Room Temperature, Creep Frame	0514
Low-temperature 2	2	VWSG-B, VWSG-R, DEMEC	120 days	Cold Room, Creep Frame	0514
Temperature dependence	1	VWSG-NA	7 days	MTS, Environ. Chamber	0405
	1	VWSG-B	26 days	MTS, Environ. Chamber	0819
Stress dependence	1 (53kips)	VWSG-B	15 days	MTS, Environ. Chamber	0516
	1 (160 kips)	VWSG-B	10 days	MTS, Environ. Chamber	0624
Thermal cycling	2	VWSG-B, VWSG-R	30 days	Cold Room, Creep Frame	0514

B.3 Test Results

B.3.1 Long-Term 1

In this test, concrete cylinders were loaded in the concrete creep frame at room temperature (66°F – 72°F). Two specimens made from the 0125-F batch, VW3 and VW6, were loaded at 7 days after molding. A compressive stress of 3,749 psi was applied to the specimens. On the 7th day, the compressive strength of concrete was 7,512 psi, therefore, the load ratio to the strength was 3,749 psi/7,512 psi = 0.50. One additional unloaded φ6″×12″ cylinder specimen, VW5, was placed next to the creep frame to measure shrinkage strain. In all three cylinders, VWSG-NA sensors were installed.

The 28-day strength of the concrete at -40°F was 10,992 psi. If a strength ratio between ambient and -40°F from the 0125-S batch was used, the expected 28-day strength will be 10,992 psi × 0.833 = 9,155 psi at ambient temperature. Based on the applied stress and elastic modulus (Table B-3), the initial strain of the specimen is 1,024με. Figure B-11 shows the total strain measured from the three specimens.

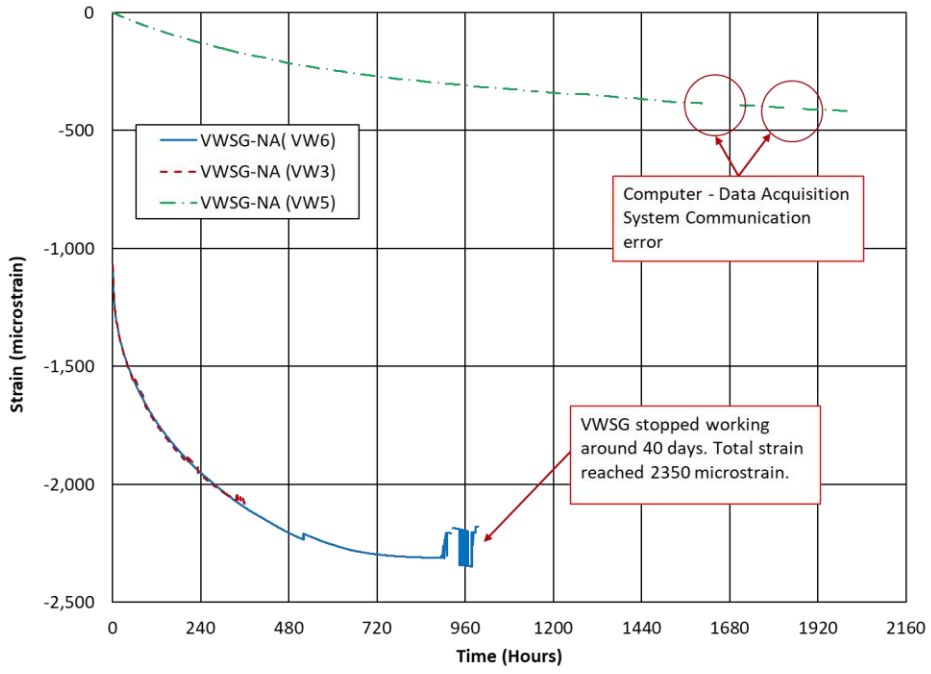

Figure B-11. Strain measurement from the long-term 1 test

The total strain reached the maximum measurement range of the VWSG-NA sensors. The VWSG-NA in VW6 stopped working at 42-day, and the sensor in VW3 stopped at 25-day. From VW6, the initial strain was 1,024με, and the total strain at 37-day was

2,312με. The strain from creep and shrinkage was 1,288με. The shrinkage strain at 37-day was 299με. Therefore, the creep strain at 37-day was 989με, and the creep coefficient was 989με/1,024με = 0.97. The shrinkage strain from VW5 reached 420με at 84 days and was continuously increasing.

From the shape of strain curve for VW6, most of total strain had occurred in 40 days. The total strain can be around 2,500με from this trend. This amount of total strain cannot be reliably measured by VWSG-NA type sensors.

B.3.2 Low-Temperature 1

Two φ6″×12″ cylinders from the 0125-S batch, VW2 and VW7, were loaded to 3,714 psi in the concrete creep frame at 8-day after molding. The strength measured on the 5th day was 7,859 psi. The load ratio was 3,714 psi/7,859 psi = 0.47 if the 5-day strength was used. An additional unloaded specimen, VW1, was placed next to the frame for shrinkage strain measurement. The 28-day strength of concrete was 9,286 psi at ambient temperature and 11,149 psi at -40°F. VWSG-NA type sensor was installed in all three specimens. Bases on the applied stress and measured elastic modulus (Table B-3), the initial strain was 947με for VW2 and 985με for VW7.

At the 14th day after molding (6th day after loading), the refrigeration system in the cold room was turned on, and the temperature was set to -40°F. The refrigeration system was turned off again and the temperature reached a room temperature of 81°F on the 54th day. Figure B-12 shows the strains measured from three specimens.

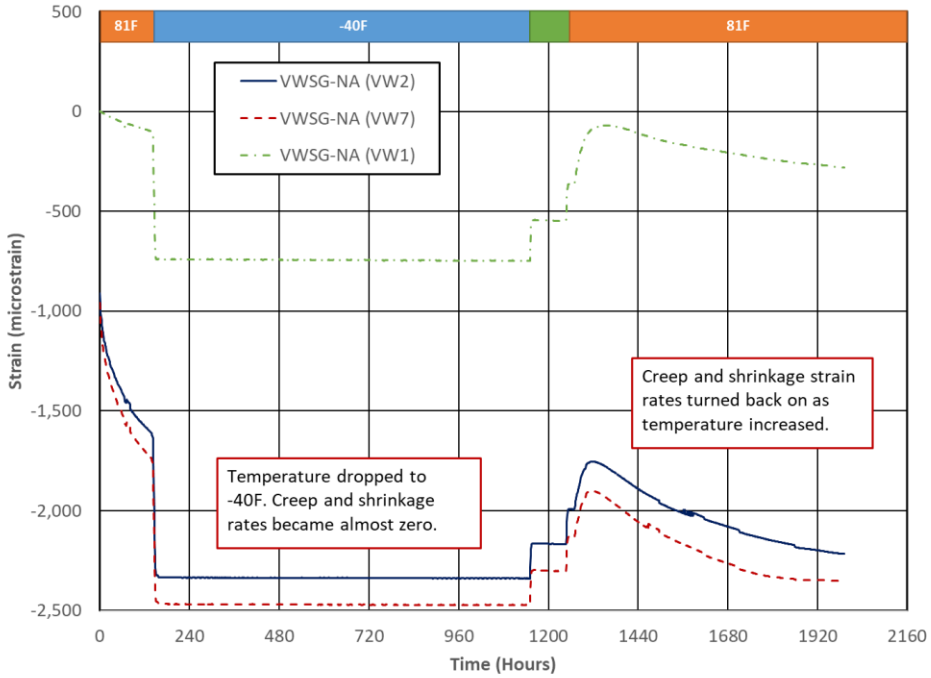

Figure B-12. Strain measurement from the low-temperature 1 test

The strains in Figure B-12 are actual strain (total strain) in Eq. (B-14) after temperature correction. The temperature before loading (81°F) was used as a reference temperature in the correction. Sudden drops and rises of strains during temperature changes correspond to concrete thermal strain.

The measured strain shows that total strain and shrinkage strain stopped increasing when the temperature was -40°F. Strains increased again once the temperature increased to 81°F. After 83 days (1,990 hours), the total strain became 2,217με for VW2 and 2,352με for VW7. The shrinkage strain reached 281με. Based on measured initial strain, total strain, and shrinkage strain, the creep coefficient was 989με/947με = 1.04 for VW2 and 1,086με/985με = 1.10 for VW7 on the 83rd day.

B.3.3 Long-Term 2

The same concrete creep frame in the long-term 1 test was used. Three φ6″×12″ concrete cylinders were loaded to 3,537 psi at 5-day when the concrete strength reached 8,771 psi. The ratio of load to the strength was 3,537 psi/8,771 psi = 0.40. VWSG-B, VWSG-R, and FOSG were installed in each specimen. Also, VW5 specimen was continuously used from the long-term 1 test in order to measure shrinkage strain. The 28-day strength of concrete was 10,090 psi. The initial strain was 874με for the VWSG-B specimen and 841με for the VWSG-R specimen. The specimens were unloaded and reloaded to check the workability and to remove the FOSG specimen. Figure B-13 shows measured strain from specimens.

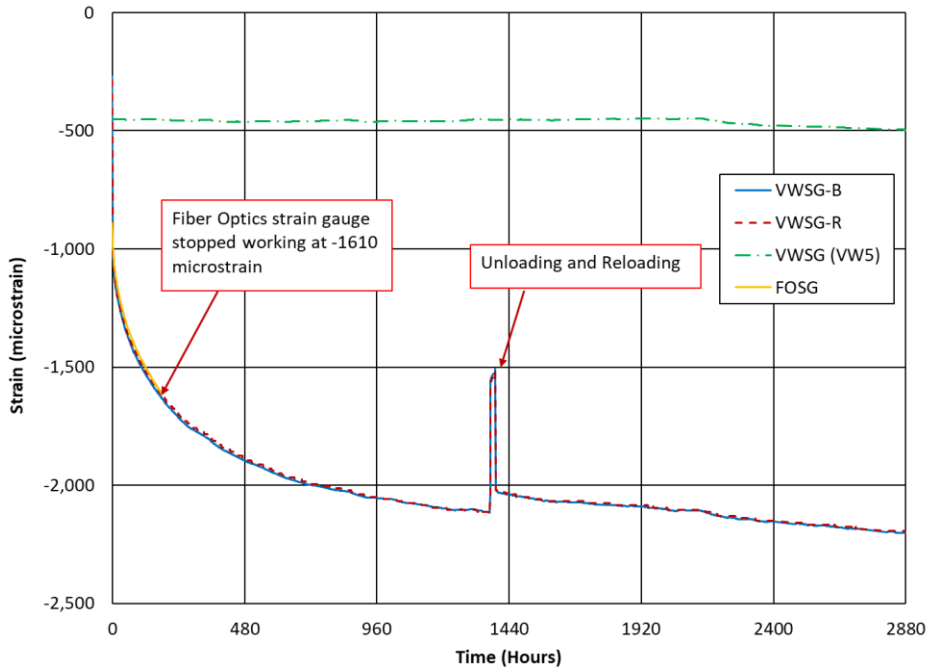

Figure B-13. Strain measurement from the long-term 2 test

The measured strains from three sensors were very close. However, the FOSG sensor stopped working at 7.5-day (180 hours) when the total strain reached 1,610με. The initial reading of the FOSG sensor before loading was 788με in compression. The sensor reached its measurable range (788+1,610 = 2,398με) when it stopped working.

At 120-day, the total strain reached 2,223με in the VWSG-B specimen and 2,221με in the VWSG-R specimen. If the shrinkage strain is 450με, the creep coefficients are 899με / 874με = 1.03 for the VWSG-B specimen and 930με/841με = 1.11 for the VWSG-R specimen. The shrinkage strain from VW5 was continuously measured from 2/1/2019, and the amount reached 509με at 234 days.

Both VWSG-B and VWSG-R sensors measured the total strain for more than 120 days. Also, strains from both sensors were very close. Since, VWSG-R has been calibrated individually, this type of sensor would be more reliable and accurate for a longer-term measurement.

B.3.4 Low-Temperature 2

Two concrete cylinders in the low-temperature 2 test were cast from the same batch (0514 batch) as the long-term 2 test. The concrete strength was 8,771 psi when the two concrete cylinders were loaded to 3,537 psi at 5-day. The ratio of load to the strength was

3,537 psi/8,771 psi = 0.40. A VWSG-B strain gauge was installed in one cylinder and VWSG-R in the other cylinder. For measuring shrinkage strain, VW1 specimen was continuously used from the low-temperature 1 test. Based on the applied stress and measured elastic moduli in Table B-3, the initial strain was 735με for the VWSG-B specimen and 792με for the VWSG-R specimen. Figure B-14 shows measured strains for 120 days. The strains suddenly dropped and rose as the temperature changed. Those amounts correspond to thermal strain of concrete.

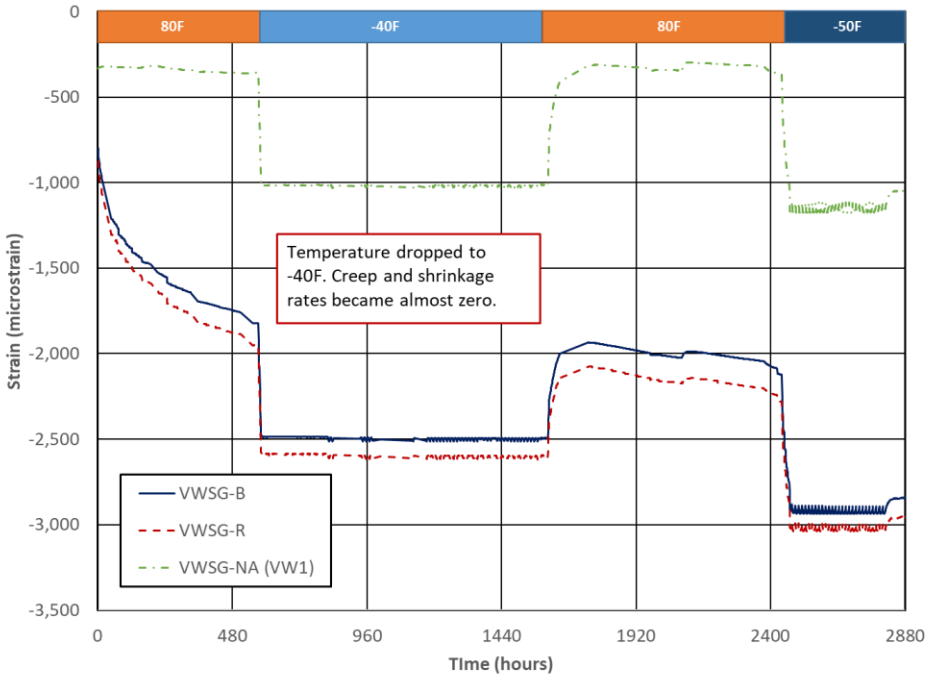

Figure B-14. Strain measurement from the low-temperature 2 test

As observed during the low-temperature 1 test, total strain from VWSG-B and VWSG-R and shrinkage strain from VW1 stopped increasing when the temperature decreased. For temperature correction, Eq. (B-14) was used for the VWSG-B sensor, and Eqs. (15) and (16) were used for the VWSG-R sensor. Between the two sensors, the difference in strain was 75με at the beginning and 120με at the end of the measurement.

In Table B-6, measured strains at 20-day (480 hours) from two sensors in the low-temperature 2 and the long-term 2 tests are compared. Since the same batch was used to mold cylinders in the two tests, the variation from concrete material was minimized. Also, cylinders were loaded with the same amount at the same age.

Table B-6. Strains between long-term 2 and low-temperature 2 tests (at 20-day)

Sensor	Test	Total (με)	Initial (με)	Shrinkage (με)	Creep (με)	Creep Coefficient
VWSG-R	Long-Term 2	1,885	841	214	830	0.99
	Low-Temp 2	1,877	792	214	871	1.10
VWSG-B	Long-Term 2	1,895	874	214	807	0.92
	Low-Temp 2	1,747	735	214	798	1.09

To decompose the measured total strain, the shrinkage strain from VW5 at the same age was used for all specimens. The creep strain and a creep coefficient were evaluated for each case. The creep coefficients evaluated from VWSG-R sensors are closer between the two tests than those from VWSG-B sensors. The measurement from VWSG-R sensors were more consistent than VWSG-B sensors.

B.3.5 Temperature Dependence

The temperature dependence of creep was investigated in two tests. The first specimen was made from the 0405 batch, and a VWSG-NA sensor was installed in the cylinder. The coating on the specimen for ambient curing was removed on the 6th day. The strength reached 9,260 psi. The specimen was dried and recoated before loading. Then, the specimen was loaded to have a compressive stress of 3,537 psi on the 12th day after molding. The strength on the loading day was 10,642 psi. The ratio of load to strength was 3,537 psi/10,642 psi = 0.33. The process of uncoating, drying, and recoating took 6 days, and the specimen became too strong when it was loaded. After this, all other specimens were not recoated. The initial strain was 769με. Figure B-15 shows the measured strain for 10,000 minutes after loading.

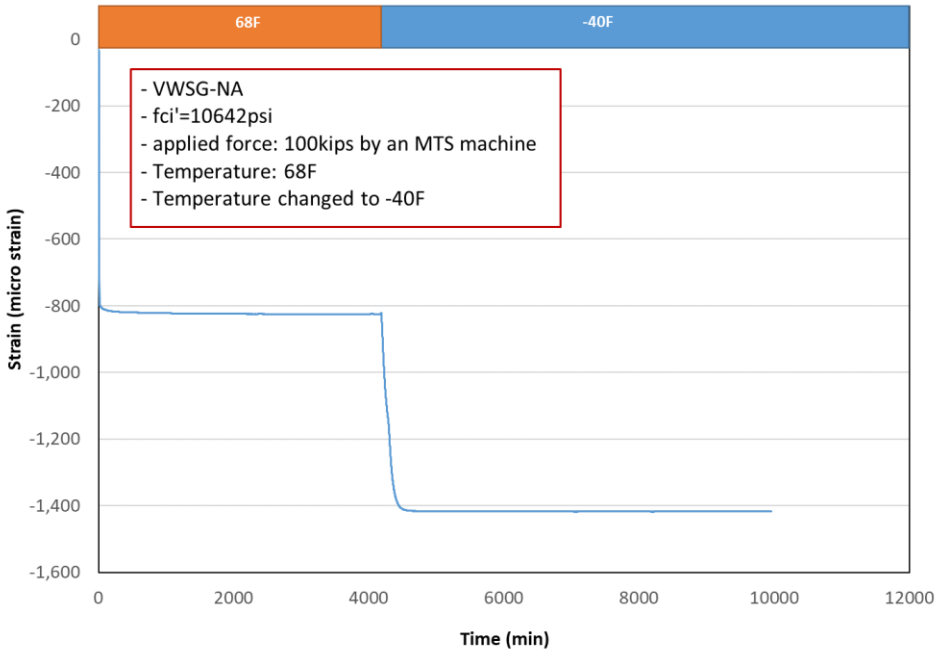

Figure B-15. Strain measurement from the temperature dependence test (0405 batch)

During the loading, the environmental chamber was set to maintain 68°F. After 70 hours (4,180 minutes), the temperature dropped to -40°F. In the figure, the total strain was corrected for temperature changes based on Eq. (B-14). Therefore, the sudden strain change when the temperature decreased was thermal strain for concrete. Since the concrete was substantially hardened when it was loaded, there was not a significant change in the total strain at 68°F. Also, the total strain did not change when the temperature was -40°F. During the temperature was -40°F, the strain changed by 4με for 90 hours (5,415 minutes).

The concrete cylinder for the 2nd temperature dependence test was made from the 0819 batch where a VWSG-B sensor was installed. On the 3rd day when concrete strength reached 7,804 psi, the specimen was set in the environmental chamber, and lowered the temperature to -40°F for two days. Then the specimen was stressed to 1,874 psi. The load ratio was 1,874 psi/7,804 psi = 0.24 based on the 3-day strength. Five stress cycles (354 psi – 3,537 psi) were applied at 264 hours after loading. The temperature increased to 68°F at 284 hours after loading. Then, five stress cycles (354 psi – 3,537 psi) were applied at 385 hours. Additional five stress cycles (354 psi – 3,537 psi) were applied at 405 hours. During the last two stress cycles, the temperature was 75°F. Figure B-16 shows the strain measured during this test.

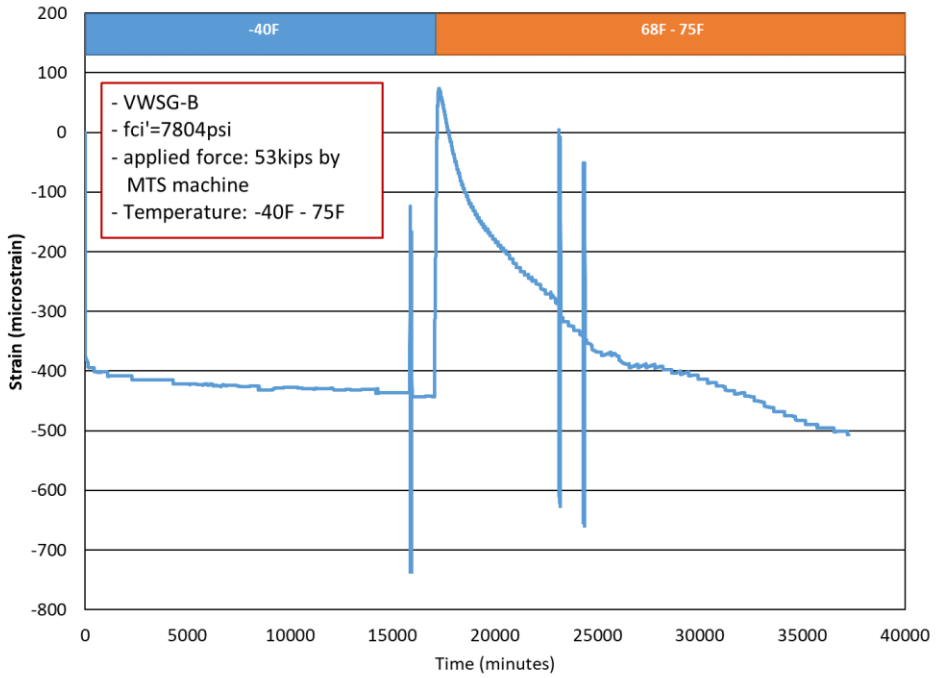

Figure B-16. Strain measurement from the temperature dependence test (0819 batch)

The initial strain was 377με based on the elastic modulus in Table B-3 that was measured at -40°F. The change in total strain between 45 minutes and 15,847 minutes after loading was 56με. The amount of change was greater than the changes observed in other tests under the cold temperature since the temperature decreased at earlier age of concrete in this test.

Figures B-17, B-18, and B-19 show the change of total strain measured during the stress cycling. In Figure B-17, the total strain changed between 167με and 735με as stress cycles of 354 psi – 3,537 psi were applied. The amplitude was 568με at -40°F. The total strain changed between 8με and 618με in Figure B-18, and between 51με and 655με in Figure B-19. At 75°F, the amplitude of total strain change was 610με in the second cycle and 604με in the third cycle. The smaller amplitude of strain (568με) at -40°F compared to the amplitude of 610με and 604με could be caused by the stiffening effect of concrete due to cold temperature. It can be mentioned that the VWSG-B sensor was responsive to the change of stress, and the measured strains were reasonable in the cold temperature.

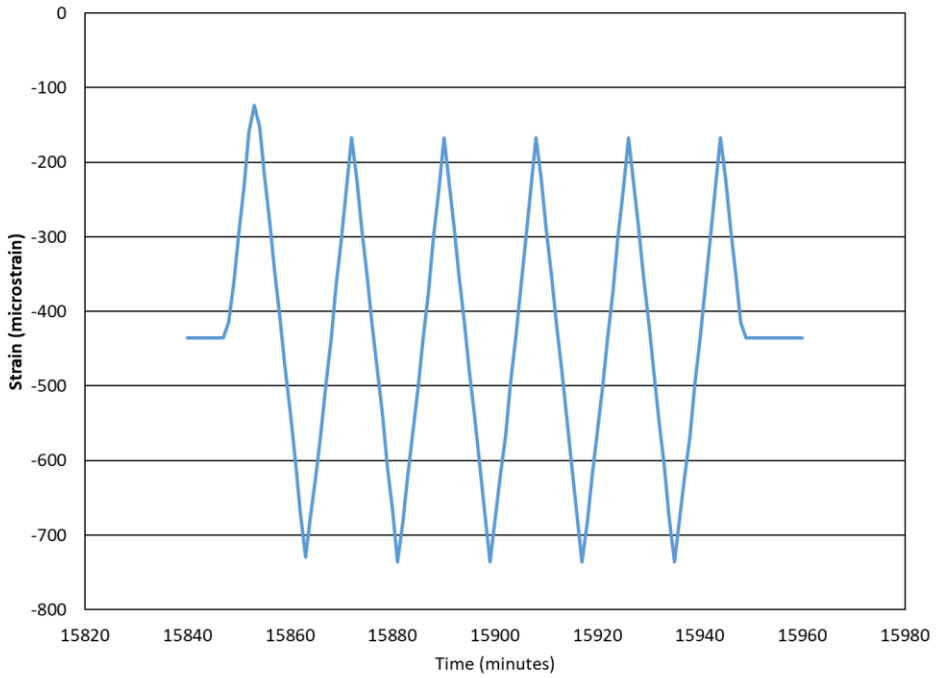

Figure B-17. Results from the 1st stress cycling (applied stress: 354 psi – 3,537 psi, temperature: -40°F)

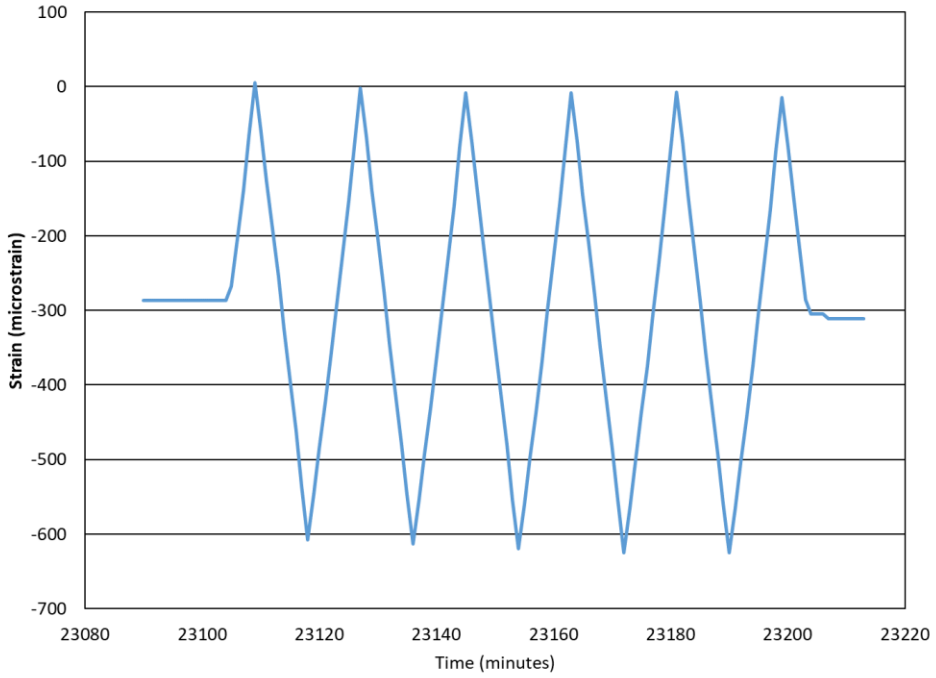

Figure B-18. Results from the 2nd stress cycling (applied stress: 354 psi – 3,537 psi, temperature: 75°F)

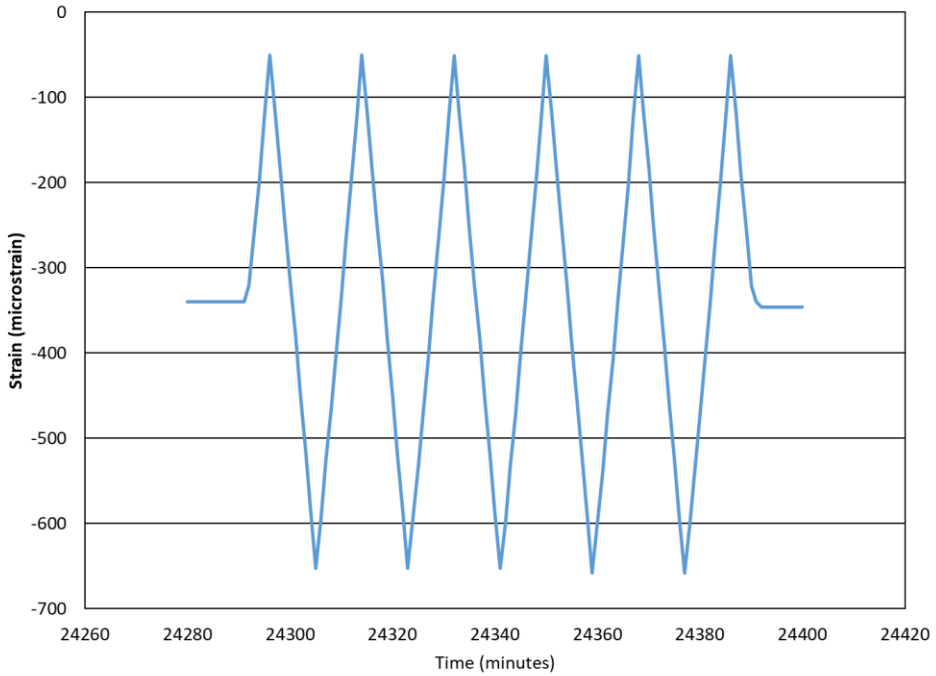

Figure B-19. Results from the 3rd stress cycling (applied stress: 354 psi – 3,537 psi, temperature: 75°F)

B.3.6 Stress Dependence

Stress dependence test was to investigate the characteristics of creep strain with different amounts of applied stress. In the long-term 2 test, the applied stress force was 3,537 psi. In the stress dependence test, 1,874 psi and 5,659 psi were applied.

A concrete cylinder made from the 0516 batch was loaded to 1,874 psi in the MTS testing machine at 6-day after molding. The concrete strength at 6-day was 8,199 psi, and the load ratio to the strength was 1,874 psi/8,199 psi = 0.23. In the specimen, a VWSG-B sensor was installed. Based on the measured elastic modulus in Table B-3, the initial strain of the specimen was 433με at 68°F. The specimen was unloaded/reloaded at 287 hours (17,234 minutes) after loading, and the temperature decreased to -40°F at 319 hours (19,117 minutes). Figure B-20 shows the measured total strain from the test.

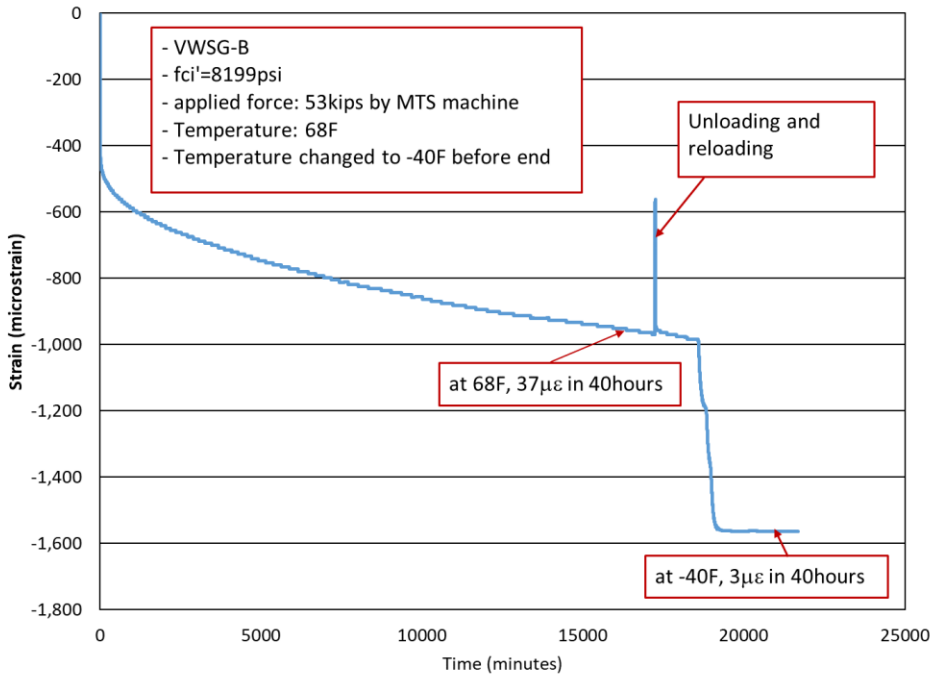

Figure B-20. Strain measurement from the stress dependence test (0516 batch)

At 200 hours (12,000 minutes) after loading, the total strain was 895με. The shrinkage strain from VW5 (specimen for measuring shrinkage strain in the long-term 1 test) at 200 hours was 115με. Therefore, the creep strain was 895-433-115 = 347με. The creep coefficient becomes 347με/433με = 0.8 for a load ratio of 0.23.

In addition, the total strain change at the cold temperature was compared. The strain change for 40 hours was 37με at 68°F. For the same time period, the total strain changed 3με at -40°F. This test also showed that the total strain change becomes dormant in cold temperature.

For the second specimen in this test, a concrete cylinder from the 0624 batch was loaded to 5,659 psi in the MTS testing machine at 4-day after molding. The concrete strength was 7,900 psi on the 4th day, and the load ratio was 5,659 psi/7,900 psi = 0.72. In the concrete cylinder, a VWSG-B sensor was installed. The initial strain was 1,658με based on measured elastic modulus in Table B-3. Figure B-21 shows the measured strain in the test.

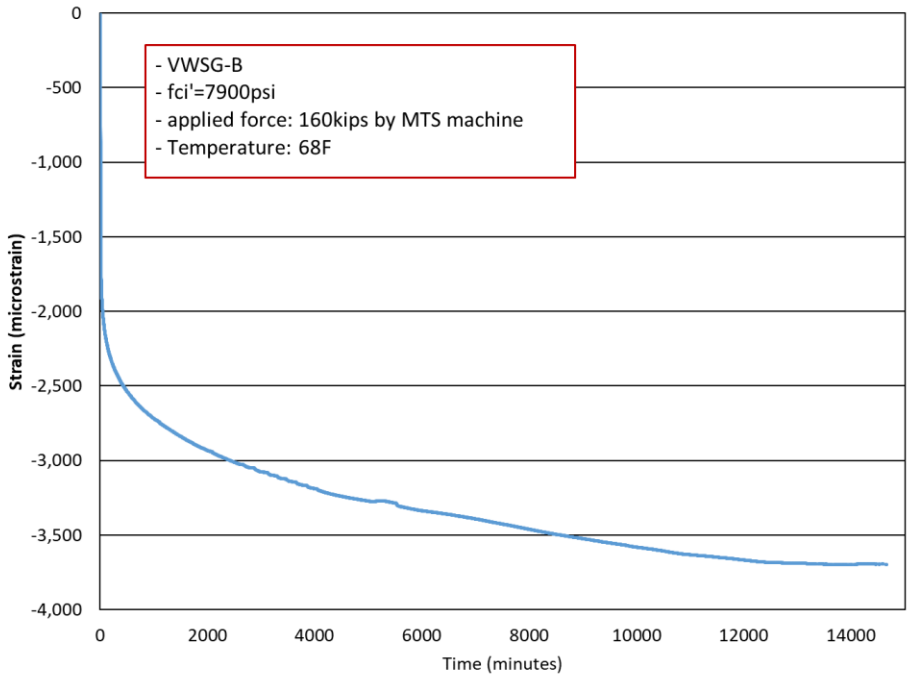

Figure B-21. Strain measurement from the stress dependence test (0624 batch)

At 200 hours (12,000 minutes), the total strain was 3,668με. Based on a shrinkage strain of 115με, the creep strain was 3,668-1,658-115 = 1,895με. The creep coefficient was 1,895με/1,658με = 1.14 for a load ratio of 0.72.

At 5,229 minutes after loading, the strain became 3,272με, and the frequency reading of VWSG-B changed from 400Hz to 1,200Hz indicating the sensor reached its lowest measurable range for the 1st mode of vibration. The following frequency reading corresponded to the 3rd mode, and n=3 was used in Eq. (B-10) to evaluate the strain. If VWSG-R was used instead of VWSG-B, larger strains could be measured from the 1st mode of vibration.

B.3.7 Thermal Cycling

The change of strain due to thermal cycling was observed from the two specimens used in the low-temperature 2 test. Five thermal cycles were applied, and the temperature changed between -40°F and 73°F in each cycle. The first cycle started at 128 days after the loading of the specimens. Each cycle took 3 – 6 days. Figure B-22 shows the change of total strain from the two specimens during the thermal cycling.

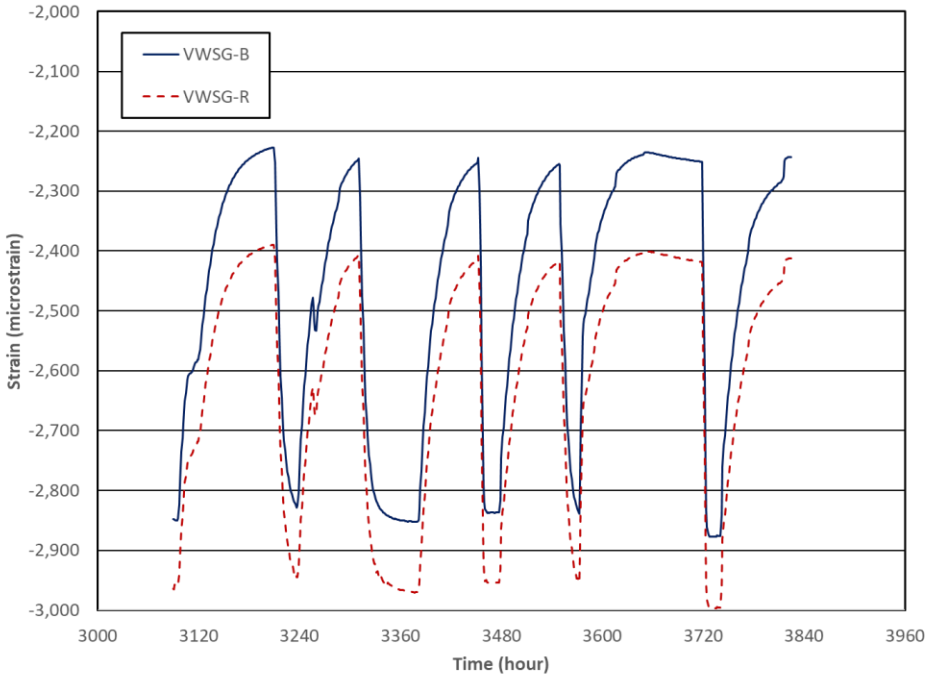

Figure B-22. Strain Measurement from the Thermal Cycling Test

The strain changes during temperature cycles correspond to the thermal strain of concrete. In Table B-7, total strains are collected and compared when the temperature was -39°F and 68°F in each temperature cycle. The two sensors were responsive to the wide temperature change in a short period of time. The difference in total strain between the two temperatures varied 566 – 581με for VWSG-B and 519 – 533με for VWSG-R sensor. The change in shrinkage strain from VW1 was 617 – 631με.

Table B-7. Strains during thermal cycles

Cycle	Temperature (°F)	Total Strain (με)		Shrinkage Strain (με)
		VWSG-B	VWSG-R	VW1
	68	2,249	2,409	402
1st	-39	2,820	2,939	1,018
	68	2,248	2,409	400
2nd	-39	2,824	2,939	1,015
	68	2,258	2,420	398
3rd	-39	2,833	2,946	1,023
	68	2,264	2,427	396
4th	-39	2,838	2,952	1,021
	68	2,257	2,419	397
5th	-39	2,873	2,994	1,039
	68	2,301	2,468	408

B.4 Summary

From seven types of test, the long-term characteristics of concrete strain were studied. Effects on total strain from cold temperature and different amount of applied stress were the main interests of the study. Information collected from tests was utilized to select concrete strain sensor for long-term, pre-stress loss monitoring.

During the two long-term tests, concrete total strain was measured for 41 days and 120 days. The load ratio (applied stress / concrete strength at loading) was 0.4 and 0.5. The total strain reached 2,400 με and 2,300 με. The total strain can increase up to 3,000 με for 5 years. From the low-temperature tests, concrete total strain and shrinkage strain became dormant when the temperature was -40°F. The same behavior was observed in other tests, but the amount of strain was greater when the specimen was loaded at earlier age in cold temperature. The creep strain increased as the applied stress increased. The stress dependent test showed that the creep coefficient at 200 hours was 0.8 for a load ratio of 0.23. At the same temperature (68°F), the creep coefficient was 1.14 for a load ratio of 0.72 at the same age.

It was estimated that the total strain can reach 3,000 με for 5 years. This exceeds the measurement range of VWSG-NA and FOSG sensors. The measurement range of VWSG-B is marginal. VWSG-B and VWSG-R were responsive to the wide change of

temperature. Also, VWSG-B was able to measure strain change induced by stress cycle at -40°F. The measured strains were comparable with the strains measured at 75°F considering the stiffening effect of concrete in cold temperature. After applying five thermal cycles (-40°F ~73°F), VWSG-B and VWSG-R accurately measured the strain without indicating deterioration by cold temperature. When the load ratio was 0.72 in the stress dependent test, strains exceeded the measurement range for the fundamental frequency of the VWSG-B sensor. In such cases, the VWSG-R sensor would better perform. Overall, the VWSG-R sensor is more accurate since each sensor was individually calibrated. Also, the measurement range of VWSG-R (5,000 με) is wide enough for the expected strain change.

APPENDIX C.

SAMPLE PRE-STRESS LOSS CALCULATION: TULSONA CREEK BRIDGE

To demonstrate differences in pre-stress loss evaluation, the Tulsona Creek bridge (# 1250) was used in this appendix. The Tulsona Creek bridge is a single span, DBT girder bridge as shown in Figure C-1.

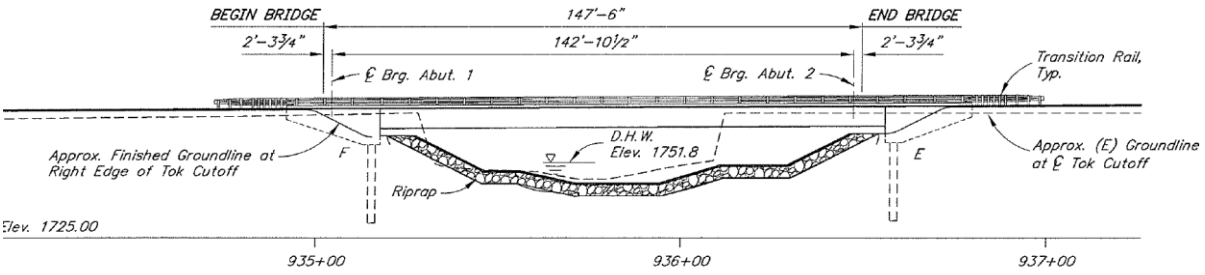

Figure C-1. Elevation of Tulsona Creek Bridge

In the bridge, seven DBT girders were employed as shown in Figure C-2. The length of a girder was 144′-6″, and the height was 5′-6″.

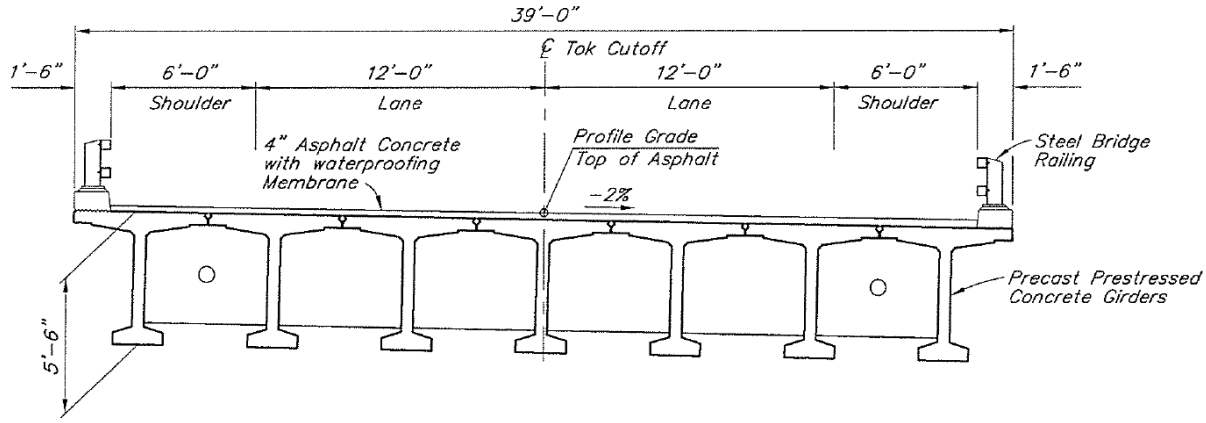

Figure C-2. Typical Section of Tulsona Creek Bridge

Figure C-3 shows the shape of a girder and the location of pre-stressing tendons. Sectional properties of a girder were evaluated based on the dimensions given in the figure.

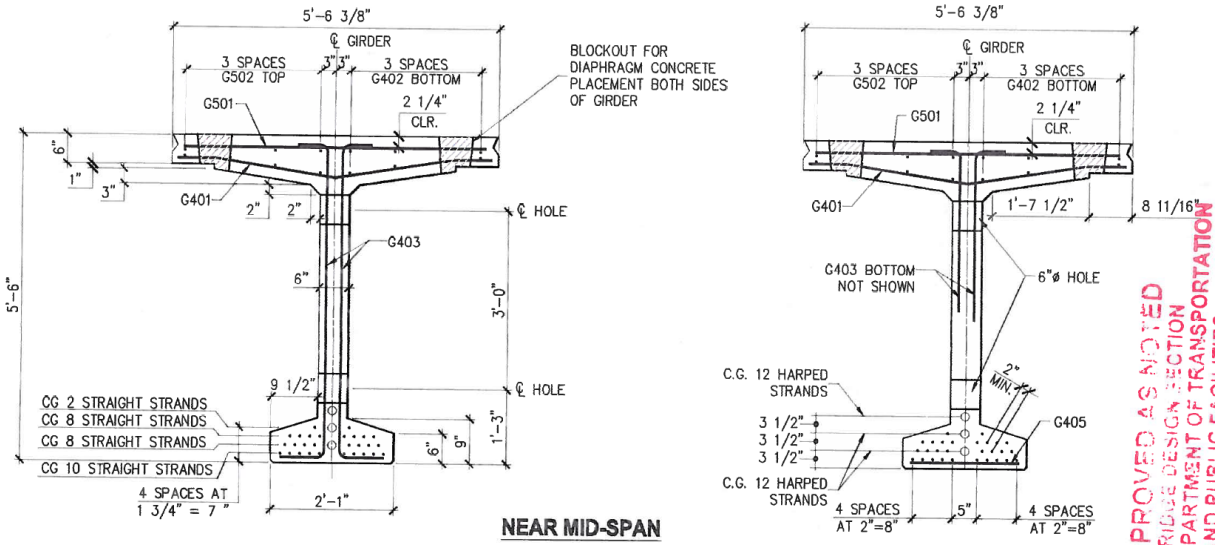

Figure C-3 Typical Cross Section of a DBT Girder in the Tulsona Creek Bridge

The detailed pre-stress loss was calculated in MathCAD worksheet, and they are attached to this appendix. In summary, the following are evaluated pre-stress losses from various procedures.

- 2004 AASHTO Lump-Sum method: 29.8 ksi
- 2004 AASHTO Refined Method: 38.9 ksi
- 2017 AASHTO Approximate Estimation: 23.2 ksi
- 2017 AASHTO Refined Estimation: 23.1 ksi

In addition, pre-stress loss calculation in the MS-Excel worksheet from NCHRP Report 496 was attached for a comparison with the value from 2017 AASHTO Refined Estimation. The long-term loss from the Excel worksheet was 25.2 ksi. This value was different from 23.1 ksi calculated from the MathCAD. The reason was the different formula to estimate the elastic modulus. The equation was revised in the 2017 AASHTO-LRFD, and it produces a greater elastic modulus than that from the previous equation used in the MS-Excel worksheet.

Part	Shape	height	width	Ai	yi	Aiyi	I I'	Ai di2	Perimeter length
		in	in				in^4	in^4	in
A	SQ	6.0	66.4	398.3	63.0	25089.8	1194.75	167068.70	95.75
B	SQ	60.0	6.0	360.0	30.0	10800.0	108000.00	56413.27	96.00
C	SQ	1.0	43.0	43.0	59.5	2558.5	3.58	12400.51	2.00
D	TR	3.0	39.0	58.5	58.0	3393.0	29.25	14021.77	39.46
E	SQ	3.0	4.0	12.0	57.5	690.0	9.00	2693.48	0.00
F	TR	2.0	4.0	4.0	55.3	221.3	0.89	656.92	5.66
G	TR	3.0	19.0	28.5	7.0	199.5	14.25	35953.82	19.92
H	SQ	6.0	19.0	114.0	3.0	342.0	342.00	178031.79	31.00
			Sum	1018.25		43294.08	109593.72	467240.26	289.79
					y_bar	42.52	from the bottom		
					I_g	576833.98			

Ap 0.153 in^2

Group	number of strands	CGS	
	ni	in	ni yi
Harped	36	7	252
Straight	28	3.625	101.5
Sum	64		353.5
CGS	5.523	in	from the bottom

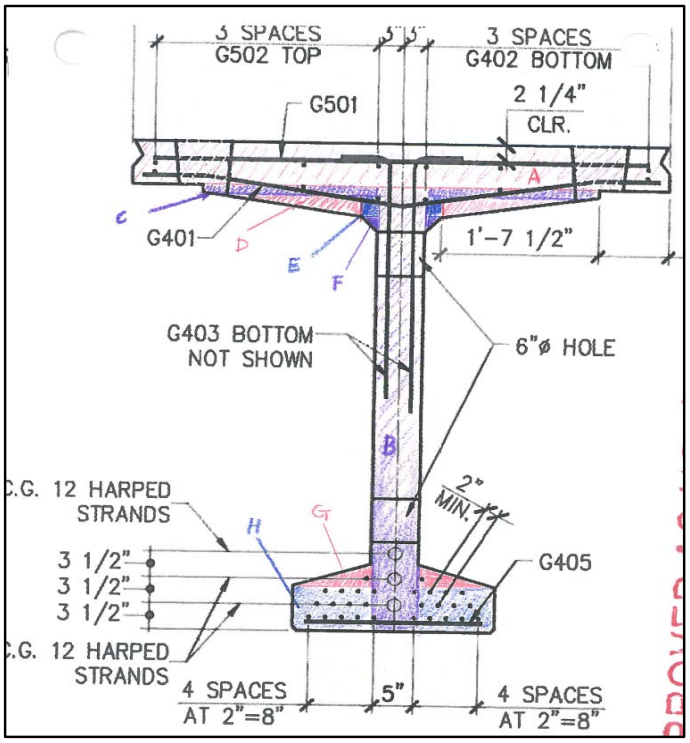

Girder

length	1734	in
Section A	1018.25	in^2
Volume	1765645.5	in^3
Side S	502496.818	in^2
End S (two)	2036.5	in^2
Total S	504533.318	in^2

	number	section	per girder	
		in^2	lb/ft	
Rail support	2	180	54.64	
	number	volume	per girder	
		in^3	lb	lb/ft
diaphragm	6	25803	1958.263	13.552

Prestress Loss Calculation Example

References:

- Garber et al. 2013. Effect of New Prestress Loss Estimations on Pretensioned Concrete Bridge Girder Desjgn (FHWA/TX-12/0-6374-2). University of Texas at Austin; Texas DOT.
- Tadros et al. 2003. Prestress Losses in Pretensioned High-Strength Concrete Bridge Girders (NCHRP Report 496). Transportation Research Board.

Reviewed by Elmer Marx (AK DOT&PF)

1. Design Parameters

1.1 Concrete

$w_c := 153\ pcf$	weight of concrete (weight of AggPro concrete)
$w_{RC} := 158\ pcf$	unit weight of PC (RC)
$f'_{ci} := 6250\ psi$	concrete strength at transfer
$f'_c := 7500\ psi$	concrete strength at 28 days

1.2 Strand

$A_p := 0.153\ in^2$	Area of strand (1/2" dia. round low-relaxation)
$f_{pu} := 270\ ksi$	tensile strength of a strand
$E_p := 28500\ ksi$	Young's modulus of a strand
$f_{pj} := 189\ ksi$	jacking stress (drawings)
$f_{pi} := 171\ ksi$	after initial losses; immediately after transfer (design value in the drawing)

1.3 Girder

$length_{girder} := 144\ ft + 6\ in = 144.5\ ft$	length of a girder (end-to-end)
$length_{girder\_b} := 142\ ft + 10.5\ in = 142.875\ ft$	length of a girder (bearing-to-bearing)
$width_{girder} := 5.53\ ft$	width of a girder
$n_{strands} := 36 + 28$	number of strands in a girder
$A_{ps} := A_p \cdot n_{strands} = 9.792\ in^2$	total area of strands
$A_g := 1018.25\ in^2$	gross area of a girder section
$I_g := 576834\ in^4$	second moment of inertia (gross section)
$e_p := 42.518\ in - 5.523\ in = 36.995\ in$	distance between cgs and cgp

Non-Commercial Use Only

$V_{girder} := 1765645.5\ in^3$ volume of a girder (Excel)

$A_{surface} := 504533.32\ in^2$ surface area of a girder (Excel)

$V\_S_{girder} := \frac{V_{girder}}{A_{surface}} = 3.5\ in$ volume-to-surface ratio of a girder

girder weight

$weight_{girder} := A_g \cdot length_{girder} \cdot w_{RC} = 161.442\ kip$

$weight_{wear} := 50\ psf$ weight for wearing surface

$w_{girder} := \frac{weight_{girder}}{length_{girder\_b}} = 1.13\ \frac{kip}{ft}$ Dead load (girder weight)

$w_{wearr} := weight_{wear} \cdot width_{girder} = 0.277\ \frac{kip}{ft}$ wearing surface load

$w_{SDL} := 0.7\ \frac{kip}{ft}$ all superimposed dead load

1.4 Site Information

$H_{relative\_humidity} := 70\%$ relative humidity in % [LRFD Figure 5.4.2.3.3-1]

Non-Commercial Use Only

2. Prestress loss calculation (2004 AASHTO)

2.1 Elastic shortening

$$M_g := \frac{w_{girder} \cdot length_{girder\_b}^{\ 2}}{8} = \left(3.46 \cdot 10^4\right)\ in \cdot kip$$

moment due to girder weight (@midspan)

$$E_{ci} := 120000\ ksi \cdot \left(\frac{w_c}{1000\ pcf}\right)^{2.0} \cdot \left(\frac{f'_{ci}}{ksi}\right)^{0.33}$$

concrete elastic modulus on the day of load transfer (= 2 days) [LRFD 5.4.2.4-1]

$w_c = 153\ pcf$ $\quad E_{ci} = \left(5.143 \cdot 10^3\right)\ ksi$

$$f_{cgp} := \frac{E_{ci}}{E_p} \cdot \left(\frac{0.7 \cdot f_{pu} \cdot A_{ps} \cdot \left(I_g + e_p^{\ 2} \cdot A_g\right) - e_p \cdot M_g \cdot A_g}{A_{ps} \cdot \left(I_g + e_p^{\ 2} \cdot A_g\right) + \frac{A_g \cdot I_g \cdot E_{ci}}{E_p}}\right) = 3.375\ ksi$$

approximate estimation of elastic shortening

$$\Delta f_{pES} := \frac{E_p}{E_{ci}} \cdot f_{cgp} = 18.704\ ksi$$

Prestress loss due to elastic shortening

2.2 Creep

$$M_{sd} := \frac{w_{SDL} \cdot length_{girder\_b}^{\ 2}}{8} = \left(2.143 \cdot 10^4\right)\ in \cdot kip$$

moment due to superimposed dead load (@midspan)

$$\Delta f_{cdp} := \frac{M_{sd} \cdot e_p}{I_g} = 1.375\ ksi$$

change in concrete stress

$$\Delta f_{pCR} := 12 \cdot f_{cgp} - 7 \cdot \Delta f_{cdp} = 30.879\ ksi$$

Prestress loss due to creep

2.3 Shrinkage

Prestress loss due to shrinkage

$$\Delta f_{pSR} := 17.0\ ksi - 0.15\ ksi \cdot H_{relative\_humidity} \cdot 100$$

$$\Delta f_{pSR} = 6.5\ ksi$$

2.4 Strand Relaxation (after transfer)

$k_{SR} := 0.3$ factor for low relaxation strands

$$\Delta f_{pR2} := k_{SR} \cdot \left(20\ ksi - 0.4 \cdot \Delta f_{pES} - 0.2 \cdot \left(\Delta f_{pCR} + \Delta f_{pSR}\right)\right)$$

Non-Commercial Use Only

$\Delta f_{pR2} = 1.513\ ksi$ Prestress loss due to relaxation

2.5 Total Long-Term Loss

$$\Delta f_{pLT} := \Delta f_{pCR} + \Delta f_{pSR} + \Delta f_{pR2} = 38.892\ ksi$$

3. 2004 AASHTO Lump-Sum Method (AKDOT method)

$$\Delta f_{pLT} := 33\ ksi \cdot \left(1 - 0.15 \cdot \left(\frac{\frac{f'_c}{1000\ psi} - 6}{6}\right)\right) - 2\ ksi = 29.763\ ksi$$

4. 2017 AASHTO LRFD (8th) Approximate Estimation [LRFD 5.9.3.3]

$f_{pj} = 189\ ksi$ prestressing steel stress immediately prior to transfer (jacking stress)

$A_{ps} = 9.792\ in^2$

$\gamma_h := 1.7 - 0.01 \cdot H_{relative\_humidity} \cdot 100 = 1$ correction factor for relative humidity

$$\gamma_{st} := \frac{5}{1 + \frac{f'_{ci}}{1000\ psi}} = 0.69$$ correction factor for specified concrete atrength at time of prestress transfer

$\Delta f_{pR} := 2.4\ ksi$ an estimate of relaxation loss taken as 2.4ksi for low-relaxation strand

$$\Delta f_{pLT} := 10.0 \cdot \frac{f_{pj} \cdot A_{ps}}{A_g} \cdot \gamma_h \cdot \gamma_{st} + 12.0\ ksi \cdot \gamma_h \cdot \gamma_{st} + \Delta f_{pR} = 23.21\ ksi$$

Time-dependent losses based on approximate estimate

5. 2017 AASHTO LRFD (8th) Refined Estimates [LRFD 5.9.3.4]

[AASHTO 5.9.3.4.4]
The equations in Article 5.9.3.4.2 and Article 5.9.3.4.3 are applicable to girders with noncomposite deck or topping, or with no topping. ... Time of "deck placement" in Article 5.9.3.4.3 may be taken as time of noncomposite deck placement or values at time of installation of precast members without topping.

5.1 Factors for creep and shrinkage calculation

Non-Commercial Use Only

$$k_{shape} := \max\left(1.45 - 0.13 \cdot \frac{V\_S_{girder}}{in}, 1.0\right) = 1$$ volume-to-surface factor [Eq. 5.4.2.3.2-2]

$$k_{hc} := 1.56 - 0.008 \cdot H_{relative\_humidity} \cdot 100 = 1$$ humidity factor for creep

$$k_{hs} := 2 - 0.014 \cdot H_{relative\_humidity} \cdot 100 = 1.02$$ humidity factor for shrinkage

$$k_f := \frac{5}{1 + \frac{f'_{ci}}{ksi}} = 0.69$$ concrete strength factor

$t_{ini} := 2$ age of concrete at time of load application (day); assume that the prestress force was applied on the day equivalent to 2 days (16 hour steam cure)

$t_{60d} := 60$ when girders are assembled at the site with welding connecting plates (assumed that 60 days after)

$t_{final} := 75 \cdot 365 = 2.738 \cdot 10^4$ final age in days (assume 75 years of service)

$$k_{td\_ini\_60d} := \frac{\left(t_{60d} - t_{ini}\right)}{12 \cdot \left(\frac{100 - 4 \cdot \frac{f'_{ci}}{ksi}}{\frac{f'_{ci}}{ksi} + 20}\right) + \left(t_{60d} - t_{ini}\right)} = 0.628$$ time development factor between ini and t60d

$$k_{td\_60d\_final} := \frac{\left(t_{final} - t_{60d}\right)}{12 \cdot \left(\frac{100 - 4 \cdot \frac{f'_{ci}}{ksi}}{\frac{f'_{ci}}{ksi} + 20}\right) + \left(t_{final} - t_{60d}\right)} = 0.999$$ time development factor between 60d and final

$$k_{td\_ini\_final} := \frac{\left(t_{final} - t_{ini}\right)}{12 \cdot \left(\frac{100 - 4 \cdot \frac{f'_{ci}}{ksi}}{\frac{f'_{ci}}{ksi} + 20}\right) + \left(t_{final} - t_{ini}\right)} = 0.999$$ time development factor between ini and final

Non-Commercial Use Only

$\Psi_{creep\_ini\_60d} := 1.9 \cdot k_{shape} \cdot k_{hc} \cdot k_f \cdot k_{td\_ini\_60d} \cdot t_{ini}^{-0.118} = 0.759$ creep coefficient ini - 60d

$\Psi_{creep\_60d\_final} := 1.9 \cdot k_{shape} \cdot k_{hc} \cdot k_f \cdot k_{td\_60d\_final} \cdot t_{60d}^{-0.118} = 0.807$ creep coefficient 60d - final

$\Psi_{creep\_ini\_final} := 1.9 \cdot k_{shape} \cdot k_{hc} \cdot k_f \cdot k_{td\_ini\_final} \cdot t_{ini}^{-0.118} = 1.206$ creep coefficient ini - final

$$E_{ci} := 120000\ ksi \cdot \left(\frac{w_c}{1000\ pcf}\right)^{2.0} \cdot \left(\frac{f'_{ci}}{ksi}\right)^{0.33}$$

concrete elastic modulus on the day of load transfer (= 2 days) [LRFD 5.4.2.4-1]

$w_c = 153\ pcf$ $E_{ci} = \left(5.143 \cdot 10^3\right)\ ksi$

5.2 Losses: time of transfer to time of deck placement (installation on the 60th days)

5.2.1 Shrinkage of girder concrete

$$\varepsilon_{bid} := k_{shape} \cdot k_{hs} \cdot k_f \cdot k_{td\_ini\_60d} \cdot 0.48 \cdot 10^{-3}$$

$$\varepsilon_{bid} = 2.122 \cdot 10^{-4}$$

concrete shrinkage strain [Eq. 5.4.2.3.3-1]

$$K_{id} := \frac{1}{1 + \left(\frac{E_p}{E_{ci}}\right) \cdot \left(\frac{A_{ps}}{A_g}\right) \cdot \left(1 + \frac{A_g \cdot e_p^{\,2}}{I_g}\right) \cdot \left(1 + 0.7 \cdot \Psi_{creep\_ini\_final}\right)}$$

$$K_{id} = 0.749$$

transformed section coefficient

$\Delta f_{pSR} := \varepsilon_{bid} \cdot E_p \cdot K_{id} = 4.528\ ksi$ loss due to shrinkage

5.2.2 Creep of girder concrete

(a) f_{cgp} calculation based on equation

$$f_{cgp\_eq} := \frac{E_{ci}}{E_p} \cdot \left(\frac{0.7 \cdot f_{pu} \cdot A_{ps} \cdot \left(I_g + e_p^{\,2} \cdot A_g\right) - e_p \cdot M_g \cdot A_g}{A_{ps} \cdot \left(I_g + e_p^{\,2} \cdot A_g\right) + \frac{A_g \cdot I_g \cdot E_{ci}}{E_p}}\right) = 3.375\ ksi$$

concrete stress @cgp immediately after transfer; AK uses $0.7 \cdot f_{pu}$ for jacking stress [LRFD C5.9.3.2.3a-1]

Non-Commercial Use Only

(b) f_{cgp} calculation based on iteration

iteration 1

use stress at transfer as initial

$$f_{p\_ini} := 0.7 \cdot f_{pu} = 189 \ ksi$$

$$f_{cgp\_1} := f_{p\_ini} \cdot A_{ps} \cdot \left(\frac{1}{A_g} + \frac{e_p^{\,2}}{I_g} \right) - \frac{M_g \cdot e_p}{I_g} = 3.99 \ ksi$$

$$f_{p\_1} := f_{p\_ini} - f_{cgp\_1} \cdot \frac{E_p}{E_{ci}} = 166.891 \ ksi$$

iteration 2

$$f_{cgp\_2} := f_{p\_1} \cdot A_{ps} \cdot \left(\frac{1}{A_g} + \frac{e_p^{\,2}}{I_g} \right) - \frac{M_g \cdot e_p}{I_g} = 3.263 \ ksi$$

$$f_{p\_2} := f_{p\_ini} - f_{cgp\_2} \cdot \frac{E_p}{E_{ci}} = 170.916 \ ksi$$

iteration 3

$$f_{cgp\_3} := f_{p\_2} \cdot A_{ps} \cdot \left(\frac{1}{A_g} + \frac{e_p^{\,2}}{I_g} \right) - \frac{M_g \cdot e_p}{I_g} = 3.396 \ ksi$$

$$f_{p\_3} := f_{p\_ini} - f_{cgp\_3} \cdot \frac{E_p}{E_{ci}} = 170.183 \ ksi$$

iteration 4

$$f_{cgp\_4} := f_{p\_3} \cdot A_{ps} \cdot \left(\frac{1}{A_g} + \frac{e_p^{\,2}}{I_g} \right) - \frac{M_g \cdot e_p}{I_g} = 3.371 \ ksi$$

$$f_{p\_4} := f_{p\_ini} - f_{cgp\_4} \cdot \frac{E_p}{E_{ci}} = 170.317 \ ksi$$

iteration 5

$$f_{cgp\_5} := f_{p\_4} \cdot A_{ps} \cdot \left(\frac{1}{A_g} + \frac{e_p^{\,2}}{I_g} \right) - \frac{M_g \cdot e_p}{I_g} = 3.376 \ ksi$$

$$f_{p\_5} := f_{p\_ini} - f_{cgp\_5} \cdot \frac{E_p}{E_{ci}} = 170.292 \ ksi$$

result from iteration is the same as the one from the equation

$$f_{cgp\_it} := f_{cgp\_5} = 3.376 \ ksi$$

Non-Commercial Use Only

(c) using f_{cgp} from equation

$f_{cgp} := f_{cgp\_eq} = 3.375\ ksi$ use result from the equation

$\Delta f_{pCR} := \frac{E_p}{E_{ci}} \cdot f_{cgp} \cdot \Psi_{creep\_ini\_60d} \cdot K_{id} = 10.626\ ksi$ loss due to creep

5.2.3 Relaxation

$\Delta f_{pR1} := 1.2\ ksi$ for low-relaxation strands [LRFD 5.9.3.4.2c]

5.3 Losses: Time of deck placement to final time

Wearing surface load is applied to the girder

$w_{wear\_SDL} := w_{wearr} = 0.277\ \frac{kip}{ft}$ load at 60 days

$M_{SD} := \frac{w_{wear\_SDL} \cdot length_{girder\_b}^{2}}{8} = \left(8.466 \cdot 10^{3}\right)\ in \cdot kip$ moment at mid-span

5.3.1 Shrinkage of girder concrete

$\varepsilon_{bif} := k_{shape} \cdot k_{hs} \cdot k_f \cdot k_{td\_ini\_final} \cdot 0.48 \cdot 10^{-3}$ final concrete shrinkage strain [Eq. 5.4.2.3.3-1]

$\varepsilon_{bif} = 3.372 \cdot 10^{-4}$

$\varepsilon_{bdf} := \varepsilon_{bif} - \varepsilon_{bid} = 1.25 \cdot 10^{-4}$ shrinkage between 60d and final

$K_{df} := K_{id}$ transformed section coefficients are the same for DBT girders

$\Delta f_{pSD} := \varepsilon_{bdf} \cdot E_p \cdot K_{df} = 2.668\ ksi$ loss due to shrinkage

5.3.2 Creep of girder concrete

$\Delta P_{pre} := -\left(\Delta f_{pSR} + \Delta f_{pCR} + \Delta f_{pR1}\right) \cdot A_{ps} = -160.14\ kip$ pre-stress force change due to loss (ini - 60d)

$\Delta f_{cd} := \frac{\Delta P_{pre}}{A_g} + \frac{\Delta P_{pre} \cdot e_p^{2}}{I_g} - \frac{M_{SD} \cdot e_p}{I_g} = -1.08\ ksi$ change in concrete stress [Eq. 5.9.3.4.3b-1]

Non-Commercial Use Only

$$E_c := 120000\ ksi \cdot \left(\frac{w_c}{1000\ pcf}\right)^{2.0} \cdot \left(\frac{f'_c}{ksi}\right)^{0.33}$$ final concrete elastic modulus [LRFD 5.4.2.4-1]

$w_c = 153\ pcf$ $E_c = \left(5.462 \cdot 10^3\right)\ ksi$

$$\Delta f_{pCD} := \frac{E_p}{E_{ci}} \cdot f_{cgp} \cdot \left(\Psi_{creep\_ini\_final} - \Psi_{creep\_ini\_60d}\right) \cdot K_{df} + \frac{E_p}{E_c} \cdot \Delta f_{cd} \cdot \Psi_{creep\_60d\_final} \cdot K_{df}$$

$\Delta f_{pCD} = 2.854\ ksi$ loss due to creep

5.3.3 Relaxation

$\Delta f_{pR2} := \Delta f_{pR1} = 1.2\ ksi$

5.4 Total prestress loss

$\Delta f_{pLT} := \Delta f_{pSR} + \Delta f_{pCR} + \Delta f_{pR1} + \Delta f_{pSD} + \Delta f_{pCD} + \Delta f_{pR2} = 23.075\ ksi$

Non-Commercial Use Only

Tulsona Bridge (Gross Section)

Proposed Detailed Method Using Estimated Material Properties

AK DBT Girder

Nabil Al-Omaishi Il-Sang Ahn

23-Mar-02 8/30/2019

Span	144.5	ft		H	70	%	
A	1018.25	in^2		f_{ci}	6.250	ksi	
I	576834	in^4		f'_c	7.500	ksi	
y_b	42.52	in	location of centroid				
h	66	in	height				
V/S	3.5	in					
Deck							
Width	0	in		f'_{cd}	0.00	ksi	
Thickness	0	in					
Area	0	in^2					
Steel				Age at release t_i	2	days	
A_{ps}	9.792	in^2		Age at deck placement	60	days	
f_{pi}	171	ksi	after transfer	Age at Final	27375	days	
E_s	28500	ksi					
y_{pb}	5.52	in					

Loads

Girder self wt	1.1300	kip/ft	**Midspan Moments**			
Deck wt	0.000	kip/ft	Girder self wt		35392	kip-in
Haunch wt	0.000	kip/ft	Deck wt	0 kip-in		
Diaph. wt	0.000	kip/ft	Haunch wt	0 kip-in		
SI dead ld.	0.277	kip/ft	Diaph. Wt	0.0 kip-in	0	kip-in
			SI dead ld.		8676	kip-in
			Live load plus impact		20284	kip-in

Solution

Modulus of Elasticity $33000*w^{1.5}*(f'_c)^{0.5}$

$w=0.140+f'_c/1000$ (kcf)

		Beam	E_{ci}	4204	
			E_c	4664	
		Deck	E_{cd}	0	
Shrinkage	$0.00043(5/(1+f_{ci}))k_s k_h k_{td}$	Beam	ε_{bif}	0.000330	
k_h	2.0-0.0143H		ε_{bid}	0.000204	
k_{td}	$t/(61-4f_{ci}+t)$	Precast	ε_{bdf}	0.000126	
		Deck	ε_{ddf}	0.003463	
Creep	$1.80*k_s*k_h*(5/(1+f_{ci}))*k_{la}*k_{td}$	Beam	ψ_{bif}	1.230	
k_h	(1.58-0.008*H)		ψ_{bid}	0.760	
k_{la}	$t_i^{-0.118}$	Formula for girder only	ψ_{bdf}	0.823	
k_{td}	$t/(61-4f_{ci}+t)$	Deck	ψ_{ddf}	13.260	

Section Properties				Precast Gross Section	Precast Transf. Rel	Precast Tr. Final	Deck	Composite Gross	Composite Tr.
Steel modular ratio,n_i	E_s/E_{ci}	6.7800	A	1018.25	1074.85	1068.29	0.00	1018.25	1068.29
Steel modular ratio,n	E_s/E_c	6.1107	y_b (to bottom fiber of beam)	42.52	40.57	40.79	66	42.52	40.79
Deck modular ratio	E_d/E_c	0.0000	I	576834	650224	642125	0	576834	642124.8
			e_p	37.00	35.05	35.26		37.00	35.26
			e_d					-23.48	
			α=1+A*e2/I	3.4162				3.416	
Transfromed section factors, K			K_r Elastic (at release)	0.81784	K_{dc} Elastic(at SIDL)				0.83281
K=1/(1+n*α*A_s/A_c*(1+0.7*C))			K_d Elastic(at deck pl.)	0.83281					
			K_{rd} Long-term	0.70696	K_{df} Long-term				0.70696

Stress Calculation		Steel Stress Change	Steel Stress Net	Gross Section Concrete Stress Change	Gross Section Concrete Stress Net	Transf. Section Concrete Stress Change	Transf. Section Concrete Stress Net
			171.000				
(1) Elastic due to P_i	$P_i*\alpha*K_r*n_i/A$	31.150	139.850	4.594	4.594	4.721	4.721
(2) Elastic due to self weight	$M*e/I*K_r*n_i$	-12.587	152.437	-1.856	2.738	-1.908	2.813
(3) Shrinkage between release and deck place	$\varepsilon_{bid}*E_p*K_{rd}$	4.111	148.326				
(4) Creep between release and deck place	$n_i*f_{cir}*K_r*\psi_{bid}*K_{rd}$	9.973	138.353				
(5) Relaxation between release and deck place		1.200	137.153	-0.502	2.236	-0.422	2.392
(6) Elastic due to deck weight	$n*\delta f_{cdp}*K_d$	0.000	137.153	0.000	2.236	0.000	2.392
(7) Elastic due to superimposed DL (on composite section)	$n*\delta f_{csp}*K_{dc}$	-2.832	139.985	-0.463	1.772	-0.476	1.915
(8) Shrinkage of beam bet.deck place and final	$\varepsilon_{bdf}*E_p*K_{df}$	2.543	137.442				
(9) Creep of beam bet.deck place and final, due to initial loads	$n_i*f_{pc}*(\psi_{bif}-\psi_{bid})*K_{df}$	6.169	131.273				
(10) Creep of beam due to deck and SIDL	$n*df_{pc}*\psi_{bdf}*K_{df}$	-3.434	134.708				

(11) Relaxation between deck place and final	$\phi_d * L_d * K_{df}$	1.200	133.508				
(12) Shrinkage of deck	$\varepsilon_{bdf} * E_{cd} / (1+0.7*\psi_{ddf}) * A_d * \alpha / A * K_{df} * n * (1+0.7*\psi_{bdf})$	0.000	133.508	-0.213	1.560	-0.182	1.733
Total Prestress Loss prior to Live Load Application		**37.492**					

Long Term ***25.196***

APPENDIX D.

SENSOR DATA SHEET

Concrete Embedment Strain Gauges

Applications

The Model 4200, 4202 and 4210 are designed to measure strains in or on...

- Foundations
- Piles
- Bridges
- Dams
- Containment vessels
- Tunnel liners
- Mass concrete with coarse aggregates
- Laboratories and/or where space limitations exist

- *Model 4200ER (5,000 µstrain) and 4200ER (10,000 µstrain) Strain Gauges.*

- *Model 4200L (low modulus) Strain Gauge.*

- *Model 4200HT-T High Temperature Strain Gauge.*

Operating Principle

The Model 4200 Series Vibrating Wire Embedment Strain Gauges are designed for direct embedment in concrete. The Model 4200 (standard model) has a 153 mm gauge length and is commonly used for strain measurements in foundations, piles, bridges, dams, containment vessels, tunnel liners, etc. The Model 4210 has a 250 mm gauge length and is designed for use in mass concrete with coarse aggregates. It is extra rugged to resist bending and has large flanges to provide greater engagement area. The 4202 and 4204 (51 mm and 102 mm gauge lengths, respectively) are designed for laboratory use and/or where there are space limitations.

Strains are measured using the vibrating wire principle: a length of steel wire is tensioned between two end blocks that are embedded directly in concrete. Deformations (i.e. strain changes) of the concrete mass, will cause the two end blocks to move relative to one another, thus altering the tension in the steel wire. The tension is measured by plucking the wire and measuring its resonant frequency of vibration using an electromagnetic coil.

Advantages and Limitations

The Model 4200 Series Strain Gauges enjoy all the advantages of vibrating wire sensors, which includes excellent long term stability, maximum resistance to the effects of water, and a frequency output suitable for transmission over very long cables.

All components are made from stainless steel for corrosion protection and the gauges are fully waterproof. The Model 4210 is very rugged and designed to withstand the rigors of concrete placement.

Each gauge incorporates a thermistor so that the temperature can be read and displayed by the readout.

Extended range, low modulus and high temperature versions are also available. The Model 4200ER is designed for measuring large strains up to 10,000 µstrain. The Model 4200L (low modulus version) is particularly suitable for measuring curing strains in concrete. The Model 4200HT is designed for short-term use at temperatures up to 200 °C while the Model 4200HT-T is designed for long-term use at temperatures up to 220 °C, making it particularly suitable for installation in steam-cured spun concrete piles.

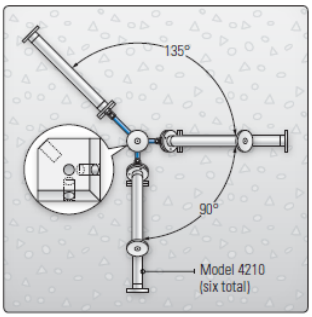

Top view of a Model 4210 strain gauge rosette configuration. Inset shows rosette fixture (enlarged for detail).

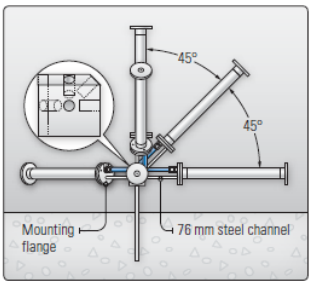

Front view of a Model 4210 strain gauge rosette configuration. Inset shows rosette fixture (enlarged for detail).

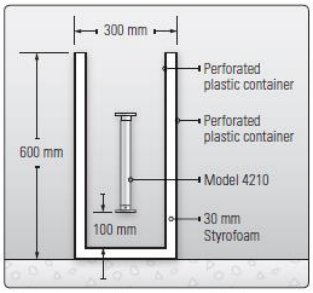

"No stress-strain" enclosure using the Model 4210.

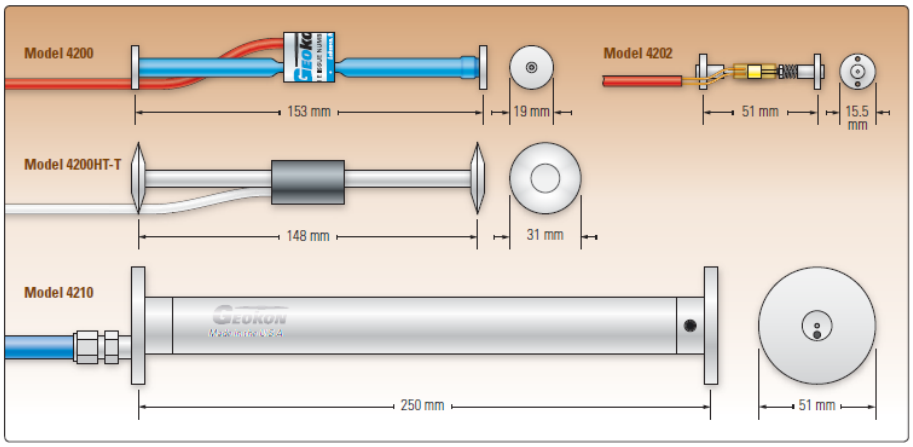

Dimensions of the 4200 Series Strain Gauges.

System Components

The strain gauges are shipped ready for installation with the correct amount of cable attached. Installation is accomplished by attaching the strain gauge to any steel reinforcement bar, or, in mass concrete, to special rosette fixtures designed to hold multiple strain gauges in different orientations to allow the measurement of strain in three dimensions.

Also available are no stress-strain enclosures for use in concrete dams. These enclosures are double-wall, plastic containers, lined with Styrofoam, designed to isolate one or more strain gauges from the stress field in the concrete, and to allow an estimate of, and correction for the effects of moisture, temperature, autogenous growth, etc.

All models are equipped with integral thermistors for the simultaneous measurement of temperature.

Readout is accomplished using the Model GK-404 or GK-405 Readouts, which can, when used with the Model 4200, display the strain directly in microstrain.

Technical Specifications

	4200	4200ER	4200L	4200HT	4200HT-T	4202	4204	4210
Range[1]	3,000 με	5,000 to 10,000 με	3,000 με	3,000 με	3,000 με	3,000 με	3,000 με	3,000 με
Resolution	1.0 με	2.0-5.0 με	1.0 με	1.0 με	1.0 με	0.4 με	1 με	0.4 με
Accuracy[2]	±0.5% F.S.[3]	±0.5% F.S.	±0.5% F.S.[3]	±0.5% F.S.[3]	±0.5% F.S.	±0.5% F.S.[3]	±0.5% F.S.[3]	±0.5% F.S.[3]
Nonlinearity	< 0.5% F.S.	±2.5-4.0% F.S.	< 0.5% F.S.	< 0.5% F.S.	< 0.5% F.S.	< 0.5% F.S.	< 0.5% F.S.	< 0.5% F.S.
Coil Resistance	180 Ω	180 Ω	180 Ω	120 Ω	50 Ω	50 Ω	180 Ω	180 Ω
Frequency Datum[4]	800 Hz	800 Hz	800 Hz	800 Hz	800 Hz	2600 Hz	1250 Hz	2600 Hz
Thermal Coefficient of Expansion	12.0 ppm/°C	variable	12.0 ppm/°C	12.0 ppm/°C	12.0 ppm/°C	12.0 ppm/°C	12.0 ppm/°C	12.0 ppm/°C
Temperature Range	–20 °C to +80 °C[1]	–20 °C to +80 °C[1]	–20 °C to +80 °C[1]	–20 °C to +200 °C	–20 °C to +220 °C	–20 °C to +80 °C[1]	–20 °C to +80 °C[1]	–20 °C to +80 °C[1]
Cable Type	4-conductor, 2 twisted pairs, 22 AWG *(for all models)*							
Cable Jacket	Red PVC, 4.75 mm ∅	Red PVC, 4.75 mm ∅	Red PVC, 4.75 mm ∅	White Teflon® 5.20 mm ∅	White Teflon® 5.20 mm ∅	Red PVC, 4.75 mm ∅	Red PVC, 4.75 mm ∅	Blue PVC, 6.35 mm ∅
Active Gauge Length	153 mm	153 mm	153 mm	153 mm	148 mm	51 mm	102 mm	250 mm[5]

[1]Other ranges available on request. | [2]Transducer accuracy established under laboratory conditions: ±0.5% F.S. with standard batch calibration. [3]±0.1% F.S. with individual calibration. | [4]Typical. | [5]Other lengths available on request.

GEOKON | TRUSTED MEASUREMENTS™

GEOKON
48 Spencer Street
Lebanon, NH 03766 · USA

www.geokon.com
e: info@geokon.com
p: +1·603·448·1562

GEOKON is an
ISO 9001:2015
registered company

The GEOKON® logo and word mark are registered trademarks with the United States Patent and Trademark Office. | GEOKON maintains an ongoing policy of design review and reserves the right to amend products and specifications without notice. | Teflon® is a registered trademark of E.I. du Pont de Nemours and Company or its affiliates.

©GEOKON. All Rights Reserved. | Rev-I-4/23/2019

Embeddable Strain Sensor | os3500

Description

The os3500 Embeddable Strain Sensor measures average strain over the length of the gage while providing integrated temperature compensation. It is based on fiber Bragg grating (FBG) technology. The os3500 is intended exclusively for embedding in concrete structures. Disk ends form a solid bond to surrounding concrete or grout.

A rugged, stainless steel body, ruggedized cables and optional connector protection fittings make the os3500 suitable for harsh environments.Two FBGs are well protected inside the os3500 body. One FBG measures strain, and the other provides for integrated temperature compensation. Since there are no epoxies holding the fiber to the carrier, long-term stability is ensured by design.

All the advantages of an **optical sensor** in a **conventional**, vibrating-wire type **package**

In side-by-side comparisons with vibrating-wire and foil strain gages, the os3500 is equally sensitive and accurate, while providing 100 times more fatigue life. The os3500 strain gage is qualified for use in harsh environments and delivers the many advantages inherent to all FBG based sensors.

This sensor can be used alone or in series as part of an FBG sensor array. Installation and cabling for such arrays is much less expensive and less cumbersome than comparable electronic gage networks.

Key Features

Temperature compensation sensor integrated inside. Measurement of relative temperature for compensation of strain measurements.

Qualified to same rigorous standards applied to comparable electronic gages.

Connector protection fittings available for **harsh environments.**

Fast, Simple, repeatable installation

Non-metallic ruggedized sensor package.

Double ended design supports multiplexing of many sensors on one fiber

Micron Optics' **patented micro opto-mechanical** technology.

Deployments

Structures (bridges, dams, tunnels, mines, buildings, oil platforms)

Energy (wind turbines, oil wells, pipelines, nuclear reactors, generators)

Transportation (railways, trains, roadways, specialty vehicles, cranes)

Marine vessels (hull, deck, cargo containers)

Aerospace (airframes, composite structures, wind tunnels, static and dynamic tests)

MICRON OPTICS

Embeddable Strain Sensor | os3500

Performance Properties	os3500
Strain; Temperature Sensitivity [1]	~1.2 pm/ue; 23.8 pm/C
Temperature Compensation	Integrated into each package
Gage Length	110 mm
Operating Temperature Range	-40 to 80 C
Strain Limits	+/- 2,500 ue
Water Resistant	Suitable for wet, high humidity environments (IP67)
Fatigue Life	> 1x10^8 cycles @ +/- 2,000 ue
Physical Properties	
Dimension; Weight	See diagram below; 98 g
Material	Stainless Steel/Polyolefin construction
Cable type / length	6 mm/3 mm ruggedized cable/1 m (+/- 10 cm), each end
Cable Bend Radius	≥17 mm
Anchoring Methods [2]	Embeddable
Optical Properties	
Peak Reflectivity (Rmax)	> 70%
FWHM (-3 dB point)	0.25 nm (+/- .05 nm)
Isolation	> 15 dB (@ +/- 0.4 nm around center wavelength)

Ordering Information

os3500-ggg-tttt/ssss-1xx-1yy

tttt/ssss Strain/Temp Wavelengths (+/- 1nm)
Standard - 1462/1466, 1472/1476 1482/1486, 1492/1496, 1502/1506, 1512/1516, 1522/1526, 1532/1536, 1542/1546, 1552/1556, 1562/1566, 1572/1576, 1582/1586, 1592/1596, 1602/1606, 1612/1616

xx Termination type
1xx Cable 1, Length & Connector
1 1 m Standard, Cable Length
UT Unterminated
FC FC/APC Connector

yy Termination type
1yy Cable 2, Length & Connector
1 1 m Standard, Cable Length
UT Unterminated
FC FC/APC Connector

Ordering Information Example

o3500-1512/1516-1FC-1FC

Accessories

PF Universal IP67 Connector Protection Fitting

Notes

1 Actual gage factor provided with gage.

2 See http://www.micronoptics.com/products/sensing-solutions/support/ for installation details.

MICRON OPTICS
1852 Century Place NE
Atlanta, GA 30345 USA
www.micronoptics.com

All rights reserved.
Specifications subject to change without further notice.